Generalized Multi-Commodity Network Flows: Case Studies in Space Logistics and Complex Infrastructure Systems

by

Takuto Ishimatsu

B.E., Aeronautics and Astronautics, The University of Tokyo (2004)
M.E., Aeronautics and Astronautics, The University of Tokyo (2006)
S.M., Aeronautics and Astronautics, Massachusetts Institute of Technology (2008)

Submitted to the Department of Aeronautics and Astronautics
in partial fulfillment of the requirements for the degree of

Doctor of Philosophy

at the

MASSACHUSETTS INSTITUTE OF TECHNOLOGY

June 2013

Author .....
Department of Aeronautics and Astronautics
May 23, 2013

Certified by .....
Olivier L. de Weck
Associate Professor of Aeronautics and Astronautics and Engineering Systems
Thesis Supervisor

Certified by .....
Jeffrey A. Hoffman
Professor of the Practice
Thesis Committee Member

Certified by .....
Yoshiaki Ohkami
Professor of System Design and Management, Keio University
Thesis Committee Member

Certified by .....
Robert Shishko
Principal Systems Engineer, NASA Jet Propulsion Laboratory
Thesis Committee Member

Accepted by .....
Eytan H. Modiano
Professor of Aeronautics and Astronautics
Chair, Graduate Program Committee

Generalized Multi-Commodity Network Flows: Case Studies in Space Logistics and Complex Infrastructure Systems

by

Takuto Ishimatsu

Submitted to the Department of Aeronautics and Astronautics
on May 23, 2013, in partial fulfillment of the
requirements for the degree of
Doctor of Philosophy

Abstract

In transition to a new era of human space exploration, the question is what the next-generation space logistics paradigm should be. The past studies on space logistics have been mainly focused on a "vehicle" perspective such as propulsive feasibility, cargo capacity constraints, and manifesting strategies, with the arbitrarily predetermined logistics network. But how do we select an optimal logistics network? Especially if we can utilize in-situ resources on the Moon and Mars, it will add complexity to network selection problem. The objective of this thesis is to develop a comprehensive graph-theoretic modeling framework to quantitatively evaluate and optimize space exploration logistics from a "network" perspective.

In an attempt to create such a modeling framework, we develop a novel network flow model referred to as the generalized multi-commodity network flow (GMCNF) model. On top of the classical network flow problems, the GMCNF model proposed in this thesis introduces three types of matrix multiplications (requirement, transformation, and concurrency), and also allows loop edges associated with nodes (graph loops) and multiple edges between the same end nodes (multigraph). With this modification, the model can handle multiple commodities that interact with each other in the form of requirement at nodes, transformation on edges, and concurrency within edges. A linear programming (LP) formulation and a mixed integer linear programming (MILP) formulation of the GMCNF model are described in preparation for the two case studies. For the MILP formulation, in addition to the flow, we introduce two more variables, capacity expansion and decision binary, and additional constraints including the big-$\mathcal{M}$ method.

The first case study applies the GMCNF LP model to human exploration of Mars. First we solve the baseline problem with a demand that is equivalent to that of the NASA's Mars Design Reference Architecture (DRA) 5.0 scenario. It is found that the solution saves 67.5% from the Mars DRA 5.0 reference scenario in terms of the initial mass in low-Earth orbit (IMLEO) primarily because chemical (LOX/LH_2) propulsion is used along with oxygen-rich ISRU. We also present one possible scenario with two "gateway" resource depots at GTO and DTO with orbital transfer vehicles (OTVs) running in the cislunar and Martian systems. Then we solve variant problems that have different settings to see the effect of each factor. Findings include: taking advantage of oxygen-rich ISRU, LOX/LH_2 is preferred to nuclear thermal rocket (NTR), the aerobraking option as well as ISRU availability on the Moon make great contributions in reducing the total mass to be launched from Earth, and as the ISRU production rate decreases, ISRU in each location becomes worthless at a

certain threshold and the network topology changes toward direct paths using NTR.

The other case study applies the GMCNF MILP model to the complex infrastructure systems in Saudi Arabia, focusing on the couplings between water and energy. Considering the capacity of the online infrastructures as of 2010 as a basis, we solve the problems with the 2030 demand and the 2050 demand. The objective function is a weighted sum of the total cost and the total CO_2 emission. The key findings include: the network tends to be less connected, more isolated when putting more emphasis on minimizing the CO_2 emissions, and some of the resulting networks suggest the possibility of the long-distance pipeline network connecting the west coast and the east coast via the central region (trans-peninsula pipeline).

Thesis Supervisor: Olivier L. de Weck
Title: Associate Professor of Aeronautics and Astronautics and Engineering Systems

Acknowledgments

In the course of this thesis work, every time I slowed down, I was lucky to find a "planet" to fly by and regained energy to propel myself forward.

First of all, I would like to thank my advisor Prof. Olivier de Weck for his guidance and support in the last five years. He gave me a number of opportunities and experiences as a researcher and broadened my world. He was always generous and broad-minded, letting me do whatever I wanted, from which I learned to be creative myself. Also I was encouraged by his understanding of what it is to have a family during PhD. I would like to express my gratitude to my thesis committee members, Prof. Jeffrey Hoffman, Prof. Yoshiaki Ohkami from Keio University, and Dr. Robert Shishko from NASA JPL for their interests in my research and inspiring suggestions in and outside the committee meetings. I truly enjoyed the opportunity to work with them on this topic. I am also appreciative of Prof. Nancy Leveson for giving me an opportunity to work on another project, which broadened my academic experience and expanded my professional relationship. I would also like to acknowledge my colleagues in the MIT Strategic Engineering Research Group (SERG) and in the MIT Complex Systems Research Laboratory (CSRL). Specifically, I would like to mention two of my oldest colleagues in SERG, Paul Grogan, who has constantly supported me with technical and non-technical discussions, and Thomas Coffee, who shed light on the starting line of my research.

On the more personal side, I could not have survived the challenging days without my friends. Wasabis and Japanese Association of MIT (JAM) are an irreplaceable part of my life at MIT. I personally thank Shinya Umeno, Kei Kobayashi, Ken Endo, Michinao Hashimoto, Masahiro Ono, Takuji Matsumoto, Sho Sato, and all the members for sharing the best time with me.

Last but not least, I sincerely thank my father Satoru, mother Yayoi, brother Yuto, sister Yui, and grandmother Yoshiko for their love and support. My special thanks also go to my parents-in-law Yasufumi and Mieko Aizono. Finally, I owe what I am today to my wife Yoshiko and daughter Cosmo. Yoshiko lived in America with me and gave birth to a lovely girl. In an unfamiliar environment, she must have experienced more hardships than I thought. Cosmo has taken over my life and become my reason for living since she was born in May 2011. This is a PhD that will be awarded to my family together.

This research was supported partly by NASA Jet Propulsion Laboratory (JPL) and partly by Center for Complex Engineering Systems (CCES) at King Abdulaziz City for Science and Technology (KACST) and MIT.

This thesis is dedicated to the memories of my grandfather Tomizo Fukuhara, who passed away in November 2012 at age 96 (1916-2012), and our baby Totora, who did not survive to be born in August 2012.

Contents

List of Figures

List of Tables

Nomenclature

Abbreviations

ABM	agent-based model
AIAA	American Institute of Aeronautics and Astronautics
ATV	Automated Transfer Vehicle
BCD	Baikonur Cosmodrome
BWRO	brackish water reverse osmosis
CAPEX	capital expenditure
CCART	cargo category allocation rates table
CCES	Center for Complex Engineering Systems
CEV	crew exploration vehicle
COS	class of supply
COTS	Commercial Orbital Transportation Services
CPI	collaborative planning interface
CRS	Commercial Resupply Services
DEIM	Deimos
DRA	design reference architecture
DSS	decision support system
DTO	Deimos transfer orbit
ECLSS	environmental control and life support system
EDL	entry, descent, and landing
EML	Earth-Moon Lagrange point
ERV	Earth return vehicle
EVA	extra-vehicular activity
GC	Gale Crater

GDP	gross domestic product
GEO	geostationary Earth orbit
GMCNF	generalized multi-commodity network flow
GPS	Global Positioning System
GSC	Guiana Space Center
GTO	geostationary transfer orbit
GUI	graphical user interface
HFO	heavy fuel oil
HMP	Haughton-Mars Project
HTV	H-II Transfer Vehicle
ILP	integer linear programming
IMLEO	initial mass in LEO
IP	integer programming
ISRU	in-situ resource utilization
ISS	International Space Station
JIT	just-in-time
JPL	Jet Propulsion Laboratory
JSC	Johnson Space Center
KACST	King Abdulaziz City for Science and Technology
KPI	key performance indicator
KSA	Kingdom of Saudi Arabia
KSC	Kennedy Space Center
LEO	low-Earth orbit
LH_2	liquid hydrogen
LLO	low lunar orbit
LMO	low Mars orbit
LOX	liquid oxygen
LP	linear programming
LSP	lunar south pole
MCNF	multi-commodity network flow
MED	multi-effect distillation
MILP	mixed integer linear programming

MINLP	mixed integer nonlinear programming
MIT	Massachusetts Institute of Technology
MOE	measure of effectiveness
MSF	multi-stage flash distillation
MSL	Mars Science Laboratory
MTH	Mars transit habitat
NASA	National Aeronautics and Space Administration
NATO	North Atlantic Treaty Organization
NEO	near-Earth object
NLP	nonlinear programming
NP	non-deterministic polynomial-time
NTR	nuclear thermal rocket
OPEX	operational expenditure
OTV	orbital transfer vehicle
PAC	Pacific Ocean splashdown
PHOB	Phobos
PTO	Phobos transfer orbit
RFID	radio frequency identification
RHS	right-hand side
RLL	reusable lunar lander
RO	reverse osmosis
SCM	supply chain management
SD	system dynamics
SEP	solar electric propulsion
SHAB	surface habitat
SIPS	Sustainable Infrastructure Planning System
SLTC	Space Logistics Technical Committee
SoS	system-of-systems
SR	Saudi riyal
SWCC	Saline Water Conversion Corporation
SWRO	sea water reverse osmosis
TDN	time-expanded decision network

TOF	time of flight
TSC	Tanegashima Space Center
TSP	Traveling Salesman Problem
ULA	United Launch Alliance
USD	United States dollar
VRP	vehicle routing problem
ZBO	zero boil-off
ZOLP	zero-one linear programming

Symbols

$\boldsymbol{A}$	requirement matrix
$\mathcal{A}$	set of directed edges
$\boldsymbol{B}$	transformation matrix
$\boldsymbol{C}$	concurrency matrix
D	pipe diameter
E_p	pumping energy
$\mathcal{G}$	directed network graph
H	hydraulic head
H_f	friction head loss
H_p	pumping head
I_sp	specific impulse
$\mathcal{J}$	objective function
$\mathcal{K}$	set of commodities
L	length of pipeline/powerline
$\mathcal{M}$	"sufficiently large" number for big-$\mathcal{B}$ method
N	dimension of LP problem
$\mathcal{N}$	set of nodes
P	electricity required for processing unit feed water
b	net supply/demand
$\boldsymbol{b}$	net supply/demand vector

c	cost per unit flow
c	consumables consumption per crew member per unit time
$\boldsymbol{c}$	unit cost vector
$\boldsymbol{c}^x$	vector of cost involved with operation
$\boldsymbol{c}^y$	vector of cost involved with capacity expansion
$\boldsymbol{c}^z$	vector of fixed cost
f	Darcy-Weisbach friction coefficient
f_{inert}	inert mass fraction
g_0	standard gravity ($= 9.80665$ m/s^2)
i	node index ($\in \mathcal{N}$)
i	variable index
j	node index ($\in \mathcal{N}$)
(i, j)	edge from node i to node j ($\in \mathcal{A}$)
k	commodity index ($\in \mathcal{K}$)
k	number of types of commodities
l	edge lower bound
l	number of concurrency constraints on each edge
m	number of directed edges
m	mass
m_{as}	aeroshell mass
m_{crew}	crew mass
m_{dr}	dry mass
m_{p}	mass of water pumped
m_{pr}	propellant mass
m_{sc}	spacecraft mass
m_{st}	structure mass
m_{vehicle}	vehicle mass
n	number of nodes
n_x	number of variables
n_{eq}	number of equality constraints
n_{ineq}	number of inequality constraints
p	commodity index ($\in \mathcal{K}$)

q	commodity index ($\in \mathcal{K}$)
r	concurrency constraint index
r	noninteger value
r_{bo}	boil-off rate
r_{e}	electricity loss per unit distance of powerline
r_{w}	water loss per unit distance of pipeline
$s_{\mathrm{CO_2}}$	rescaling factor for CO_2 emission
s_{cost}	rescaling factor for total cost (CAPEX + OPEX)
u	edge capacity
$\boldsymbol{u}$	edge capacity vector
v	flow velocity of water pipe
w	waste generation per crew member per unit time
x	flow variable
$\boldsymbol{x}$	flow variable vector
$\boldsymbol{y}$	capacity expansion variable vector
$\boldsymbol{z}$	decision binary variable vector
Δh	elevation difference
Δm	change in mass
Δt	duration of edge
ΔV	change in velocity
α	proportional constant for ISRU maintenance mass
β	proportional constant for ISRU resource production
γ	minimum vehicle mass per crew member
η	ratio of structure mass to propellant mass
θ	aeroshell mass fraction
μ	multiplier for generalized network flow
μ	mixture ratio of oxidizer to fuel
ϕ	propellant mass fraction

Superscripts and Subscripts

$(\cdot)^{+}$	outflow from tail node
$(\cdot)^{-}$	inflow into head node
$(\cdot)^{\pm}$	both outflow and inflow
$(\cdot)^{\mathrm{T}}$	transpose
$(\cdot)^{k}$	commodity k
$(\cdot)_{i}$	node i
$(\cdot)_{j}$	node j
$(\cdot)_{ii}$	graph-loop associated with node i
$(\cdot)_{ij}$	edge (i, j)
$(\cdot)_{pq}$	(p, q) entry of a matrix
$(\cdot)_{\mathrm{eq}}$	equality constraint
$(\cdot)_{\mathrm{ineq}}$	inequality constraint

Chapter 1

Introduction

The final touchdown of the Space Shuttle Atlantis on July 21, 2011, marked the end of NASA's Space Shuttle Program after 30 years of operation and 135 space missions. At the same time, however, it was the dawn of a new era of human space exploration. The time has come to refocus our eyes on the outer world beyond geospace. The next destinations could be the Moon, near-Earth objects (NEOs), Lagrangian points, the moons of Mars, and ultimately Mars. The Red Planet has been a long-held goal of human spaceflight ever since NASA's two Viking probes landed there in 1976. It is still fresh in our minds that JPL's Mars Science Laboratory (MSL) successfully landed Curiosity, a Mars rover, in Gale Crater in August 2012. Investigating Mars' habitability, MSL is hoped to be a positive precursor to human exploration of Mars.

As shown in Figure 1-1, past human space exploration programs have followed different types of logistics paradigms. Under the Apollo program, six missions were sent to the lunar surface between 1969 and 1972. Each mission was self-contained; in other words, no space logistics network existed to support each mission. All the supplies were carried along with the astronauts to their destinations.

For the International Space Station (ISS) program, on the other hand, a "carry-along" strategy is impractical because of the long duration of the mission. Instead, the ISS logistics strategy is based on regular resupply flights by various vehicles such as the Space Shuttle, Russian Progress and Soyuz, European ATV, and Japanese HTV (also known as Kounotori). This type of strategy is appropriate for long-term missions located relatively close to a resupply source, which is the same strategy used by people replenishing their pantries from

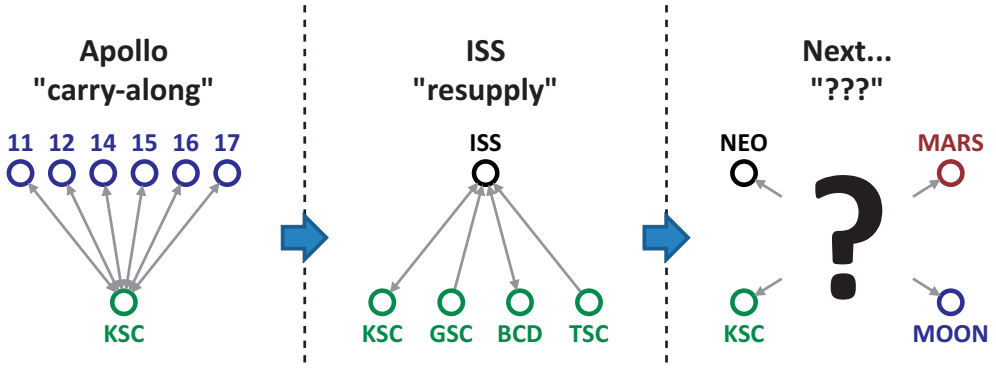

Figure 1-1: Space logistics paradigms

the nearby grocery store once a week.

Then the question is, assuming we are ultimately going to Mars, what the next logistics paradigm should be. Compared to most human activities in our daily lives, the biggest challenge in Mars exploration is its enormous scale in space and time, which may lead to most of the downstream technical challenges. Round-trip missions to Mars (380 million kilometers away) will take years while even the farthest ever reach of mankind, the Apollo missions to the Moon (380 thousand kilometers away), only took weeks. Although they utilize common technologies in many aspects, we need to explore and develop the most optimal and robust strategy to achieve this long-term grand project successfully well within a reasonable budget. One possible key to success comes from following a "travel light and live off the land" strategy that has well-served terrestrial explorers for centuries [1, 2].

1.1 Background

Announced in January 2004, the Vision for Space Exploration was to seek to implement a sustained and affordable human and robotic program to extend human presence across the solar system, starting with a human return to the Moon in preparation for human exploration of Mars [3]. This vision encouraged engineers to define and refine the top-level requirements and configurations for crew and cargo launch systems and to develop an exploration architecture concept to support sustained human and robotic Mars exploration programs.

Under increasing pressure to reconcile the budget for the Constellation Program, the Obama administration requested an independent review of NASA's Human Spaceflight pro-

gram in May 2009. NASA established a blue-ribbon panel, chaired by Norman Augustine, to perform the review over the summer of 2009. The final report of the "Augustine Committee", released in October 2009, states that "a human landing followed by an extended human presence on Mars stands prominently above all other opportunities for exploration. Mars is unquestionably the most scientifically interesting destination in the inner solar system, with a planetary history much like Earth's" [4]. The Committee proposed three classes of options for exploration beyond low-Earth orbit (LEO): a "Mars First" option with a Mars landing perhaps after a brief test of equipment and procedures on the Moon, a "Moon First" option with lunar surface exploration focused on developing the capability to explore Mars, and a "Flexible Path" option first focusing on non-lunar missions, such as NEOs, Lagrangian points, and the moons of Mars, followed by exploration of the lunar surface and/or Martian surface.

Influenced by the findings of the Augustine Committee, the Obama administration released the 2011 fiscal year budget in February 2010, which included no funding for the Constellation Program [5]. Constellation was "over budget, behind schedule, and lacking in innovation" in the Obama administration's stance. Thus Constellation was canceled while NASA's budget was to increase by 6.0 billion USD over five years to extend funding for the ISS through 2020 and support commercial space transportation while NASA develops new technology for future space exploration missions. For the ISS logistics, NASA has awarded contracts under the programs called Commercial Orbital Transportation Services (COTS) and Commercial Resupply Services (CRS) to private companies such as SpaceX and Orbital Sciences for cargo delivery to the ISS through at least 2015, during which the United Stated will not have its own access to the ISS. In his space policy speech at Kennedy Space Center in April 2010, President Obama discussed the future of US effort in human spaceflight and implied a plan for NASA that follows the Augustine Committee's "Flexible Path to Mars" option [6].

Although the Constellation Program has faced cancellation, NASA's new direction for human spaceflight reaffirms that Mars is the ultimate goal of human exploration of the inner solar system [6, 7]. In response to this background, we can expect to see an increasing number of robotic explorations of Mars over the next several decades, followed by human missions. Eventually we envision colonies of humans and robots jointly exploring the Red Planet in a collaborative fashion.

Adding to the technical challenges of Mars exploration, logistical concerns should be considered far in advance. Far away from home with limited capability to manufacture the basic resources to sustain life, astronauts are constantly at risk of logistical lapses. A well-planned logistics strategy is essential to balance risks, ensure robustness, and achieve maximum exploration capability [8].

The importance of a well-planned logistics strategy is not limited to Mars exploration. Over the next 50 years, mission architectures are expected to transition from single, independent sorties to tightly-integrated campaigns spanning many years and involving several stakeholder organizations. As a system-of-systems, a space exploration campaign will require sophisticated logistics and supply chain planning to maintain human presence in remote, hostile environments [9]. For this reason, space logistics is an important concept for future space exploration.

1.2 Space Logistics

Reorganized in January 2004, the Space Logistics Technical Committee (SLTC) of the American Institute of Aeronautics and Astronautics (AIAA) defined space logistics as:
The theory and practice of driving space system design for operability and managing the flow of material, services, and information needed throughout the system lifecycle [10].
Another definition by the committee reads:
The science of planning and carrying out the movement of humans and material to, from and within space combined with the ability to maintain human and robotics operations within space.

As such, space logistics addresses the aspects of space operations both on Earth and in space that deal with material, people, facilities, and services.

A vast body of research exists for terrestrial transportation networks and supply chain logistics in business and military applications. For example, Simchi-Levi et al. used transportation network modeling to solve a school bus routing problem, in which the primary constraints focused on the timing restrictions inherent in school bus pickups and dropoffs [11]. Using transportation networks, they were able to find an optimal allocation of vehicles to routes and schedules. However, space exploration introduces several fundamental differences. First, unlike transports on Earth, space resupply missions are possible only at

discrete intervals corresponding to favorable positions of planetary bodies and accommodating lead times required for spacecraft manufacturing, assembly, and ground operations. For example, a typical interval of Mars mission opportunities is more than 2 years, which derives from the synodic period of Mars. Second, transports in space can last significantly longer (for weeks to months) compared to terrestrial transports which tend to take no more than hours to days with the exception of ocean freight. A typical duration of Mars transfer is 6 months or so. Finally, the fraction of usable cargo mass in spaceflight is significantly less than that of terrestrial transports. While a semi-trailer gross weight may be nearly 50% cargo and a passenger aircraft about 10%, usable cargo mass fractions for launch vehicles to LEO including to the ISS range between 0.5% to 1.5% and the Apollo lunar landings contribute a mere 0.05%.

The challenges of space logistics - infrequent launch windows, long transport durations, and minimal cargo capacity - emphasize the importance of Mars transfer trajectory design and analysis. Planning future missions requires advance trajectory data such as departure and arrival dates (time of flight) and ΔV. Considering interplanetary missions from the perspective of not individual missions but a long-term spaceflight campaign consisting of highly-coupled missions, future mission designers should have more exhaustive trajectory data by which they can perform a trade study between ΔV and time of flight within each launch window and even between neighboring launch windows [12,13]. Since the flexibility of transportation schedule in mission planning is important, it would be preferable for launch windows to be as wide as possible and we need effort to expand them by designing better transfer trajectories and propulsion systems [14].

In summary, to safely explore distant locations in space must respond to a wide range of unexpected events far enough in advance to accommodate launch window opportunities and the long-duration transports while working with severely limited mass capacities. These opposing constraints may require advanced strategies such as completely closed-loop environmental control and life support systems (ECLSS), in-situ resource utilization (ISRU) and manufacturing or repair capabilities, highly efficient packing and container design, significant part commonality between systems, and orbital supply depots.

1.3 Literature Review

Space logistics is an emerging topic in recent years as we start to see space exploration not as a set of isolated missions but as an intricately-linked exploration campaign. A great deal of scientific principles and techniques have been developed since World-War-II to improve the effectiveness and efficiency of terrestrial supply chains in the private and military sectors. However, the potential benefits of this body of knowledge were only poorly understood in the context of space exploration. Sustainable space exploration is impossible without appropriate supply chain management (SCM). Unlike the Apollo program where everything was carried along and individual missions were independent, future space exploration will have to rely on a complex supply chain network. In coordination with NASA's Constellation Program lunar architectural studies in 2004-2005, Massachusetts Institute of Technology (MIT) founded its Space Logistics Project to build a research base supporting interplanetary supply chain management and logistical analysis necessary for extended exploration campaigns.

1.3.1 Terrestrial Analogs and Classes of Supply

The project initially studied several terrestrial analogs to space exploration, investigating and contrasting lessons learned from SCM in (1) major industries specialized in "low-quantity", capital-intensive products, (2) long-range military operations such as aircraft and naval-submarine logistics, and (3) supply chains for operations in remote environments, specifically the NASA Haughton-Mars Project (HMP), which is the functional equivalent of a Mars Exploration base in the high Arctic (75°N). For six weeks during the summer of 2005, a group of researchers from MIT participated in the HMP expedition with an objective of investigating inventory, network modeling, radio frequency identification (RFID), and extra-vehicular activities (EVA) logistics [15].

One of the major challenges in human space exploration is asset management. For this project, a set of ten classes of supply (COS) in Figure 1-2 was formulated, representing a high level grouping of the primary objects used in the exploration system [16]. Each of the ten classes has several sub-classes which further refine the categorization of the supply items. This functional classification, validated by mapping the COS against the taxonomy used by NATO, the US Military, and the ISS (CCART) and also via the HMP expedition,

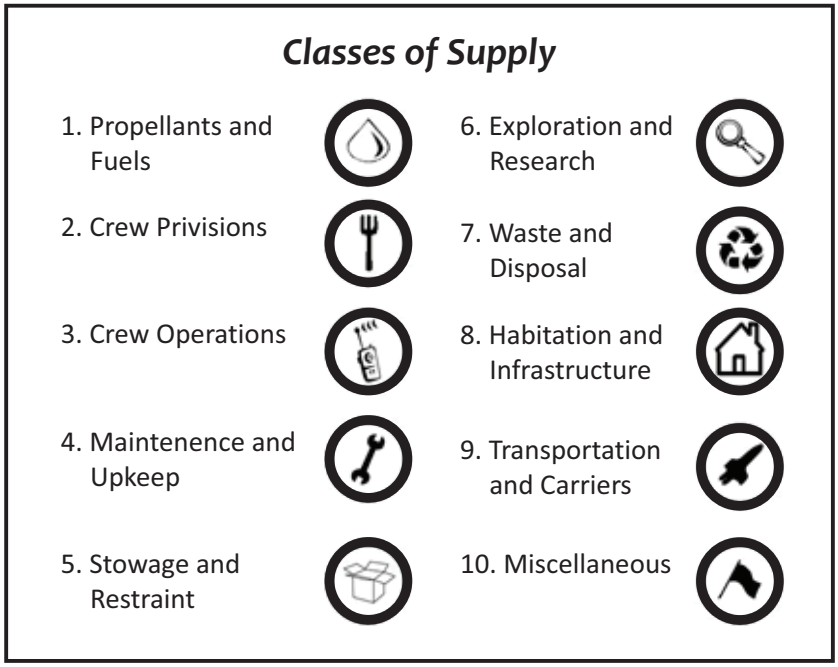

Figure 1-2: Functional classes of supply for space exploration

provides a robust multi-level supply class hierarchy that allow great flexibility when dealing with supply classes at different levels of granularity.

1.3.2 Modeling Framework for Space Logistics

In parallel with the aforementioned terrestrial analog studies, mathematical modeling and analysis of interplanetary supply chain have been carried out at the MIT Strategic Engineering Research Group, led by de Weck, to demonstrate a methodology for designing and evaluating the operational planning for spaceflight campaign. A primary question for space exploration mission design is how to best design the logistics required for a sustainable space transportation system that will enable continual exploration. Inherent to the problem of transporting astronauts to the Moon, NEOs, Mars, and beyond is sustaining the crew and the operations while in transit and at the respective destinations. Especially for long-term missions, the amount of consumables required becomes a significant issue in terms of initial mass in LEO (IMLEO), which translates to mission cost. The goal of the interplanetary supply chain logistics problem is to adequately account for and optimize the transfer of supplies from Earth to locations in space. In order to develop a sustainable architecture, we need to recognize the interdependencies between missions and how this coupling could

affect the logistics planning.

Against this background, Taylor et al. explored the requirements necessary to define the interplanetary logistics problem and extended a modeling tool traditionally utilized in terrestrial logistics to incorporate the astrodynamic relationships of space travel [17–19]. The problem fundamentally consists of three basic building blocks: the commodities or supplies that must be shipped to satisfy a mission demand, the elements or physical structures that are used to both hold and move the commodities, and the network or pathways that the elements and commodities travel on. The physical network, or static network, represents the set of physical locations, or nodes, and the connections, or edges, between them. However, the goal is the design of a sequence of missions that evolve over an extended period of time. In addition, certain properties of the space network are time-varying. For these reasons, they introduced time-expanded networks as a modeling tool. In the time-expanded network, a copy of each static node is made for each of the discretized time points. They mathematically defined these three building blocks and performed a heuristic optimization in the case study of a lunar outpost scenario. Silver et al. used the concept of time-expanded decision networks (TDN) to design and analyze flexibility in large-scale complex systems [20].

Gralla et al. further refined the definitions of the three building blocks [21, 22]. For example, elements are characterized by a wide set of characteristics: they can hold other supply items, be propulsive or non-propulsive, carry crew or not carry crew, be launched from Earth, be reused, refueled, disposed of (staged), pre-deployed, and be "docked" with other elements to form a (temporary) stack. They described a modeling framework that enables visualization, simulation, optimization, and evaluation of various types of logistics strategies using the metrics (termed measures of effectiveness or MOEs). The MOEs provide a quantitative way to evaluate specific space exploration scenarios and interplanetary supply chains in general [23]. The framework was embodied in SpaceNet, a discrete event simulation and optimization software program, which is described later in the next section.

Siddiqi et al. proposed a matrix-based modeling approach for analyzing spaceflight campaign logistics [24, 25]. A campaign is considered to be a series of coordinated flights delivering cargo at a location or node. The goal is to understand and then quantify how to optimally deliver what to a particular location and when, given future demand and consumption. In other words, it is important to understand how a mix of prepositioning,

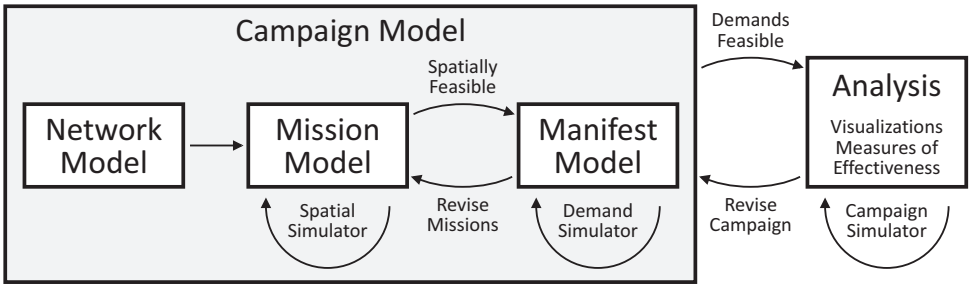

Figure 1-3: SpaceNet campaign modeling and analysis sequence

carry-along, and resupply manifesting strategies can be optimized to ultimately maximize exploration. With this goal, they formulated a matrix representation of the cargo carried by flights for consumption in different time periods (or missions), defining a logistics strategy index for identifying important flights from a cargo-delivery perspective and assessing impact of flight cancellations, failures, and delays. The method was demonstrated on a lunar outpost establishment and was also applied in modeling the logistics of the ISS. Grogan et al. further expanded this method to model and determine optimal manifests for multi-transport, multi-node space exploration systems [26–28].

1.3.3 SpaceNet

SpaceNet is a software implementing the established space logistics framework within a discrete event simulation environment to support campaign analyses and trade studies [8, 9, 29]. SpaceNet models space exploration from a supply chain and logistics perspective, and has been under continuous development over the past seven years. Demands originate from crew members requiring food, water, gases, and hygiene items, infrastructure elements requiring spares or replacement parts, and vehicles requiring propellant required to complete transports. For feasible campaigns (those in which all demands can be satisfied), sensitivity and trade studies evaluate system responses to change and inform design decisions.

SpaceNet 1.3 was released to the public in 2007 as a MATLAB® application and graphical user interface (GUI) supported by an Excel database [30–32]. SpaceNet 1.4 included additional development to improve the ability to analyze long-duration lunar surface campaigns [33]. In 2008, there was an effort to migrate SpaceNet from MATLAB® to a cross-platform, web-accessible implementation. SpaceNet 2.0 served as an internal Java Web Start prototype that utilized modular aspects of object-oriented programming to provide a

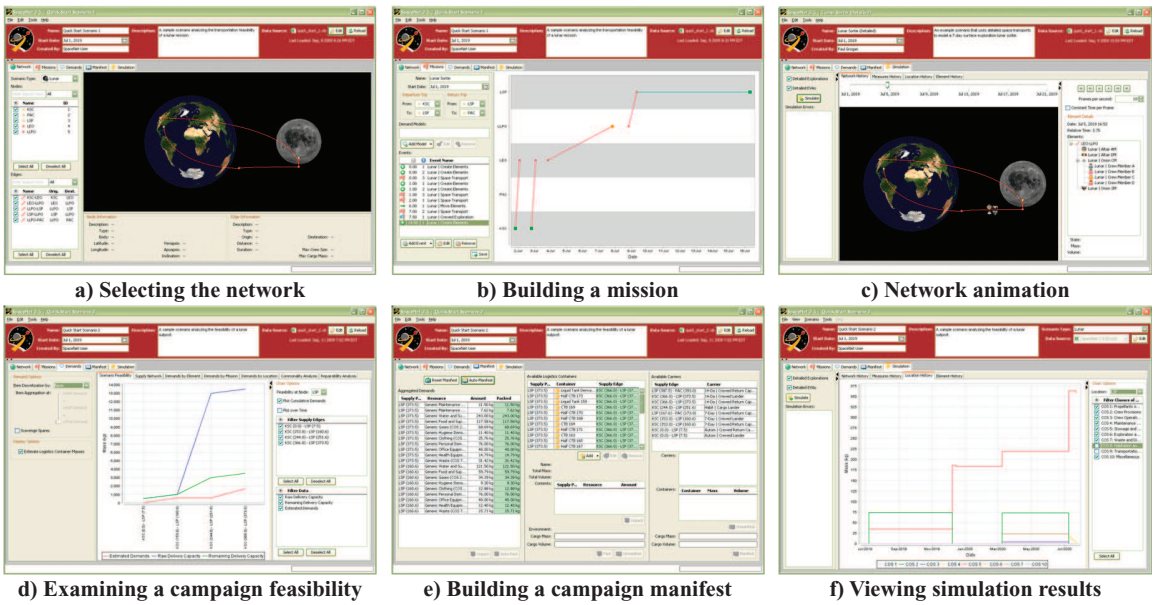

Figure 1-4: SpaceNet screenshots

platform for future extension and development. This version implemented the algorithms to optimize the mission cargo allocations [34]. SpaceNet 2.5 was released to the public in 2009 as a Java executable program, implementing a revised and expanded model for flexible space exploration analysis [35, 36] The most recent version is SpaceNet 2.5r2, released in 2010.

Modeling and analyzing space exploration within SpaceNet is comprised of four steps, as illustrated in Figure 1-3. First, a time-expanded network model is constructed which encompasses all of the surface and orbital locations (nodes) to be reached and the available paths between nodes (edges) over time. Physics-based network constraints including selected trajectories' ΔV requirements are included in the network model inputs. Second, a baseline mission sequence is defined. Each mission model is comprised of events such as element initialization, transportation segments, and exploration processes which drive a discrete event simulation. Propulsive feasibility, i.e., verifying sufficient fuel is available to complete all propulsive transportation burns, is established during the mission definition phase. Third, a demands analysis is performed to inspect the generation of demands by various elements throughout the simulation. The demanded resources are sequentially packed into logistics containers and manifested onto various transports for consumption. During manifesting, logistical feasibility is established if the defined transports have suffi-

cient capacity for all demanded resources - revision of the baseline scenario may be required to close the logistics loop. Finally, the full campaign is simulated to quantify measures of effectiveness and build final visualizations. The screenshots are shown in Figure 1-4.

Yue et al. used SpaceNet to analyze four application cases: ISS resupply campaign, lunar outpost campaign, NEO sortie, and Mars exploration campaign [37, 38].

1.4 Graph-Theoretic Modeling Approach to Space Logistics

As described in Section 1.3, the past studies on space logistics have been mainly focused on a "vehicle" perspective such as propulsive feasibility, cargo capacity constraints, and manifesting strategies. When evaluating these performances, we have to define a logistics network first. In these previous works, however, a logistics network seems to have been arbitrarily determined or has to be predetermined by the user without a strong rationale behind the network selection [19, 35]. It is obvious that there is more than one way to define a logistics network between origin and destination. Then a research question is raised on how we select an optimal logistics network. We can readily imagine that ISRU on the surface nodes and resource depots in orbital nodes or Lagrangian nodes will add complexity to network selection problem. Therefore, the objective of this thesis is to develop a comprehensive graph-theoretic modeling framework to quantitatively evaluate and optimize space exploration logistics from a network perspective. Once the framework for optimization of network selection has been established, it can be implemented as a front end to SpaceNet for logistics network auto-generation.

Figure 1-5 shows an example of Earth-Moon-Mars logistics network. Surface nodes include Kennedy Space Center (KSC) and Pacific Ocean splashdown (PAC), lunar south pole (LSP), Phobos (PHOB), Deimos (DEIM), and Gale Crater (GC) on Mars, where JPL's Curiosity landed recently, while orbital nodes include low-Earth orbit (LEO), geostationary orbit (GEO) and its transfer orbit (GTO), low lunar orbit (LLO), Earth-Moon Lagrange points (EML), Phobos/Deimos transfer orbits (PTO/DTO), and low Mars orbit (LMO). Edges between those nodes represent possible movements or transports between two locations. Therefore, no direct edge between two nodes means that a direct transport between the two nodes are not allowed. For instance, we must go through LLO to reach the lunar surface.

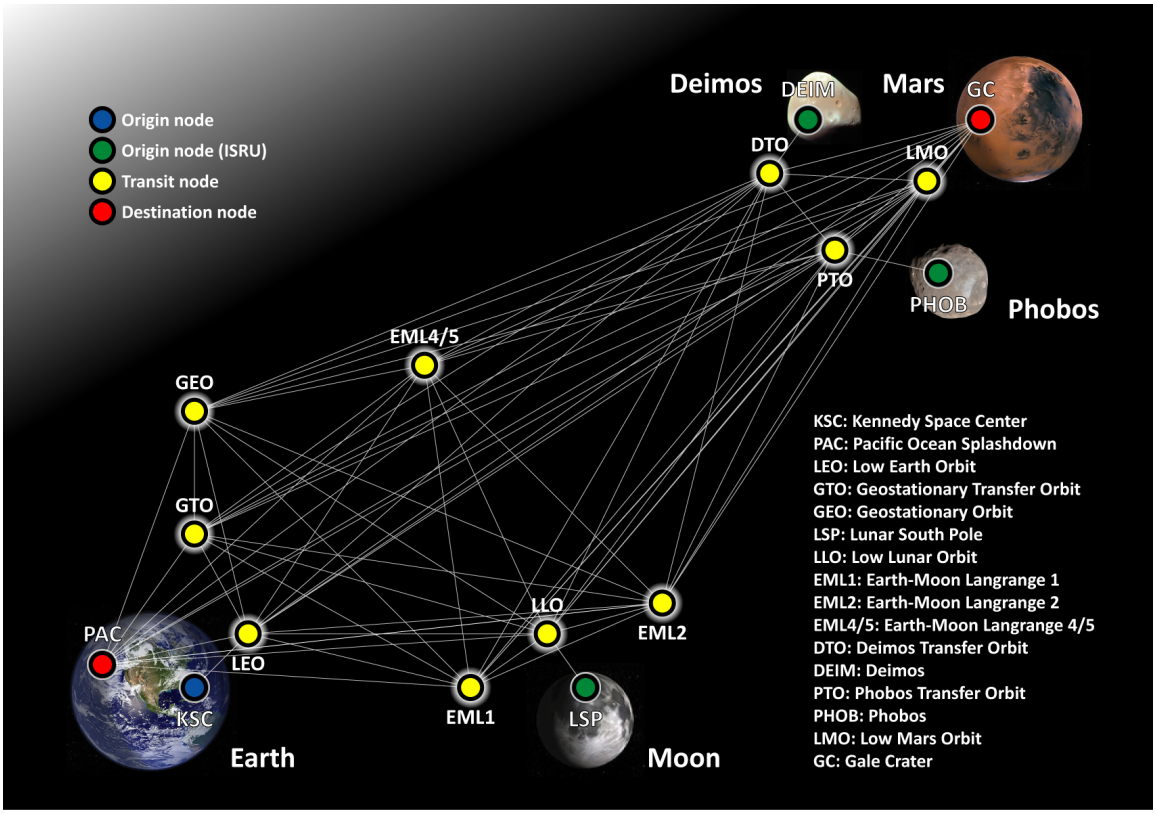

Figure 1-5: Example of Earth-Moon-Mars logistics network

One of the goals of this study is, given a mission objective, to find the best route(s) in the network. In other words, the optimization result should be able to figure out which nodes and edges to use. This result could be translated to "where to deploy what", providing insights on the best transportation architecture and infrastructure concept. Therefore it should be noted that Figure 1-5 just includes all the possibilities and it does not necessarily mean we must have something deployed at each node. For this reason, we can add or remove as many nodes and edges as we can think of.

1.4.1 Resource-Economy in Space

First, "resource-economy" should be defined in the context of space logistics. "Fuel-economy" is a term that is often used in transportation systems on Earth. Fuel-economy is a major portion of "resource-economy" in space logistics as well, but in the case of manned spaceflight, we must also take crew provisions into consideration. As shown in Figure 1-2 in Section 1.3.1, supplies are classified into ten classes. Among these classes, (1) Propellants and Fuels and (2) Crew Provisions have major contributions to resource-economy in space

in terms of mass. Crew provisions mainly consist of water, food, and gases. Unlike on Earth, we cannot get extra food quickly once we fly out to space. Since we can assume a total demand for crew provisions is roughly a linear function of a total mission duration, it definitely contributes to one of the major cargo masses because of the long duration of the mission. For this reason, we use the term "resource-economy" in stead of fuel-economy in this study.

Fuel-economy in space should not be defined in a narrow sense as used in transportation on Earth. It should not be a propulsion system performance of individual vehicles but it should be viewed as a system performance of the overall exploration architecture and logistics network. In addition to a propulsion system performance, a fuel consumption is driven by an exploration architecture and a logistics network in terms of the number of stages and whether there exist ISRU plants and resource depots in some locations or not. Moreover, ΔV required for transfer is highly time-variant in interplanetary exploration such as Mars missions, which means that a fuel consumption is also a function of a mission duration and timing. Resource-economy in space is, therefore, closely coupled with the selection of logistics network, exploration architecture, infrastructure, time and mission duration as well as propulsion system.

1.4.2 Network Graph

A logistics network is represented by the set of physical locations (nodes) and connections (edges) between them. With respect to mass flow, nodes can generally be classified into three types: mass-origin nodes, mass-transit nodes, and mass-destination nodes. A payload is originated or resource is generated at mass-origin nodes. A vehicle stays at mass-transit nodes for a while for rendezvous, transshipment, or refueling. A payload is deployed at mass-destination nodes. Mathematically these three types of nodes can be unified by defining a supply/demand b for each node. A positive value of b represents a positive supply while a negative value of b a negative supply, that is, a positive demand. Hence, if b is positive, it is a mass-origin node; if b is negative, it is a mass-destination node; and if b is equal to zero, it is neither provides nor requires so that only a mass-transit occurs at this node.

Edges represent movements or transports between two locations and are associated with "costs" in general. In space transportation, one major cost is a propulsive burn. In a transport from node i and node j, for instance, the relationship between total masses at

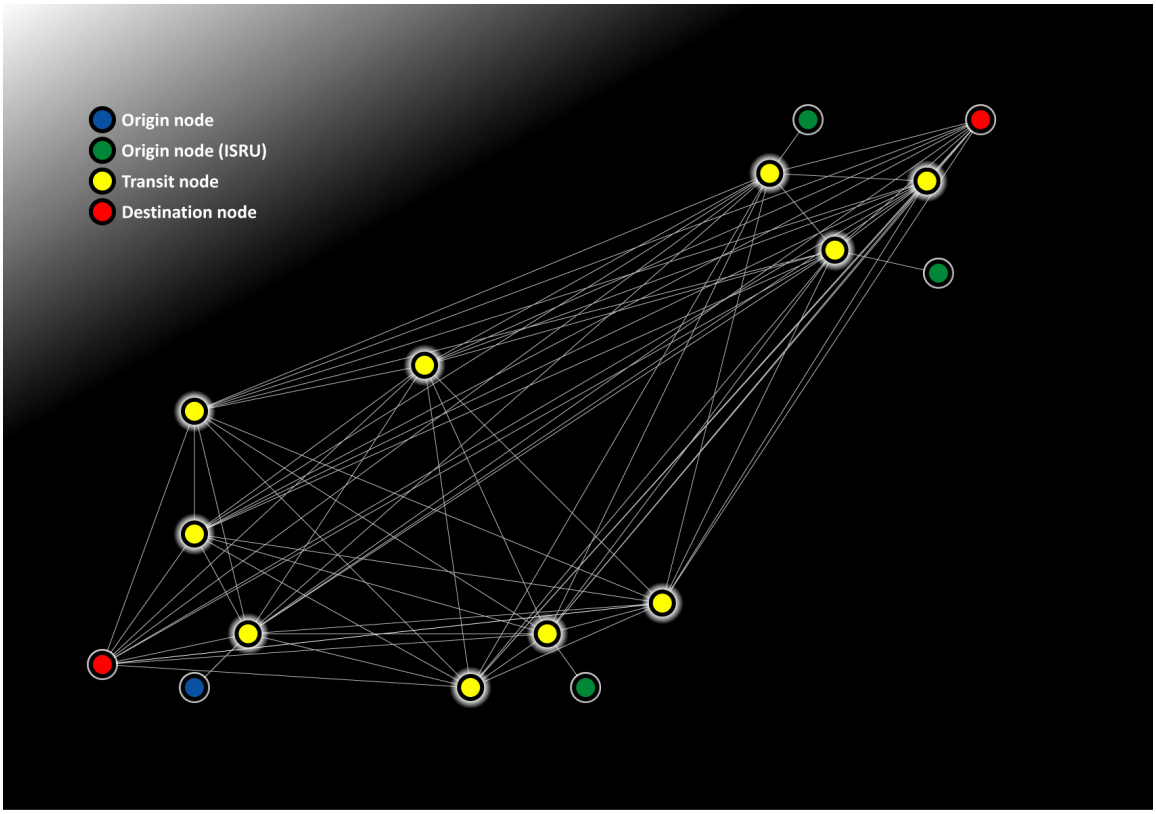

Figure 1-6: Notional network graph extracted from Figure 1-5

nodes i and j is represented by the rocket equation:

$$m_j = m_i \exp\left(-\frac{\Delta V_{ij}}{I_{\mathrm{sp}} g_0}\right) \tag{1.1}$$

where ΔV_{ij} represents ΔV required for transfer from node i to node j and $I_{\mathrm{sp}} g_0$ represents the effective exhaust velocity. The cost for this burn is the amount of propellant consumed and expressed as a mass reduction:

$$\Delta m_{ij} = m_i - m_j = m_i \left[1 - \exp\left(-\frac{\Delta V_{ij}}{I_{\mathrm{sp}} g_0}\right)\right] \tag{1.2}$$

Other possible major costs associated with space transports include crew provisions consumption and propellant boil-off.

Then the question is how to translate this to a mathematical problem. Figure 1-6 shows a notional network graph, which extracts only the relationship between nodes and edges from a logistics network in Figure 1-5. By extracting only mathematically meaningful components, we can formulate a purely mathematical problem. Chapter 2 discusses how to associate each

(a) ISRU plant (image courtesy of NASA JSC)

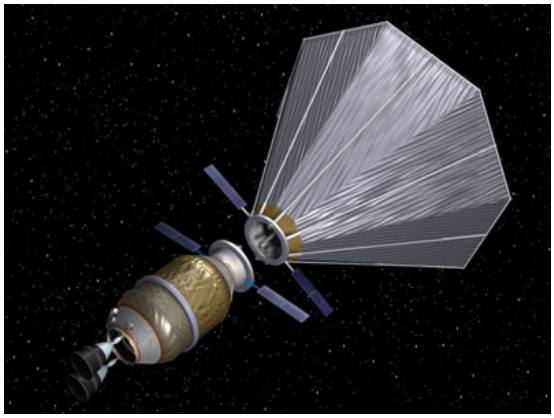

(b) Space fuel depot (image courtesy of ULA)

Figure 1-7: Sample images of ISRU plant and space fuel depot

node and edge with their own properties mentioned above and formulate a network flow problem. Chapter 3 describes how to solve the network flow problem computationally.

1.4.3 ISRU and Resource Depots

One of the goals of this research is to evaluate the potential benefits of ISRU from a long-term perspective. According to NASA, "*in-situ resource utilization will enable the affordable establishment of extraterrestrial exploration and operations by minimizing the materials carried from Earth and by developing advanced, autonomous devices to optimize the benefits of available in-situ resources*" [39]. Various ISRU systems have been proposed so far such as: hydrogen reduction, methane carbothermal reduction, molten electrolysis (electrowinning), volatile extraction, and polar water extraction on the lunar surface, and Sabatier reaction, reverse water gas shift reaction, and atmosphere electrolysis on the Martian surface [40–48]. The two moons of Mars, Phobos and Deimos, the dwarf planet, Ceres, and near-Earth asteroids could also be sources of raw materials for ISRU [49, 50]. As such, ISRU or the ability to produce water, gases, and propellants somewhere halfway to the destination, along with resource depots or the ability to store them, is expected to be one of the most important key concepts in resource-economy in space. Sample images of ISRU plant and space fuel depot are shown in Figure 1-7. In the graph-theoretic analysis, ISRU capability can be modeled as a mass-origin node where a production rate translates to a mass generation rate while storage capability of resource depots can be modeled as a mass-transit node.

The graph-theoretic approach for space logistics essentially models the movement of

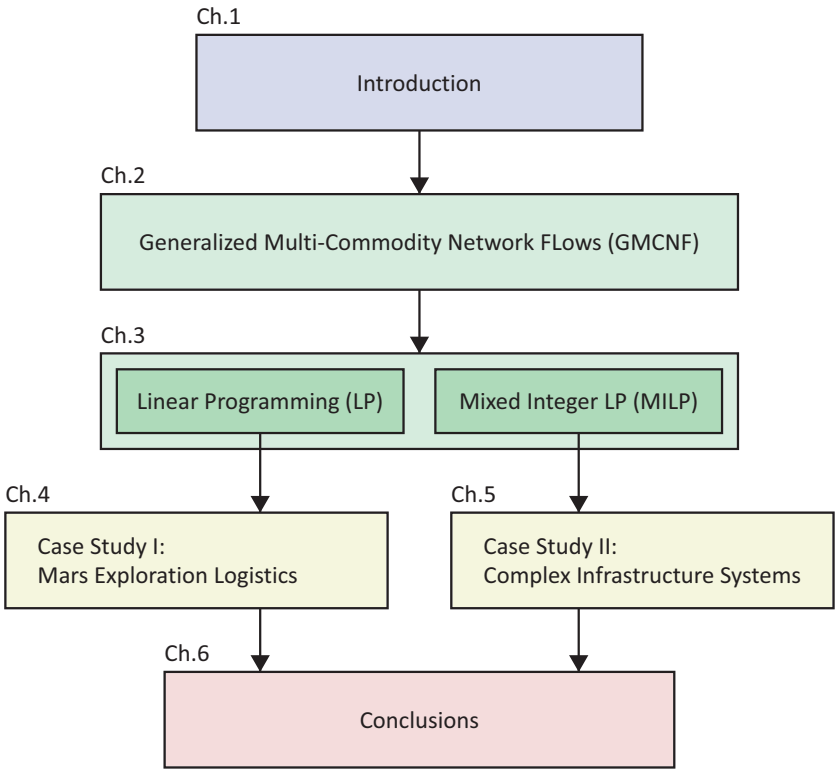

Figure 1-8: Thesis roadmap

cargo in a flow network. ISRU allows resources to be available in locations other than Earth surface. Therefore we need to deal separately with materials that are only available on Earth (e.g., science payload) and resources that are also available in other locations. For this reason, the problem is formulated as a multi-commodity network flow problem, which is described in detail in Chapter 2.

1.5 Thesis Overview

The objective of this thesis is to develop a comprehensive graph-theoretic modeling framework to quantitatively evaluate and optimize space exploration logistics from a network perspective. A thesis roadmap is shown in Figure 1-8. Chapter 2 presents a mathematical formulation of generalized multi-commodity network flows and a couple of mathematical concepts in graph theory that help formulating the problem to be addressed in this study. In Chapter 3, network flow optimization problems formulated as a Linear Programming (LP) problem and a Mixed Integer LP (MILP) problem are described, followed by the optimization structure used in this study. Chapter 4 presents a case study for space exploration

logistics as an LP application while Chapter 5 is dedicated to a case study for terrestrial complex infrastructure systems as a MILP application. Chapter 6 reviews the key ideas and contributions presented in this dissertation, discusses the potential benefits as well as limitations of the methodology, and concludes with suggestions for future work in this research area.

Chapter 2

Generalized Multi-Commodity Network Flows

As discussed earlier in Section 1.4, this thesis formulates a multi-commodity network flow problem. This chapter first reviews fundamentals of network flows and classical generalized flows and multi-commodity flows. Subsequently a new formulation for generalized multi-commodity network flows and its examples are presented. A couple of mathematical concepts in graph theory that help formulating the problem to be addressed in this study are also introduced such as "multi-graph" and "graph-loop".

2.1 Fundamentals of Network Flows

Before stepping into generalized multi-commodity network flows, the fundamentals of network flows are reviewed based on the textbook by Ahuja, Magnanti, and Orlin [51]. While there are many applications of network flow models, the minimum cost flow model is the most fundamental of all network flow problems. The special versions of the minimum cost flow problem that play a central role in the theory and applications of network flows include:

- Shortest path problem
- Maximum flow problem
- Assignment problem
- Transportation problem
- Circulation problem

Also the generalizations of the minimum cost flow problem include:

- Convex cost flow problem
- Generalized flow problem
- Multi-commodity flow problem

The most fundamental minimum cost flow problem wishes to determine a least cost shipment of a single commodity through a network in order to satisfy demands at certain nodes from available suppliers at other nodes. A mathematical programming formulation of the minimum cost flow problem is presented below.

Let $\mathcal{G} = (\mathcal{N}, \mathcal{A})$ be a directed network defined by a set $\mathcal{N}$ of n nodes and a set $\mathcal{A}$ of m directed edges. Each edge $(i, j) \in \mathcal{A}$ has an associated *cost* c_{ij} that denotes the cost per unit flow on that edge. We assume that the flow cost varies linearly with the amount of flow. We also associate with each edge $(i, j) \in \mathcal{A}$ a *capacity* u_{ij} that denotes the maximum amount that can flow on the edge and a *lower bound* l_{ij} that denotes the minimum amount that must flow on the edge. We associate with each node $i \in \mathcal{N}$ a number b_i representing its supply/demand. If $b_i > 0$, node i is a *supply node*; if $b_i < 0$, node i is a *demand node* with a demand $-b_i$; and if $b_i = 0$, node i is a *transshipment node*. The decision variables in the minimum cost flow problem are edge flows and we represent the flow on an edge $(i, j) \in \mathcal{A}$ by x_{ij}. The relationship between these building blocks is depicted in Figure 2-1. The minimum cost flow problem is an optimization model formulated as follows:
Minimize

$$\mathcal{J} = \sum_{(i,j)\in\mathcal{A}} c_{ij} x_{ij} \tag{2.1}$$

subject to

$$\sum_{j:(i,j)\in\mathcal{A}} x_{ij} - \sum_{j:(j,i)\in\mathcal{A}} x_{ji} = b_i \qquad \forall\ i \in \mathcal{N} \tag{2.2a}$$

$$l_{ij} \le x_{ij} \le u_{ij} \qquad \forall\,(i,j) \in \mathcal{A} \tag{2.2b}$$

where

$$\sum_{i\in\mathcal{N}} b_i = 0 \tag{2.3}$$

We refer to the constraints in Eq. (2.2a) as *mass balance constraints*. The first term in this constraint for a node represents the total *outflow* of the node (i.e., the flow emanating from the node) and the second term represents the total *inflow* of the node (i.e., the flow entering the node). The mass balance constraint states that the outflow minus inflow must

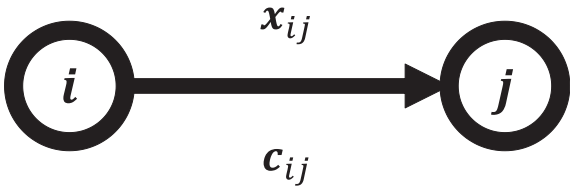

Figure 2-1: Nodes i and j, directed edge (i, j), flow x_{ij}, and unit cost c_{ij}

equal the supply/demand of the node. If the node is a supply node, its outflow exceeds its inflow; if the node is a demand node, its inflow exceeds its outflow; and if the node is a transshipment node, its outflow equals its inflow. The flow must also satisfy the lower bound and capacity constraints in Eq. (2.2b), which we refer to as *flow bound constraints*. The flow bounds typically model physical capacities or restrictions imposed on the flows' operating ranges. In most applications, the lower bounds on edge flows are zero; therefore, if we do not state lower bounds for any problem, we assume that they have value zero.

2.2 Classical Generalized Flows and Multi-Commodity Flows

Having introduced the fundamentals of minimum cost flow problem, this section reviews its two generalizations: generalized flow problems and multi-commodity flow problems.

2.2.1 Generalized Flow Problems

In the minimum cost flow problem described in the previous section, we have made one very fundamental, yet almost invisible, assumption: we conserve flow on every edge, that is, the amount of flow on any edge that leaves its tail node equals the amount of flow that arrives at its head node. This assumption is very reasonable in many application settings. Other practical contexts, however, violate this conservation assumption. In generalized flow problems, edges might "consume" or "generate" flow. Generalized network flow problems arise in several application contexts: for example, (1) power transmission through electric lines, with power lost with distance traveled; (2) flow of water through pipelines or canals that lose water due to seepage or evaporation; (3) transportation of a perishable commodity; and (4) cash management scenarios in which edges represent investment opportunities and multipliers represent appreciation or depreciation of an investment's value.

In a basic generalized network flow model for addressing these situations, we associate a positive multiplier μ_{ij} with every edge (i, j) of the network and assume that if we send

x_{ij} unit from node i to node j along the edge (i,j), then $\mu_{ij}x_{ij}$ units arrive at node j. This model is a generalization of the minimum cost flow problem in the sense that if every multiplier has value 1, the generalized network flow model becomes the minimum cost flow problem. The generalized flow problem is formulated as follows:
Minimize

$$\mathcal{J} = \sum_{(i,j)\in\mathcal{A}} c_{ij}x_{ij} \tag{2.4}$$

subject to

$$\sum_{j:(i,j)\in\mathcal{A}} x_{ij} - \sum_{j:(j,i)\in\mathcal{A}} \mu_{ji}x_{ji} \leq b_i \qquad \forall\, i \in \mathcal{N} \tag{2.5a}$$

$$0 \leq x_{ij} \leq u_{ij} \qquad \forall\, (i,j) \in \mathcal{A} \tag{2.5b}$$

If $0 < \mu_{ij} < 1$, the edge is *lossy*, and if $1 < \mu_{ij} < \infty$, the edge is *gainy*. In this model we assume that the lower bound on every edge flow is zero.

Since the supply does not necessarily have to equate to the demand, Eq. (2.5a) is an inequality constraint instead of equality in Eq. (2.2a). Hence, the supply/demand zero-sum in Eq. (2.3) is not considered hereafter.

2.2.2 Multi-Commodity Flow Problems

Throughout our discussion to this point, we have considered network models composed of a single commodity. In many application contexts, several physical commodities, vehicles, or messages, each governed by their own network flow constraints, share the same network. Examples include (1) the transportation of passengers from different origins to different destinations within a city; (2) the routing of non-homogeneous tankers (non-homogeneous in terms of speed, carrying capability, and operating costs); (3) the worldwide shipment of different varieties of grains to those that consume it; and (4) the transmission of messages in a communication network between different origin-destination pairs. If the commodities do not interact in any way, then to solve problems with several commodities, we would solve each single-commodity problem separately. In other situations, however, because the commodities do share common facilities, the individual single-commodity problems are not independent, so to find an optimal flow, we need to solve the problems in concert with each other. In the multi-commodity flow problem introduced in the textbook by Ahuja, Magnanti, and Orlin, the individual commodities share the common edge capacities, that

is, each edge has a capacity u_{ij} that restricts the total flow of all commodities on that edge [51].

Let x_{ij}^k denote the flow of commodity k (out of a set $\mathcal{K}$) on edge (i,j), and let c_{ij}^k denote the unit cost for commodity k on edge (i,j). Using this notation we can formulate the multi-commodity flow problem as follows:
Minimize

$$\mathcal{J} = \sum_{k \in \mathcal{K}} \sum_{(i,j) \in \mathcal{A}} c_{ij}^k x_{ij}^k \tag{2.6}$$

subject to

$$\sum_{j:(i,j) \in \mathcal{A}} x_{ij}^k - \sum_{j:(j,i) \in \mathcal{A}} x_{ji}^k \leq b_i^k \qquad \forall\ i \in \mathcal{N} \text{ and } \forall\ k \in \mathcal{K} \tag{2.7a}$$

$$\sum_{k \in \mathcal{K}} x_{ij}^k \leq u_{ij} \qquad \forall\, (i,j) \in \mathcal{A} \tag{2.7b}$$

$$0 \leq x_{ij}^k \leq u_{ij}^k \qquad \forall\, (i,j) \in \mathcal{A} \text{ and } \forall\ k \in \mathcal{K} \tag{2.7c}$$

The "bundle" constraints in Eq. (2.7b) tie together the commodities by restricting the total flow of all commodities on each edge (i,j) to at most u_{ij}. Note that we also impose individual flow bounds u_{ij}^k on the flow of commodity k on edge (i,j).

If $\boldsymbol{x}_{ij}$ and $\boldsymbol{c}_{ij}$ are respectively the vector notations of x_{ij}^k and c_{ij}^k with respect to commodity, then the above formulation can be rewritten as:
Minimize

$$\mathcal{J} = \sum_{(i,j) \in \mathcal{A}} {\boldsymbol{c}_{ij}}^{\mathrm{T}} \boldsymbol{x}_{ij} \tag{2.8}$$

subject to

$$\sum_{j:(i,j) \in \mathcal{A}} \boldsymbol{x}_{ij} - \sum_{j:(j,i) \in \mathcal{A}} \boldsymbol{x}_{ji} \leq \boldsymbol{b}_i \qquad \forall\ i \in \mathcal{N} \tag{2.9a}$$

$$\boldsymbol{0} \leq \boldsymbol{x}_{ij} \leq \boldsymbol{u}_{ij} \qquad \forall\, (i,j) \in \mathcal{A} \tag{2.9b}$$

In some applications including the ones described later in Chapter 4 and 5, the individual commodities do not share common edge capacities while they interact in other ways. For this reason, the bundle constraints in Eq. (2.7b) are not imposed hereafter.

2.3 Generalized Multi-Commodity Network Flows (GMCNF)

The previous two sections reviewed the background knowledge of network flows in preparation for introducing the generalized multi-commodity network flow model, which is proposed in this thesis. The generalized multi-commodity network flow problem is literally a mix of the generalized flow problem in Section 2.2.1 and the multi-commodity flow problem in Section 2.2.2. As discussed earlier in Section 1.4, the problem addressed in this thesis encompasses the characteristics of the two flows and therefore should be formulated as a generalized multi-commodity network flow problem because (1) major commodities such as propellant are substantially consumed during transport (generalized flows), and (2) a space exploration mission carries along multiple commodities, which could even have different origin-destination pairs especially when considering ISRU (multi-commodity flows).

2.3.1 Mathematical Formulation

One very important addition in the generalized multi-commodity network flow is the interaction between different commodities. In generalized flow problems, a single commodity could increase or decrease its quantity by passing through an edge. In generalized multi-commodity flow problems, however, we must consider not only a gain or loss of each commodity itself but also a gain or loss of a commodity due to another commodity, and even a transformation between different commodities. For example, the amount of propellant consumed is driven by the total mass (not only the propellant itself), and food is consumed by the crew turning into waste. This can all be mathematically implemented by multiplying a flow vector $\boldsymbol{x}_{ij}$ by a square matrix instead of a scalar μ_{ij} as in Eq. (2.5a). The off-diagonal entries of this matrix should be able to capture the interactions between different commodities.

Before formulating the problem, let us introduce two more additions to generalize the model more completely. When sending out a flow $\boldsymbol{x}_{ij}$ from node i, we might have additional requirements other than $\boldsymbol{x}_{ij}$ itself. For example, when we send out water through pipelines, we also need pumping energy at node i but the pumping energy itself does not flow through the pipeline. The other addition is a flow concurrency constraint. When commodity 1 flows on the edge, a certain amount of commodity 2 might also have to be carried along with commodity 1. For example, in order to perform aerobraking maneuver at Mars arrival, a

Figure 2-2: Outflow $\boldsymbol{x}_{ij}^{+}$, inflow $\boldsymbol{x}_{ij}^{-}$, and unit costs for outflow $\boldsymbol{c}_{ij}^{+}$ and inflow $\boldsymbol{c}_{ij}^{+}$

spacecraft would need an aeroshell whose mass should be around 15% of the total mass being braked.

Figure 2-2 shows the building blocks of the generalized multi-commodity network flows. In order to explicitly incorporate the above three additions (transformation, requirement, and concurrency), we split the flow into two parts: $\boldsymbol{x}_{ij}^{+}$ and $\boldsymbol{x}_{ij}^{-}$, where $\boldsymbol{x}_{ij}^{+}$ represents the outflow from node i and $\boldsymbol{x}_{ij}^{-}$ represents the inflow into node j. $\boldsymbol{c}_{ij}^{+}$ and $\boldsymbol{c}_{ij}^{+}$ denote the unit costs for outflow and inflow, respectively. Using this notation, the generalized multi-commodity network flow can be formulated as follows:
Minimize

$$\mathcal{J} = \sum_{(i,j)\in\mathcal{A}} \left(\boldsymbol{c}_{ij}^{+\mathrm{T}} \boldsymbol{x}_{ij}^{+} + \boldsymbol{c}_{ij}^{-\mathrm{T}} \boldsymbol{x}_{ij}^{-} \right) \tag{2.10}$$

subject to

$$\sum_{j:(i,j)\in\mathcal{A}} \boldsymbol{A}_{ij}^{+} \boldsymbol{x}_{ij}^{+} - \sum_{j:(j,i)\in\mathcal{A}} \boldsymbol{A}_{ji}^{-} \boldsymbol{x}_{ji}^{-} \leq \boldsymbol{b}_i \qquad \forall\, i \in \mathcal{N} \tag{2.11a}$$

$$\boldsymbol{B}_{ij} \boldsymbol{x}_{ij}^{+} = \boldsymbol{x}_{ij}^{-} \qquad \forall\, (i,j) \in \mathcal{A} \tag{2.11b}$$

$$\boldsymbol{C}_{ij}^{+} \boldsymbol{x}_{ij}^{+} \leq \boldsymbol{0} \quad \text{and} \quad \boldsymbol{C}_{ij}^{-} \boldsymbol{x}_{ij}^{-} \leq \boldsymbol{0} \qquad \forall\, (i,j) \in \mathcal{A} \tag{2.11c}$$

$$\boldsymbol{0} \leq \boldsymbol{x}_{ij}^{+} \leq \boldsymbol{u}_{ij}^{+} \quad \text{and} \quad \boldsymbol{0} \leq \boldsymbol{x}_{ij}^{-} \leq \boldsymbol{u}_{ij}^{-} \qquad \forall\, (i,j) \in \mathcal{A} \tag{2.11d}$$

We introduce three matrices: $\boldsymbol{A}_{ij}^{\pm}$, $\boldsymbol{B}_{ij}$, and $\boldsymbol{C}_{ij}^{\pm}$. We call $\boldsymbol{A}_{ij}^{\pm}$ a *requirement matrix*, $\boldsymbol{B}_{ij}$ a *transformation matrix*, and $\boldsymbol{C}_{ij}^{\pm}$ a *concurrency matrix*. As can be seen from the constraints in Eqs. (2.11a) and (2.11b), $\boldsymbol{A}_{ij}^{+} \boldsymbol{x}_{ij}^{+}$ is required at node i to send outflow $\boldsymbol{x}_{ij}^{+}$ into edge (i,j), $\boldsymbol{x}_{ij}^{+}$ is transformed into $\boldsymbol{x}_{ij}^{-} = \boldsymbol{B}_{ij} \boldsymbol{x}_{ij}^{+}$, and $\boldsymbol{A}_{ij}^{-} \boldsymbol{x}_{ij}^{-}$ is received at node j with inflow $\boldsymbol{x}_{ij}^{-}$ from edge (i,j). Also in the concurrency constraints in Eq. (2.11c), the relationship between commodities on each edge (i,j) is self-constrained such that the dot product with $\boldsymbol{C}_{ij}^{\pm}$ is

less than or equal to zero. With this modification, we can treat the flow gain and loss due to the interaction between commodities, transformation between commodities, additional requirements at nodes, and concurrency on edges. If we consider k types of commodities, that is, the decision variable vector includes k components, then the $\boldsymbol{A}_{ij}^{\pm}$ and $\boldsymbol{B}_{ij}$ matrices must be k-by-k square matrices while the $\boldsymbol{C}_{ij}^{\pm}$ matrix is a l-by-k matrix, where l is the number of concurrency constraints on edge (i, j).

$$\boldsymbol{A}_{ij}^{\pm} = \begin{bmatrix} A_{11} & \cdots & A_{1p} & \cdots & A_{1q} & \cdots & A_{1k} \\ \vdots & \ddots & \vdots & \ddots & \vdots & \ddots & \vdots \\ A_{p1} & \cdots & A_{pp} & \cdots & A_{pq} & \cdots & A_{pk} \\ \vdots & \ddots & \vdots & \ddots & \vdots & \ddots & \vdots \\ A_{q1} & \cdots & A_{qp} & \cdots & A_{qq} & \cdots & A_{qk} \\ \vdots & \ddots & \vdots & \ddots & \vdots & \ddots & \vdots \\ A_{k1} & \cdots & A_{kq} & \cdots & A_{1q} & \cdots & A_{kk} \end{bmatrix}_{ij}^{\pm} \tag{2.12a}$$

$$\boldsymbol{B}_{ij} = \begin{bmatrix} B_{11} & \cdots & B_{1p} & \cdots & B_{1q} & \cdots & B_{1k} \\ \vdots & \ddots & \vdots & \ddots & \vdots & \ddots & \vdots \\ B_{p1} & \cdots & B_{pp} & \cdots & B_{pq} & \cdots & B_{pk} \\ \vdots & \ddots & \vdots & \ddots & \vdots & \ddots & \vdots \\ B_{q1} & \cdots & B_{qp} & \cdots & B_{qq} & \cdots & B_{qk} \\ \vdots & \ddots & \vdots & \ddots & \vdots & \ddots & \vdots \\ B_{k1} & \cdots & B_{kq} & \cdots & B_{1q} & \cdots & B_{kk} \end{bmatrix}_{ij} \tag{2.12b}$$

$$\boldsymbol{C}_{ij}^{\pm} = \begin{bmatrix} C_{11} & \cdots & C_{1p} & \cdots & C_{1q} & \cdots & C_{1k} \\ \vdots & \ddots & \vdots & \ddots & \vdots & \ddots & \vdots \\ C_{r1} & \cdots & C_{rp} & \cdots & C_{rq} & \cdots & C_{rk} \\ \vdots & \ddots & \vdots & \ddots & \vdots & \ddots & \vdots \\ C_{l1} & \cdots & C_{lp} & \cdots & C_{lq} & \cdots & C_{lk} \end{bmatrix}_{ij}^{\pm} \tag{2.12c}$$

Note that if $\boldsymbol{A}_{ij}^{\pm}$ and $\boldsymbol{B}_{ij}$ are identity matrices and $\boldsymbol{C}_{ij}^{\pm}$ is a null matrix, the constraints in Eqs. (2.11a)-(2.11d) turn back to the constraints in the classical multi-commodity flow model in Eqs. (2.9a)-(2.9b). Also, if $\boldsymbol{A}_{ij}^{\pm}$ and $\boldsymbol{B}_{ij}$ are diagonal matrices and $\boldsymbol{C}_{ij}^{\pm}$ is a null

matrix, there are no interactions between commodities and therefore the problem can be decoupled into k independent generalized flow problems. To put it the other way around, the off-diagonal entries of $\boldsymbol{A}_{ij}^{\pm}$ and $\boldsymbol{B}_{ij}$ and non-zero entries of $\boldsymbol{C}_{ij}^{\pm}$ indicate that there are interactions between commodities. For example, the (p, q) entry of $\boldsymbol{A}_{ij}^{+}$ means that if we send 1 unit of the qth commodity, we also need $[A_{pq}]_{ij}^{+}$ units of the pth commodity. The (r, p) entry of $\boldsymbol{C}_{ij}^{+}$, which is $[C_{rp}]_{ij}^{+}$, is the pth commodity's contribution to the rth concurrency constraint. In the next three sections, examples of these $\boldsymbol{ABC}$ matrices are presented.

2.3.2 Requirement Matrix $\boldsymbol{A}_{ij}^{\pm}$

The $\boldsymbol{A}_{ij}^{\pm}$ matrix can describe the commodities that are additionally required by sending out or receiving the flow but do not flow on the edge themselves. Examples of this include the electricity consumed for pumping freshwater into the pipeline, the money received from the sales of commercial products, and the workforce required for loading/unloading a freighter at the seaport.

Pumping Energy

Suppose the pumping energy is calculated as the standard gravity g_0 times the total head H_{ij} times the water pumped. If node i sends out water and electricity to edge (i, j), it is required to provide:

$$\boldsymbol{A}_{ij}^{+}\boldsymbol{x}_{ij}^{+} = \begin{bmatrix} 1 & 0 \\ g_0 H & 1 \end{bmatrix}_{ij}^{+} \begin{bmatrix} \text{water} \\ \text{electricity} \end{bmatrix}_{ij}^{+} \tag{2.13}$$

The off-diagonal entry $g_0 H$ means that if we pump 1 unit of water into the pipeline, we need to provide $g_0 H$ units of electricity for pumping aside from the electricity sent out.

Another example is a `"plant"` such as an ISRU plant and a desalination plant. In this study, a generic plant as a resource processing facility is modeled using a `"graph-loop"` instead of a node. As discussed later in Section 2.4, the $\boldsymbol{A}$ matrix also plays a key role in a graph-loop.

2.3.3 Transformation Matrix $\boldsymbol{B}_{ij}$

The $\boldsymbol{B}_{ij}$ matrix can describe the flow gain/loss or transformation between commodities. Unless the $\boldsymbol{B}_{ij}$ matrices are all identity matrices, there is no longer the underlying law of

flow conservation. Two space-related examples are provided below.

Propellant Mass Fraction

The *propellant mass fraction* is the ratio between mass of the propellant used and the initial mass of the vehicle. From the rocket equation, the propellant mass fraction ϕ_{ij} on edge (i, j) is derived as:

$$\phi_{ij} = 1 - \exp\left(-\frac{\Delta V_{ij}}{I_{\text{sp}} g_0}\right) \tag{2.14}$$

where ΔV_{ij} is the change in the vehicle's velocity on edge (i, j), I_{sp} is the specific impulse, and g_0 is the standard gravity. Let m_{dr} and m_{pr} be the dry mass and the initial propellant mass, respectively. If Δm_{pr} is consumed during the propulsive burn, then the propellant mass fraction is given by:

$$\phi \equiv \frac{\Delta m_{\text{pr}}}{m_{\text{dr}}^{+} + m_{\text{pr}}^{+}} \tag{2.15}$$

Therefore, the propellant mass right after the burn is:

$$m_{\text{pr}}^{-} = m_{\text{pr}}^{+} - \Delta m_{\text{pr}} = -\phi m_{\text{dr}}^{+} + (1 - \phi)\, m_{\text{pr}}^{+} \tag{2.16}$$

Since the dry mass does not change during the burn, then Eq. (2.11b) holds, where

$$\boldsymbol{x}_{ij}^{\pm} = \begin{bmatrix} \text{dry mass} \\ \text{propellant} \end{bmatrix}_{ij}^{\pm} \qquad \boldsymbol{B}_{ij} = \begin{bmatrix} 1 & 0 \\ -\phi & 1 - \phi \end{bmatrix}_{ij} \tag{2.17}$$

Crew Consumables and Waste

During spaceflight, consumables such as oxygen, water, and food are consumed and waste is generated by the crew. Let c and w be the consumables consumption and the waste generation per unit crew member per unit time, respectively. If Δt_{ij} is the duration of edge (i, j), then Eq. (2.11b) holds, where

$$\boldsymbol{x}_{ij}^{\pm} = \begin{bmatrix} \text{crew} \\ \text{consumables} \\ \text{waste} \end{bmatrix}_{ij}^{\pm} \qquad \boldsymbol{B}_{ij} = \begin{bmatrix} 1 & 0 & 0 \\ -c\Delta t_{ij} & 1 & 0 \\ w\Delta t_{ij} & 0 & 1 \end{bmatrix}_{ij} \tag{2.18}$$

Putting the above two examples together, Eq. (2.11b) still holds for

$$\boldsymbol{x}_{ij}^{\pm} = \begin{bmatrix} \text{payload} \\ \text{crew} \\ \text{propellant} \\ \text{consumables} \\ \text{waste} \end{bmatrix}_{ij}^{\pm} \qquad \boldsymbol{B}_{ij} = \boldsymbol{B}_{ij}^{(2)} \boldsymbol{B}_{ij}^{(1)} \tag{2.19}$$

where

$$\boldsymbol{B}_{ij}^{(1)} = \begin{bmatrix} 1 & 0 & 0 & 0 & 0 \\ 0 & 1 & 0 & 0 & 0 \\ -\phi & -\phi & 1-\phi & -\phi & -\phi \\ 0 & 0 & 0 & 1 & 0 \\ 0 & 0 & 0 & 0 & 1 \end{bmatrix}_{ij} \qquad \boldsymbol{B}_{ij}^{(2)} = \begin{bmatrix} 1 & 0 & 0 & 0 & 0 \\ 0 & 1 & 0 & 0 & 0 \\ 0 & 0 & 1 & 0 & 0 \\ 0 & -c\Delta t & 0 & 1 & 0 \\ 0 & w\Delta t & 0 & 0 & 1 \end{bmatrix}_{ij} \tag{2.20}$$

As shown in Eqs. (2.19) and (2.20), when there are multiple flow transformation events on a single edge, $\boldsymbol{B}_{ij}$ can be the product of multiple matrices, in which the subsequent transformation matrix is multiplied from the left:

$$\boldsymbol{B}_{ij} = \boldsymbol{B}_{ij}^{(n)} \cdots \boldsymbol{B}_{ij}^{(2)} \boldsymbol{B}_{ij}^{(1)} \tag{2.21}$$

In general, a non-diagonal matrix is not commutative. Therefore, if there are interactions between different commodities, that is, $\boldsymbol{B}_{ij}$ matrices have off-diagonal entries, then the order of matrix multiplication must be exactly the sequence of transformation events.

Just as a trial, let us compare $\boldsymbol{B}_{ij}^{(2)} \boldsymbol{B}_{ij}^{(1)}$ in Eq. (2.22a) with its reverse product $\boldsymbol{B}_{ij}^{(1)} \boldsymbol{B}_{ij}^{(2)}$ in Eq. (2.22b).

$$\boldsymbol{B}_{ij}^{(2)} \boldsymbol{B}_{ij}^{(1)} = \begin{bmatrix} 1 & 0 & 0 & 0 & 0 \\ 0 & 1 & 0 & 0 & 0 \\ -\phi & -\phi & 1-\phi & -\phi & -\phi \\ 0 & -c\Delta t & 0 & 1 & 0 \\ 0 & w\Delta t & 0 & 0 & 1 \end{bmatrix}_{ij} \tag{2.22a}$$

$$\boldsymbol{B}_{ij}^{(1)}\boldsymbol{B}_{ij}^{(2)} = \begin{bmatrix} 1 & 0 & 0 & 0 & 0 \\ 0 & 1 & 0 & 0 & 0 \\ -\phi & -\phi\,(1\underline{-c\Delta t + w\Delta t}) & 1-\phi & -\phi & -\phi \\ 0 & -c\Delta t & 0 & 1 & 0 \\ 0 & w\Delta t & 0 & 0 & 1 \end{bmatrix}_{ij} \tag{2.22b}$$

The $(3,2)$ entry of $\boldsymbol{B}_{ij}^{(1)}\boldsymbol{B}_{ij}^{(2)}$ is different from that of $\boldsymbol{B}_{ij}^{(2)}\boldsymbol{B}_{ij}^{(1)}$ by the underlined part, which is very intuitive in this context because the amount of propellant consumed by the propulsive burn is determined by the total mass at the time of burn.

2.3.4 Concurrency Matrix $\boldsymbol{C}_{ij}^{\pm}$

When a commodity flows on an edge, it might need a certain amount of another commodity to travel along with it. Again, we present two space-related examples below.

Inert Mass Fraction

Propellant cannot travel by itself; it needs `"structure"`. The *inert mass fraction* is defined as the ratio of structure mass to structure plus propellant mass:

$$f_{\text{inert}} \equiv \frac{m_{\text{st}}^{+}}{m_{\text{st}}^{+} + m_{\text{pr}}^{+}} \tag{2.23}$$

so that the ratio of structure mass to propellant mass is:

$$\eta \equiv \frac{m_{\text{st}}^{+}}{m_{\text{pr}}^{+}} = \frac{f_{\text{inert}}}{1 - f_{\text{inert}}} \tag{2.24}$$

If we have 1 unit of propellant, we must carry at least η units of structure along with it. Suppose that the flow vector includes payload, propellant, and structure. Then this constraint can be represented by Eq. (2.11c), where

$$\boldsymbol{x}_{ij}^{+} = \begin{bmatrix} \text{payload} \\ \text{propellant} \\ \text{structure} \end{bmatrix}_{ij}^{+} \qquad \boldsymbol{C}_{ij}^{+} = \begin{bmatrix} 0 & \eta & -1 \end{bmatrix}_{ij}^{+} \tag{2.25}$$

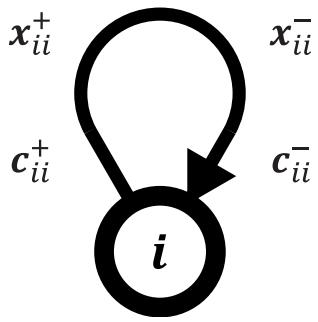

Figure 2-3: A graph loop

which is equivalent to

$$[\eta m_{\mathrm{pr}}]_{ij}^{+} \leq [m_{\mathrm{st}}]_{ij}^{+} \tag{2.26}$$

Aeroshell

It is said that when performing aerobraking, spacecraft needs aeroshell with a mass of about 15% of the total mass being braked. Let θ denote this aeroshell mass fraction. When a spacecraft with a mass of 1 performs aerobraking, it must have an aeroshell with a mass of θ. This constraint can be represented by Eq. (2.11c), where

$$\boldsymbol{x}_{ij}^{-} = \begin{bmatrix} \text{spacecraft} \\ \text{aeroshell} \end{bmatrix}_{ij}^{-} \qquad \boldsymbol{C}_{ij}^{-} = \begin{bmatrix} \theta & -1 \end{bmatrix}_{ij}^{-} \tag{2.27}$$

which is equivalent to

$$[\theta m_{\mathrm{sc}}]_{ij}^{-} \leq [m_{\mathrm{as}}]_{ij}^{-} \tag{2.28}$$

Note that aerobraking is usually performed at arrival so that this is an `"inflow"` concurrency (with a superscript of `"−"`).

2.4 Other Concepts in Graph Theory

A couple of mathematical concepts in graph theory that help formulating the problem to be addressed in this study are also introduced in this section.

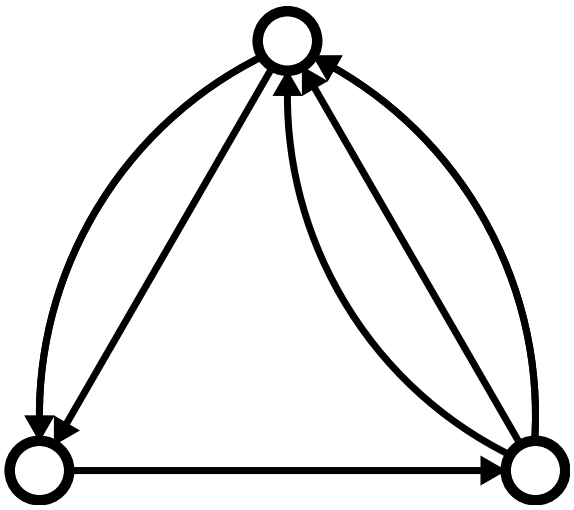

Figure 2-4: A multigraph (also called a pseudograph)

2.4.1 Graph Loop

In graph theory, a graph loop is an edge that connects a node to itself (Figure 2-3). It is also called a self-loop or a "buckle". This can be used for modeling a generic plant as a resource processing facility. A resource processing facility is likely to be modeled as a node, as opposed to a typical edge modeling transportation. In this study, however, a resource processing facility is also modeled as an edge connecting a node to itself. $\boldsymbol{ABC}$ matrices that were discussed in the previous section are also applicable to graph loops and therefore resource processing can be represented by a requirement matrix $\boldsymbol{A}$ and a transformation matrix $\boldsymbol{B}$.

Examples of a graph loop used in the space application (discussed later in Chapter 4) include (1) ISRU on the surface nodes producing resource and requiring maintenance and (2) Mars surface exploration consuming oxygen, water, and food, and generating waste. Examples of a graph loop used in the terrestrial application (discussed later in Chapter 5) include (3) desalination transforming feed water into potable water and requiring electricity and (4) waste water treatment transforming waste water into non-potable water and requiring electricity.

2.4.2 Multigraph

In graph theory, an undirected graph that has no loops and no more than one edge between any two different nodes is called a simple graph. As opposed to a simple graph, a multigraph

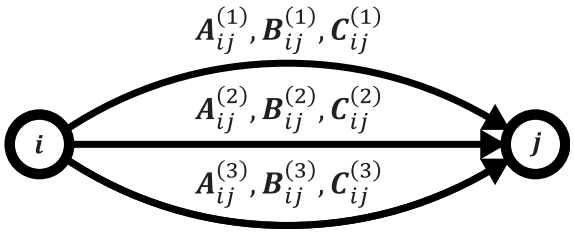

Figure 2-5: Multiple edges (parallel edges) between nodes i and j

refers to a graph in which multiple edges (also called "parallel edges") are either permitted or required between the same end nodes [52–54]. Thus, as shown in Figure 2-4, two nodes may be connected by more than one edge. A multigraph is also called a pseudograph. There are two distinct notions of multiple edges. One is that as in graphs without multiple edges, the identity of an edge is defined by the nodes it connects, but the same edge can occur several times between these nodes. Alternatively, we define edges to be first-class entities like nodes, each having its own identity independent of the nodes it connects.

For example, if we think about an interplanetary transfer from LEO to LMO, we have multiple choices on propulsion system such as chemical, nuclear thermal rocket (NTR), solar electric propulsion (SEP), and so on, each of which has different I_{sp}. We also have aerocapture option; if we perform aerocapture, we need to bring an appropriate aeroshell. Moreover, there are trade-offs between ΔV and TOF (time of flight); if we send a robotic mission, we might prefer a lower ΔV with a longer TOF while if we send human, we might prefer a shorter TOF with a compromise of ΔV. All these parameters are implemented through $\boldsymbol{ABC}$ matrices on each edge. Therefore such multiple choices can be modeled by allowing parallel edges between the same end nodes (see Figure 2-5). By implementing parallel edges that represent trades, the optimization of network flow will automatically give us a solution to the trade problem.

Some references require that multigraphs possess no graph loops, some explicitly allow them, and yet others do not include any explicit allowance or disallowance [52–57]. Tutte uses the term "multigraph" to mean a graph containing either loops or multiple edges. As a result of these many ambiguities, use of the term "multigraph" should be deprecated, or at the very least used with extreme caution.

Note that all graphs are assumed to be directed graphs in this study. A "directed" version of multigraph is called a multidigraph or a quiver. However, we have no rigid

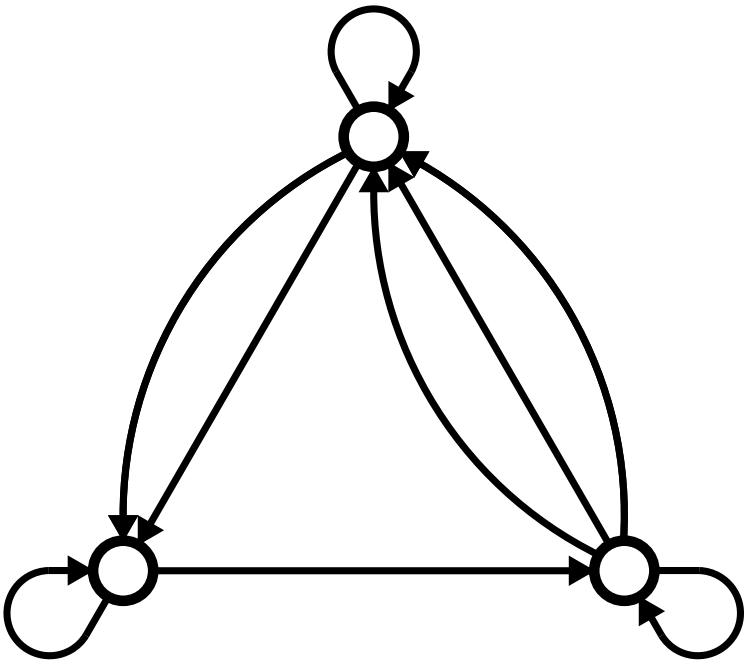

Figure 2-6: A reflexive graph

distinction in this study. As described later in Chapter 5, in a graph that we use in the terrestrial application, there is a graph loop associated with every node. As shown in Figure 2-6, a pseudograph such that each node has an associated graph loop is referred to as a reflexive graph.

This is all we need from graph theory. In Chapters 4 and 5, the problems are implemented using the $\boldsymbol{ABC}$ matrices in Eqs. (2.11) and in Sections 2.3.2 through 2.3.4 and a multigraph or a reflexive graph in Figures 2-4 and 2-6.

Chapter 3

Formulation of Optimization Problem

In the previous chapter, we presented the generalized multi-commodity network flow model using a requirement matrix $\boldsymbol{A}_{ij}^{\pm}$, a transformation matrix $\boldsymbol{B}_{ij}$, and a concurrency matrix $\boldsymbol{C}_{ij}^{\pm}$ on a multigraph that allows loops and multiple edges between the same two nodes. This chapter discusses how to actually implement and solve the optimization problem based on those mathematical formulations. While there are many fields of optimization, in order to take advantage of linearity of the constraints in Eqs. (2.11), this thesis is focused on two large and important subfields: linear programming (LP) and mixed integer linear programming (MILP). As described in more detail later, the space application in Chapter 4 formulates and solves LP problems while the terrestrial application in Chapter 5 formulates and solves MILP problems. Therefore this chapter serves as a preparation for (generalization of) the subsequent two chapters.

3.1 Linear Programming Formulation

3.1.1 Linear Programming (LP)

Linear programming (LP) is an optimization problem with a linear objective function, a set of linear equality and inequality constraints, and a set of nonnegativity restrictions imposed upon the underlying decision variables. Its feasible region is a convex polyhedron, which is a set defined as the intersection of finitely many half spaces, each of which is defined by a

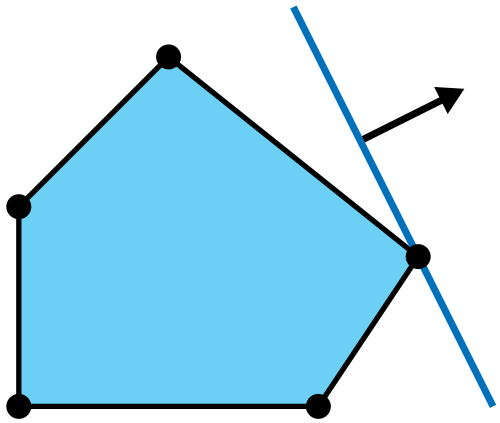

Figure 3-1: A pictorial representation of an LP with 2 variables and 5 inequalities

linear inequality. Figure 3-1 shows an example of a feasible region of a simple LP with two variables and five inequality constraints. The set of feasible solutions is depicted in light blue and forms a 2-dimensional polytope. The linear objective function is represented by the blue line and the arrow indicates the direction in which we are optimizing. As can be easily imagined by extending Figure 3-1 to N dimensions, an LP algorithm finds a corner point in the polyhedron where the objective function has the smallest (or largest) value if such a point exists.

Linear programs are problems that can be expressed in canonical form:
Minimize

$$\mathcal{J} = \boldsymbol{c}^{\mathrm{T}}\boldsymbol{x} \tag{3.1}$$

subject to

$$\boldsymbol{A}_{\mathrm{ineq}}\boldsymbol{x} \leq \boldsymbol{b}_{\mathrm{ineq}} \tag{3.2a}$$

$$\boldsymbol{A}_{\mathrm{eq}}\boldsymbol{x} = \boldsymbol{b}_{\mathrm{eq}} \tag{3.2b}$$

$$\boldsymbol{x} \geq \boldsymbol{0} \tag{3.2c}$$

where $\boldsymbol{x}$ represents the vector of variables (to be determined), $\boldsymbol{c}$, $\boldsymbol{b}_{\mathrm{ineq}}$, and $\boldsymbol{b}_{\mathrm{eq}}$ are vectors of coefficients (known), and $\boldsymbol{A}_{\mathrm{ineq}}$ and $\boldsymbol{A}_{\mathrm{eq}}$ are matrices of coefficients (known). Eq. (3.2a) represents inequality constraints, Eq. (3.2b) equality constraints, and Eq. (3.2c) nonnegativity constraints. If this problem has n_x nonnegative decision variables, n_{ineq} inequality constraints, and n_{eq} equality constraints, then the vectors $\boldsymbol{c}$ and $\boldsymbol{x}$ are n_x-dimensional column vectors, the matrix $\boldsymbol{A}_{\mathrm{ineq}}$ has n_{ineq} rows and n_x columns, the matrix $\boldsymbol{A}_{\mathrm{eq}}$ has n_{eq} rows

Table 3.1: Generalized multi-commodity network flow LP

Variables	x_{ij}^{+}	x_{ij}^{-}	x_{hi}^{-}		RHS	Σ	$\forall$
Objective Function	c_{ij}^{+}	c_{ij}^{-}	$\mathbf{0}$	$=$	$\mathcal{J}$	$(i,j) \in \mathcal{A}$	
Mass Balance (Net Supply/Demand)	A_{ij}^{+}	$\boldsymbol{O}$	$-A_{hi}^{-}$	$\leq$	b_i	$j:(i,j) \in \mathcal{A}$ $h:(h,i) \in \mathcal{A}$	$i \in \mathcal{N}$
Self-Constraints for Outflow	C_{ij}^{+}	$\boldsymbol{O}$	$\boldsymbol{O}$	$\leq$	$\mathbf{0}$		$(i,j) \in \mathcal{A}$
Self-Constraints for Inflow	$\boldsymbol{O}$	C_{ij}^{-}	$\boldsymbol{O}$	$\leq$	$\mathbf{0}$		$(i,j) \in \mathcal{A}$
Flow Transformation	B_{ij}	$-I$	$\boldsymbol{O}$	$=$	$\mathbf{0}$		$(i,j) \in \mathcal{A}$

and n_x columns, and the vectors $\boldsymbol{b}_{\text{ineq}}$ and $\boldsymbol{b}_{\text{eq}}$ are n_{ineq}-dimensional and n_{eq}-dimensional column vectors, respectively.

3.1.2 LP Formulation for GMCNF

Generalized multi-commodity network flow problems defined in Eqs. (2.10) and (2.11) can be rewritten in canonical form by translating the constraints in Eqs. (2.11) into equality and inequality constraints above. The transformation constraints in Eq. (2.11b) fall into equalities while the rest of the constraints fall into inequalities. Table 3.1 summarizes this translation. The cells shaded in light red configure the $\boldsymbol{A}_{\text{ineq}}$ while the cells shaded in light yellow configure the $\boldsymbol{A}_{\text{eq}}$ matrix.

Suppose a generalized multi-commodity network flow problem has n nodes, m edges, and k types of commodities. Since the flow is split into outflow and inflow for each edge, there are $2m$ flow vectors and $2m$ cost vectors, each of which is a k-dimensional column vector. In order to formulate an LP problem in canonical form, we need to put them together to construct one large column vector so that we can compute the objective function in Eq. (3.1) by one large vector multiplication, that is, $\boldsymbol{x}_{ij}^{+}$ and $\boldsymbol{x}_{ij}^{-}$ build up a $2km$-dimensional column vector $\boldsymbol{x}$, and $\boldsymbol{c}_{ij}^{+}$ and $\boldsymbol{c}_{ij}^{-}$ build up a $2km$-dimensional column vector $\boldsymbol{c}$. This is equivalent to an LP problem with $2km$ scalar variables.

As described in Eqs. (2.12), the $\boldsymbol{A}_{ij}^{\pm}$ and the $\boldsymbol{B}_{ij}$ matrices are k-by-k square matrices while the $\boldsymbol{C}_{ij}^{\pm}$ matrix is a l-by-k matrix, where l is the number of concurrency constraints on edge (i,j). In actuality, the number of concurrency constraints could be different with

each edge. However, for simplicity, let l denote the maximum number of concurrency constraints among edges, and for edges with less than l concurrency constraints, we can just assign zeros to avoid the unnecessary rows without any influence on the solution. Therefore there are at most lm concurrency constraints for outflows and inflows, respectively. Since the mass balance constraints are defined for each node, we have kn mass balance constraints. Putting them together, the matrix $\boldsymbol{A}_{\text{ineq}}$ has $(kn + 2lm)$ rows and $2km$ columns. On the other hand, since the flow transformation is defined for each edge, there are km transformation constraints in total. Hence, the matrix $\boldsymbol{A}_{\text{eq}}$ has km rows and $2km$ columns. To summarize, the generalized multi-commodity network flow problem has $2km$ variables, $(kn + 2lm)$ inequality constraints, and km equality constraints as well as $2km$ flow bound constraints. Thus, the problem size is determined by the four parameters: the number of nodes n, the number of edges m, the number of types of commodities to be considered k, and the maximum number of concurrency constraints among edges l. For example, a fully connected reflexive digraph with 10 nodes has 100 edges including 10 loops. If we consider 5 types of commodities and if we assume 1 concurrency constraint for each outflow and inflow, this problem has 1000 variables, 250 inequality constraints, and 500 equality constraints in addition to 1000 flow bound constraints.

While the computational time highly depends on the method that the solver uses, the computational complexity is apparently a linear function of the number of nodes n, the number of edges m, and the number of commodities k because the number of variables can be represented by $2km$ and the number of both inequality and equality constraints can be represented by $kn + km + 2lm$. The number of commodities k and the number of edges m seem to have a relatively big impact on the computational complexity compared to the number of nodes n. However, since the number of nodes and the number of edges are closely related, n can greatly contribute to the problem size through both m and itself, depending on the network topology.

3.2 Mixed Integer Linear Programming Formulation

As described later in Chapter 5, the terrestrial application extends the generalized multi-commodity network flow model to a specific mixed integer linear programming formulation, which is presented preliminarily in this section.

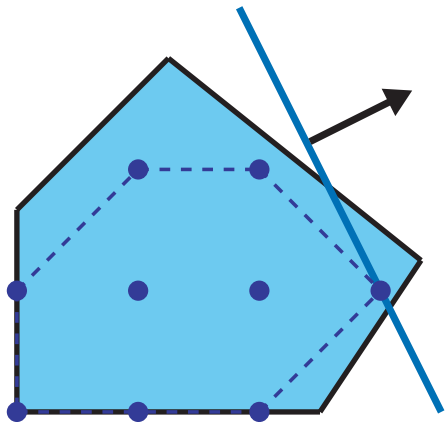

Figure 3-2: An ILP polytope with LP relaxation

3.2.1 Mixed Integer Linear Programming (MILP)

An integer programming (IP) problem is a mathematical optimization in which some or all of the variables are restricted to be integers. In many settings the term refers to integer linear programming (ILP). Integer programming is classified as an NP-hard problem while a special case, 0-1 integer linear programming, in which unknowns are binary, is an NP-complete problem.

Figure 3-2 shows an ILP version of Figure 3-1 with additional constraints of $\boldsymbol{x}$ being integers. The feasible integer points are shown in blue, and the blue dashed lines indicate their convex hull, which is the smallest convex polyhedron that contains all of these points. In this case, the original region in light blue represents the polyhedron of the LP relaxation, which is given by the inequalities without the integrality constraints. The linear objective function is represented by the blue line and the arrow indicates the direction in which we are optimizing. Compared to Figure 3-1, we can see that the blue line is set back a little bit due to the fact that a solution is limited to a grid point. It appears that a solution is constrained to a much smaller search space in ILP than in LP, but paradoxically it takes much longer time to solve the problem. Probably the most famous ILP problem is the Traveling Salesman Problem (TSP).

Mixed integer linear programming (MILP) involve problems in which only some of the variables are constrained to be integers. If the variables are restricted to be binary (either 0 or 1), the problem is also called zero-one linear programming (ZOLP). The following section presents an MILP formulation specific to the case study in Chapter 5.

3.2.2 MILP Formulation for GMCNF

In the case study in Chapter 5, we consider a large infrastructure network consisting of desalination plants, power plants, and cities, in which edges represent water pipelines or powerlines and graph loops model resource processing facilities. Thus, the flow $\boldsymbol{x}$ on edges represents how much water is transported through the pipelines or how much electricity is transmitted through the powerlines while the flow $\boldsymbol{x}$ on loops represents how much water is produced at desalination plants or how much electricity is produced at power plants.

However, as discussed in more detail later, one of the goals of solving the generalized multi-commodity network flow problem in this context is to explore the best investment in future infrastructure systems. We wish to determine where we should build a new facility and how much capacity it should have, or if we expand the capacity of the existing facility, how much it should be. This decision-making can be included in the problem by introducing another variable. Let $\boldsymbol{y}$ denote the capacity expansion. For example, $\boldsymbol{y}_{ij}^{\pm}$ can express how much we expand the transmission capacity of pipeline (i, j), and $\boldsymbol{y}_{ii}^{\pm}$ can express how much we expand the operation capacity of facility i. If $\boldsymbol{u}_{ij}^{\pm}$ is the current capacity of edge (i, j), then the new capacity is $\boldsymbol{u}_{ij}^{\pm} + \boldsymbol{y}_{ij}^{\pm}$; now the flow $\boldsymbol{x}_{ij}^{\pm}$ must be less than or equal to $\boldsymbol{u}_{ij}^{\pm} + \boldsymbol{y}_{ij}^{\pm}$. By setting $\boldsymbol{u}_{ij}^{\pm}$ to be zero, it can contain a brand-new infrastructure that does not exist yet. Hence, a brand-new infrastructure can be inclusively viewed as "capacity expansion" for the modeling purposes.

Of course the capacity expansion comes at a cost. For distinction, let $\boldsymbol{c}_{ij}^{x^{\pm}}$ and $\boldsymbol{c}_{ij}^{y^{\pm}}$ be the unit costs for $\boldsymbol{x}_{ij}^{\pm}$ and $\boldsymbol{y}_{ij}^{\pm}$, respectively. These costs, however, can only describe the proportional costs. We must also consider fixed costs. For example, if we use a pipeline, the operation and maintenance cost is incurred regardless of how much water is transported through it. As opposed to the proportional costs, this cost can be modeled as a fixed cost, which is incurred if we use the edge and not incurred if we do not use the edge. For this reason, we also introduce a binary variable $\boldsymbol{z}_{ij}$, representing whether the edge is used or not. Let $\boldsymbol{c}_{ij}^{z}$ be the fixed cost incurred by using edge (i, j).

Using these notations, a mixed integer linear programming problem of the generalized multi-commodity network flow is formulated as follows:

Minimize

$$\mathcal{J} = \sum_{(i,j)\in\mathcal{A}} \left(\boldsymbol{c}_{ij}^{x^+\mathrm{T}} \boldsymbol{x}_{ij}^{+} + \boldsymbol{c}_{ij}^{x^-\mathrm{T}} \boldsymbol{x}_{ij}^{-} + \boldsymbol{c}_{ij}^{y^+\mathrm{T}} \boldsymbol{y}_{ij}^{+} + \boldsymbol{c}_{ij}^{y^-\mathrm{T}} \boldsymbol{y}_{ij}^{-} + \boldsymbol{c}_{ij}^{z\,\mathrm{T}} \boldsymbol{z}_{ij} \right) \tag{3.3}$$

subject to

$$\sum_{j:(i,j)\in\mathcal{A}} \boldsymbol{A}_{ij}^{+} \boldsymbol{x}_{ij}^{+} - \sum_{j:(j,i)\in\mathcal{A}} \boldsymbol{A}_{ji}^{-} \boldsymbol{x}_{ji}^{-} \leq \boldsymbol{b}_i \qquad \forall\, i \in \mathcal{N} \tag{3.4a}$$

$$\boldsymbol{B}_{ij} \boldsymbol{x}_{ij}^{+} = \boldsymbol{x}_{ij}^{-} \qquad \forall\, (i,j) \in \mathcal{A} \tag{3.4b}$$

$$\boldsymbol{C}_{ij}^{+} \boldsymbol{x}_{ij}^{+} \leq \boldsymbol{0} \quad \text{and} \quad \boldsymbol{C}_{ij}^{-} \boldsymbol{x}_{ij}^{-} \leq \boldsymbol{0} \qquad \forall\, (i,j) \in \mathcal{A} \tag{3.4c}$$

$$\boldsymbol{x}_{ij}^{+} \leq \boldsymbol{u}_{ij}^{+} + \boldsymbol{y}_{ij}^{+} \quad \text{and} \quad \boldsymbol{x}_{ij}^{-} \leq \boldsymbol{u}_{ij}^{-} + \boldsymbol{y}_{ij}^{-} \qquad \forall\, (i,j) \in \mathcal{A} \tag{3.4d}$$

$$\boldsymbol{x}_{ij}^{+} \leq \mathcal{M} \boldsymbol{z}_{ij} \quad \text{and} \quad \boldsymbol{x}_{ij}^{-} \leq \mathcal{M} \boldsymbol{z}_{ij} \qquad \forall\, (i,j) \in \mathcal{A} \tag{3.4e}$$

$$z_{ij} \in \{0,1\} \qquad \forall\, (i,j) \in \mathcal{A} \tag{3.4f}$$

The objective function in Eq. (3.3) includes three types of costs: costs proportional to the flow $\boldsymbol{x}_{ij}^{\pm}$, costs proportional to the capacity expansion $\boldsymbol{y}_{ij}^{\pm}$, and fixed costs incurred by $\boldsymbol{z}_{ij}$. The $\boldsymbol{ABC}$-involved constraints in Eqs. (3.4a)-(3.4c) remain the same as in Eqs. (2.11a)-(2.11c). The flow bound constraint in Eq. (3.4d) has been changed; the capacity expansion $\boldsymbol{y}_{ij}^{\pm}$ is now involved. The constraint in Eq. (3.4e) are the so-called big-$\mathcal{M}$ method. $\mathcal{M}$ is chosen sufficiently large. The constraint $\boldsymbol{x}_{ij}^{\pm} \leq \mathcal{M} \boldsymbol{z}_{ij}$ forces $z_{ij} = 1$ whenever $x_{ij}^{\pm} > 0$ for any commodity. If, on the other hand, we do not use edge (i,j), then $\boldsymbol{z}_{ij} = \boldsymbol{0}$, which forces $\boldsymbol{x}_{ij}^{\pm} = 0$. The disadvantage of this approach is that the running time of the integer programming algorithm may depend on the choice of $\mathcal{M}$. Choosing $\mathcal{M}$ very large (e.g., $\mathcal{M} = 10^{12}$) will lead to valid formulations, but the overly large value of $\mathcal{M}$ may slow down the solution procedure. The last constraint in Eq. (3.4f) simply states that z_{ij} is binary.

Table 3.2 summarizes the translation of Eqs. (3.3) and (3.4) into canonical form in Eqs. (3.1) and (3.2). The cells shaded in light red configure the $\boldsymbol{A}_{\text{ineq}}$ while the cells shaded in light yellow configure the $\boldsymbol{A}_{\text{eq}}$ matrix.

Again, suppose a generalized multi-commodity network flow problem has n nodes, m edges, k types of commodities, and maximum l concurrency constraints for one edge outflow or inflow. The decision variables include $2m$ flow vectors, $2m$ capacity expansion vectors,

Table 3.2: Generalized multi-commodity network flow MILP

Variables	$\boldsymbol{x}_{ij}^{+}$	$\boldsymbol{x}_{ij}^{-}$	$(\boldsymbol{x}_{hi}^{-})$	$\boldsymbol{y}_{ij}^{+}$	$\boldsymbol{y}_{ij}^{-}$	$\boldsymbol{z}_{ij}$		RHS	Σ	$\forall$
Objective Function	$\boldsymbol{c}_{ij}^{x^+}$	$\boldsymbol{c}_{ij}^{x^-}$	$\boldsymbol{0}$	$\boldsymbol{c}_{ij}^{y^+}$	$\boldsymbol{c}_{ij}^{y^-}$	$\boldsymbol{c}_{ij}^{z}$	$=$	$\mathcal{J}$	$(i,j) \in \mathcal{A}$	
Mass Balance (Net Supply/Demand)	$\boldsymbol{A}_{ij}^{+}$	$\boldsymbol{O}$	$-\boldsymbol{A}_{hi}^{-}$	$\boldsymbol{O}$	$\boldsymbol{O}$	$\boldsymbol{O}$	$\leq$	$\boldsymbol{b}_i$	$j\colon (i,j) \in \mathcal{A}$ $h\colon (h,i) \in \mathcal{A}$	$i \in \mathcal{N}$
Self-Constraints for Outflow	$\boldsymbol{C}_{ij}^{+}$	$\boldsymbol{O}$	$\boldsymbol{O}$	$\boldsymbol{O}$	$\boldsymbol{O}$	$\boldsymbol{O}$	$\leq$	$\boldsymbol{0}$		$(i,j) \in \mathcal{A}$
Self-Constraints for Inflow	$\boldsymbol{O}$	$\boldsymbol{C}_{ij}^{-}$	$\boldsymbol{O}$	$\boldsymbol{O}$	$\boldsymbol{O}$	$\boldsymbol{O}$	$\leq$	$\boldsymbol{0}$		$(i,j) \in \mathcal{A}$
Capacity Expansion for Outflow	$\boldsymbol{I}$	$\boldsymbol{O}$	$\boldsymbol{O}$	$-\boldsymbol{I}$	$\boldsymbol{O}$	$\boldsymbol{O}$	$\leq$	$\boldsymbol{u}_{ij}^{+}$		$(i,j) \in \mathcal{A}$
Capacity Expansion for Inflow	$\boldsymbol{O}$	$\boldsymbol{I}$	$\boldsymbol{O}$	$\boldsymbol{O}$	$-\boldsymbol{I}$	$\boldsymbol{O}$	$\leq$	$\boldsymbol{u}_{ij}^{-}$		$(i,j) \in \mathcal{A}$
Big $\mathcal{M}$ Method for Outflow	$\boldsymbol{I}$	$\boldsymbol{O}$	$\boldsymbol{O}$	$\boldsymbol{O}$	$\boldsymbol{O}$	$-\mathcal{M}\boldsymbol{I}$	$\leq$	$\boldsymbol{0}$		$(i,j) \in \mathcal{A}$
Big $\mathcal{M}$ Method for Inflow	$\boldsymbol{O}$	$\boldsymbol{I}$	$\boldsymbol{O}$	$\boldsymbol{O}$	$\boldsymbol{O}$	$-\mathcal{M}\boldsymbol{I}$	$\leq$	$\boldsymbol{0}$		$(i,j) \in \mathcal{A}$
Flow Transformation	$\boldsymbol{B}_{ij}$	$-\boldsymbol{I}$	$\boldsymbol{O}$	$\boldsymbol{O}$	$\boldsymbol{O}$	$\boldsymbol{O}$	$=$	$\boldsymbol{0}$		$(i,j) \in \mathcal{A}$

and m binary vectors, each of which is a k-dimensional column vector. Corresponding to these decision variables, we have $2m$ cost vectors for the flow $\boldsymbol{x}_{ij}^{\pm}$, $2m$ cost vectors for the capacity expansion $\boldsymbol{y}_{ij}^{\pm}$, and m fixed cost vectors. In canonical form, $\boldsymbol{x}_{ij}^{\pm}$, $\boldsymbol{y}_{ij}^{\pm}$, and $\boldsymbol{z}_{ij}$ together construct a $5km$-dimensional column vector $\boldsymbol{x}$ while $\boldsymbol{c}_{ij}^{x^{\pm}}$, $\boldsymbol{c}_{ij}^{y^{\pm}}$, and $\boldsymbol{c}_{ij}^{z}$ build up a $5km$-dimensional column vector $\boldsymbol{c}$. This problem has $5km$ scalar variables including km binary variables.

Since the flow bound constraint and the big-$\mathcal{M}$ constraint are defined for each edge, there are $2km$ flow bound constraints and $2km$ big-$\mathcal{M}$ constraints. The matrix $\boldsymbol{A}_{\text{ineq}}$ has $(kn + 2lm + 4km)$ rows and $5km$ columns while the matrix $\boldsymbol{A}_{\text{eq}}$ has km rows and $5km$ columns, which means that there are $(kn + 2lm + 4km)$ inequality constraints and km equality constraints as well as $5km$ nonnegativity constraints. For example, if we consider a fully connected reflexive digraph with 10 nodes and 100 edges including 10 loops, 5 types of commodities, and 1 concurrency constraint for each outflow and inflow, this problem has 2500 variables, 500 of which are binary, 2250 inequality constraints, and 500 equality constraints, in addition to 2500 nonnegativity constraints.

While there are several different approaches to solving mixed integer programs, most of them are based on solving various LP relaxations of the integer program because solving linear programs is much easier than solving integer programs. Solving integer programs is NP-hard whereas linear programs can be solved in polynomial time. The simplest approach to solving mixed integer programs is to use *branch and bound*. This approach works as follows: we solve the LP relaxation of the mixed integer program. If we obtain an optimal solution in which all the variables that are required to take integer values are integer values, then we are done. Otherwise, taking some variable x_i that is required to take an integer value but is a noninteger value r in the solution to the LP relaxation, we create a new problem in which a new constraint $x_i \leq \lfloor r \rfloor$ or $x_i \geq \lceil r \rceil$ is added and continue. By repeating this procedure, a best known solution (the incumbent solution in the mixed integer program) approaches a value that bounds the best possible solution. Generally the difference between these two values is called the optimality gap. If the problem size is sufficiently big, MILP cannot be solved within a reasonable time. In that case we can terminate the MILP optimization under a variety of circumstances. One example is the optimality gap tolerance. There are two such tolerances: a relative MIP gap tolerance that is commonly used, and an absolute MIP gap tolerance that is appropriate in cases where the expected optimal objective function is quite small in magnitude. For example, if we set a relative MIP gap to be 10^{-4}, the optimization stops when an integer feasible solution has been proved to be within 0.01% of optimality.

3.3 Implementation

In this thesis, the generalized multi-commodity network flow model is implemented in MATLAB®. Whereas various numerical algorithms are available within the MATLAB Optimization Toolbox™, this study employs the IBM® ILOG® CPLEX® Optimization Studio using the MATLAB connector, especially for the more powerful algorithm for mixed integer linear programming problems.

First, a dataset including supply/demand, parameters, and assumptions is created using Microsoft Office Excel®. Then the dataset is fed into MATLAB and a generalized multi-commodity network described in Chapter 2 is constructed by defining supplies/demands at nodes, objective function coefficients, capacities, and the $\boldsymbol{ABC}$ matrices for edges. The

GMCNF problem is translated into an LP (Chapter 4) or a MILP (Chapter 5) as described in the previous two sections.

The CPLEX function to solve LP problems is `cplexlp`, using the following syntax:

```
x = cplexlp(f, Aineq, bineq, Aeq, beq, lb, ub)
```

where `f` is equivalent to $\boldsymbol{c}$ in Eq. (3.1), `Aieq` and `Aeq` are built up from the cells in light red and light yellow in Table 3.1, respectively, `bineq` and `beq` are their corresponding RHSs, `lb` is the lower bound, and `ub` is the edge capacity.

On the other hand, the CPLEX function to solve MILP problems is `cplexmilp`, using the following syntax:

```
x = cplexmilp(f,Aineq,bineq,Aeq,beq,lb,ub,[],[],[],ctype)
```

where `Aieq` and `Aeq` are built up from the cells in light red and light yellow in Table 3.2, respectively, `bineq` and `beq` are their corresponding RHSs, `ctype` is a string with possible char values in which `ctype(i)` is assigned `B`, `I`, `C`, `S`, or `N` to indicate that `x(i)` should be binary, general integer, continuous, semi-continuous, or semi-integer, respectively, and the rest are the same as above. As can be seen from Table 3.2, two large matrices `Aieq` and `Aeq` have many zero elements. Therefore for memory saving purposes we use a sparse matrix, which converts a matrix to sparse form by squeezing out any zero elements.

Since all the mathematical preparation has been presented in the previous chapter and this chapter, the following two chapters are dedicated to the case studies of the generalized multi-commodity network flow problems with LP formulation (Chapter 4) and MILP formulation (Chapter 5).

Chapter 4

Case Study I: Mars Exploration Logistics

This chapter presents the first case study in the space application using the generalized multi-commodity network flow (GMCNF) linear programming (LP) model. One advantage of the LP formulation is that it can be quickly solved and that if solved, the solution is guaranteed to be optimal. As discussed in the next chapter, mixed integer linear programming (MILP) cannot necessarily be solved in a short time. This advantage of LP allows us to solve a number of instances.

4.1 Introduction

Since the general introduction about space exploration logistics has been presented in Chapter 1, this section discusses a more specific problem description. As stated in Chapter 1, the objective of this thesis is to develop a comprehensive graph-theoretic modeling framework to quantitatively evaluate and optimize space exploration logistics from a network perspective. In the past studies a logistics network seems to have been arbitrarily determined without a strong rationale behind it while this study considers all the possibilities in the logistics network selection. Again Figure 4-1 shows the Earth-Moon-Mars logistics network with several representative nodes. The nodes include Kennedy Space Center (KSC) for launches, a Pacific Ocean splashdown zone (PAC) for crew return, a low-Earth orbit (LEO) with an altitude of 300 km, a geostationary Earth orbit (GEO) with an altitude of 35786 km and a geostationary transfer orbit (GTO), which is a Hohmann transfer orbit from LEO

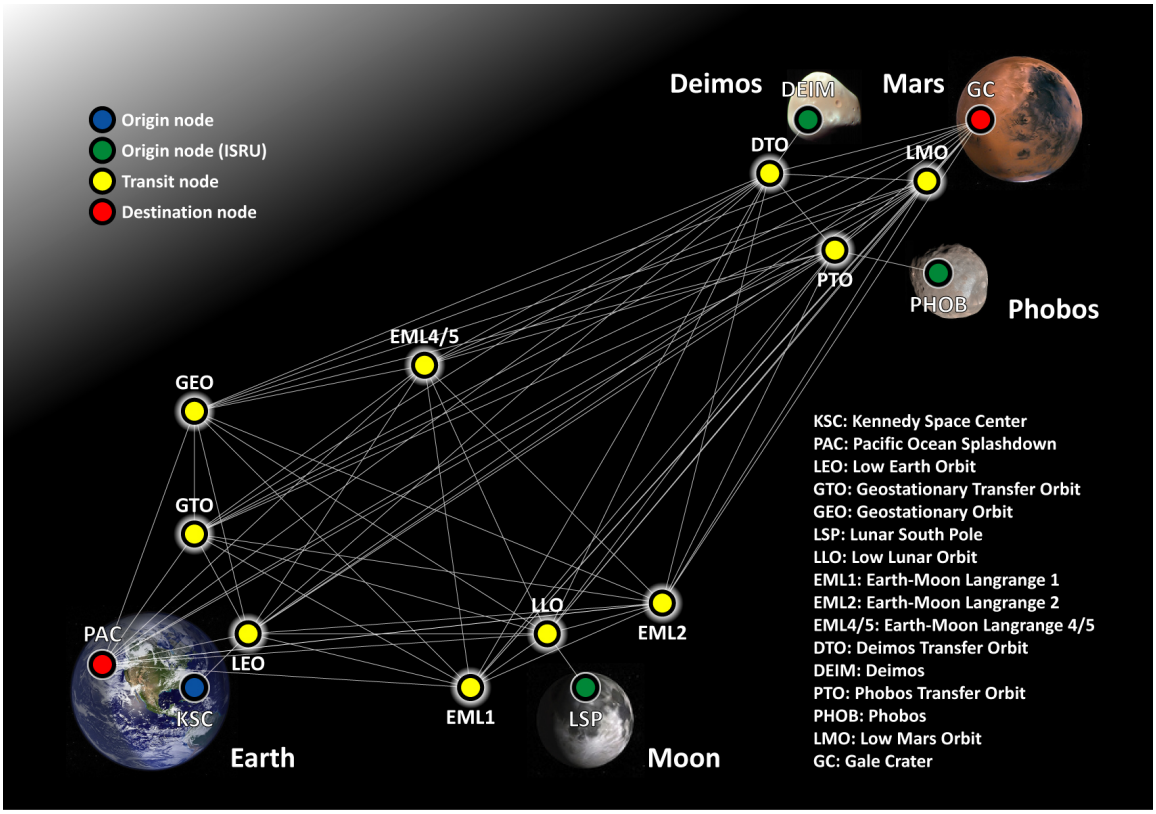

Figure 4-1: Example of Earth-Moon-Mars logistics network

to GEO, the lunar south pole (LSP), a low lunar orbit (LLO), Earth-Moon Lagrange points 1 (EML1), 2 (EML2), and 4/5 (EML4/5), Deimos (DEIM) and its transfer orbit (DTO), Phobos (PHOB) and its transfer orbit (PTO), a low Mars orbit (LMO), and Gale Crater (GC) on the Martian surface. Strictly speaking, we can define an infinite number of orbital nodes because, for example, we can think of an Earth orbit with any altitude. However, if we include an unnecessarily large number of nodes in the problem, which then creates a huge number of edges as well, it makes the problem size very large as discussed in Chapter 3. For this reason, it is wise to limit the number of nodes and edges to be considered and select a set of reasonably representative nodes. This case study discusses the space logistics network for human exploration of Mars, based on a set of nodes in Figure 4-1.

4.1.1 Mars Design Reference Architecture 5.0

NASA has undertaken substantial effort to develop a design reference architecture (DRA) for conceptual missions to Mars [58]. DRA represents the current "best" strategy for human missions and architectures and should be constantly updated as we learn. It also serves

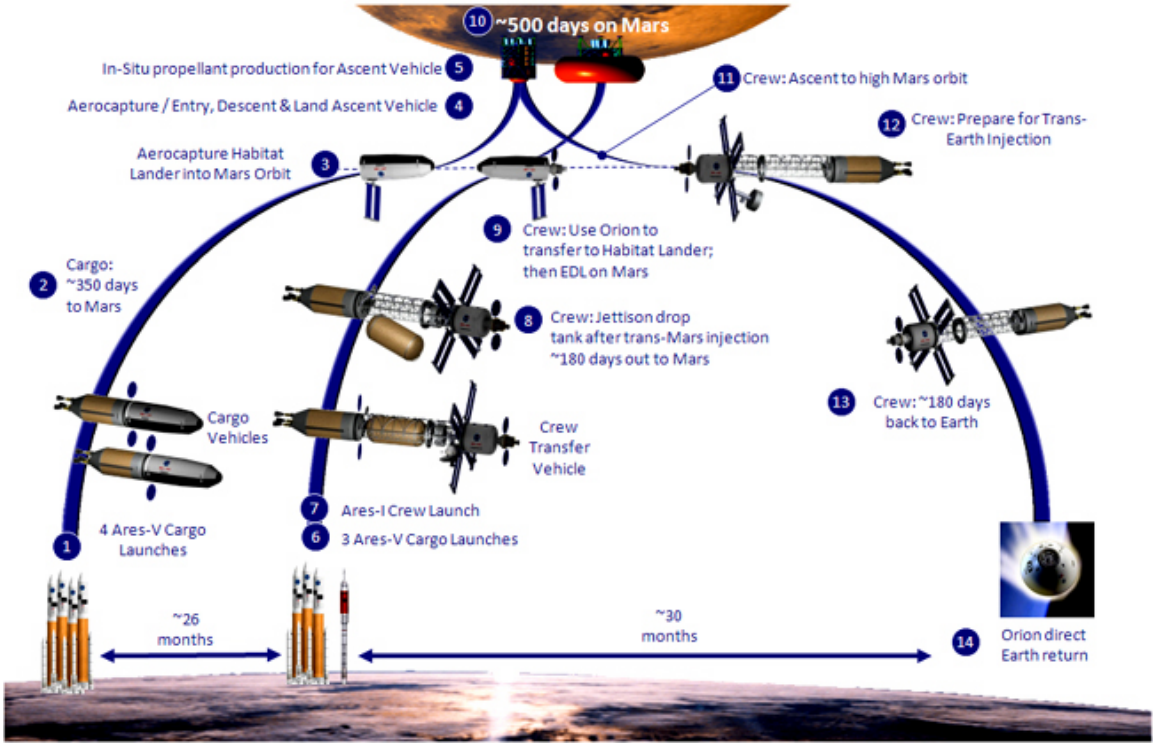

Figure 4-2: Mars Design Reference Architecture mission profile

as a benchmark against which alternative architectures can be measured. As of early 2013, the most recent publication is Mars DRA 5.0, which was published in July 2009 [59]. This design reference describes the spacecraft and missions which could be used for the first three excursions to the surface of Mars. The Mars exploration architecture is heavily based on lunar concepts from the Constellation Program, including the Ares V heavy lift launch vehicle, but also includes advanced technology concepts such as nuclear thermal rockets (NTR) for interplanetary propulsion, zero-loss cryogenic coolers for propellant transportation, aerocapture as the Mars arrival capture method, in-situ resource utilization (ISRU) for Mars ascent propellant production, and nuclear fission reactors for surface power. Figure 4-2 shows the mission profile.

4.1.2 Cislunar Propellant and Logistics Infrastructure

On the other hand, various concepts for a cislunar propellant and logistics infrastructure and transportation architecture have recently been proposed. Such concepts include a propellant depot, a reusable lunar lander (RLL), a propellant tanker, an orbital transfer vehicle (OTV) with aerobraking capability [60, 61]. These concepts are "game-changing"

because they would fundamentally affect the architecture of future space operations, providing greater access to space beyond Earth orbit. The challenge is to create the infrastructure with minimum development costs and to assure that operational costs do not diminish its benefits. These cislunar infrastructure/architecture concepts are never used in Mars DRA 5.0. Therefore one of the goals of this case study is to discuss the potential benefits of utilizing lunar resources and cislunar network for human Mars missions. As shown in Figure 4-1, there is also the Martian system including two moons. While there are various views about the possibilities of ISRU on Phobos and Deimos, we assume that surface regolith and/or water ice in the interior are available on these two moons so that we can evaluate the potential utility of Phobos/Deimos. If the cislunar system would be useful for outbound missions to Mars, it would not be surprising that the Martian system is useful for return trip to Earth.

4.2 GMCNF Model for space logistics

This section describes a mathematical formulation of the problem along the GMCNF model, including the definitions of a network graph, decision variables and an objective function, supply/demand at each node, and a requirement matrix $\boldsymbol{A}_{\boldsymbol{ij}}^{\pm}$, a transformation matrix $\boldsymbol{B}_{\boldsymbol{ij}}$, and a concurrency matrix $\boldsymbol{C}_{\boldsymbol{ij}}^{\pm}$ for each edge.

4.2.1 Network Graph

Again Figure 4-3 shows a notional network graph that extracts only the relationship between nodes and edges from a logistics network in Figure 4-1. This network graph includes 16 nodes in total. There appears to be 59 connections in the network. However, as discussed earlier in Section 2.4.2, this network graph allows both multiple edges between the same end nodes and graph-loops associated with nodes. For example, we have multiple choices on propulsion system with aerocapture option for each edge. As described in more detail later, we consider two propulsion systems: conventional chemical propulsion (LOX/LH_2) and nuclear thermal rocket (NTR). One of the advantages of the GMCNF model is that system-level trades such as the selection of propulsion system are automatically conducted in the network flow optimization by implementing multiple choices as multiple edges. Of course these multiple choices have different characteristics and constraints that must be

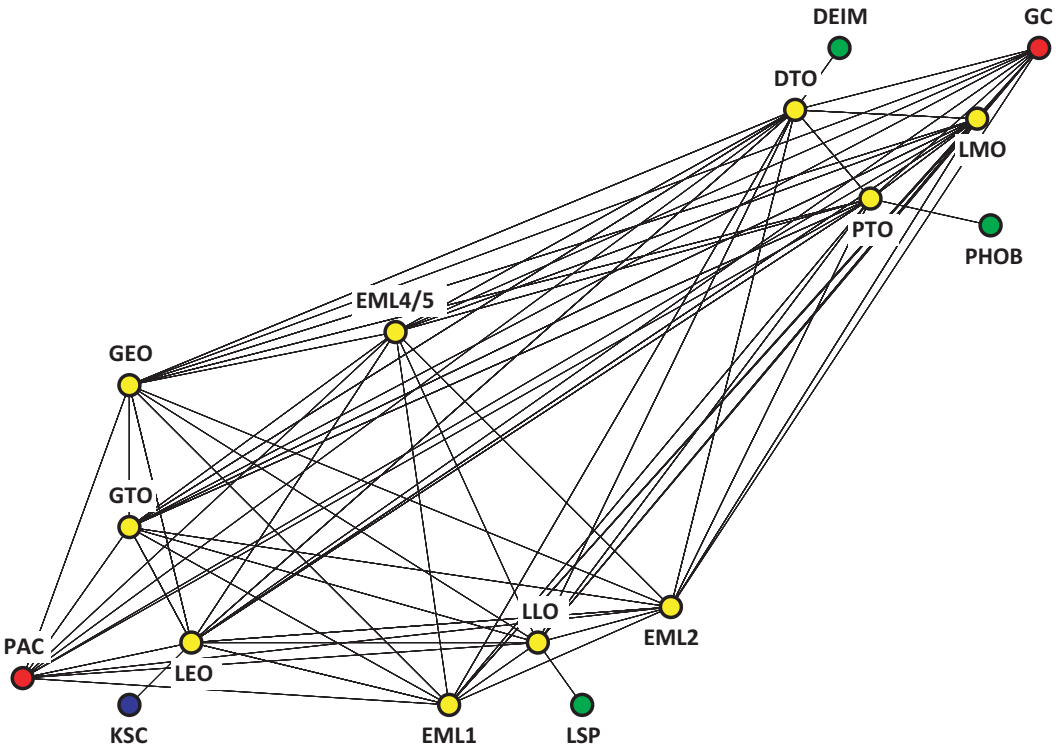

Figure 4-3: Network graph with 16 nodes and 357 edges (including 9 loops)

individually translated into the $\boldsymbol{ABC}$ matrices. In total, there are 357 directed edges including 9 loops. However, note that not necessarily all nodes and edges will be used in the optimal solution.

4.2.2 Decision Variables and Objective Functions

First, decision variables included in the flow vector and an objective function need to be selected. In the GMCNF model, everything that moves around the network (even the crew) is referred to as a "commodity". Using Figure 1-2 as a reference, the decision variables can be divided into the following categories:

$$\boldsymbol{x}_{ij}^{\pm} = \begin{bmatrix} \text{crew} \\ \text{transportation} \\ \text{resources} \\ \text{infrastructure} \end{bmatrix}_{ij}^{\pm} \tag{4.1}$$

Each category has sub-classes as follows:

$$\text{crew} = \begin{bmatrix} \text{crew} \\ \text{crewRe} \end{bmatrix} \tag{4.2a}$$

$$\text{transportation} = \begin{bmatrix} \text{vehicle} \\ \text{habitat} \\ \text{inertLOX} \\ \text{inertNTR} \\ \text{aeroshell} \end{bmatrix} \tag{4.2b}$$

$$\text{resources} = \begin{bmatrix} \text{hydrogen} \\ \text{oxygen} \\ \text{water} \\ \text{food} \\ \text{waste} \end{bmatrix} \tag{4.2c}$$

$$\text{infrastructure} = \begin{bmatrix} \text{plant} \\ \text{maintenance} \end{bmatrix} \tag{4.2d}$$

where "crewRe" represents crew returning to Earth distinguished from crew traveling outbound (the reason for this is described later), "transportation" includes a crew transfer vehicle, a surface habitat, an inert mass for LOX/LH_2 and NTR (separately defined), and an aeroshell system, "resources" includes hydrogen, oxygen, water as well as crew provisions and waste, and "infrastructure" represents an ISRU plant and maintenance mass. These variables are all evaluated in mass [kg].

While we could define any objective function with respect to which the network flow is optimized, we simply use the total mass to be launched from Earth, which in this case study is Kennedy Space Center (KSC). Using the notation of the GMCNF model in Eq. (2.10), this can be written as:

$$\boldsymbol{c}_{ij}^{+} = \begin{cases} \mathbf{1} & \text{for } i = \text{KSC} \\ \mathbf{0} & \text{otherwise} \end{cases} \qquad \text{and} \qquad \boldsymbol{c}_{ij}^{-} = \mathbf{0} \quad \forall\,(i,j) \in \mathcal{A} \tag{4.3}$$

where $\mathbf{1}$ and $\mathbf{0}$ are vectors. Since KSC is only connected to LEO, this is essentially equivalent to initial mass in LEO (IMLEO), which is often used as a measure of the mission cost as a widely accepted surrogate for estimating it.

4.2.3 Supply and Demand

Next we define supply/demand $\boldsymbol{b}_i$ at each node. In the network in Figure 4-3, Kennedy Space Center (KSC), the lunar south pole (LSP), Phobos (PHOB), Deimos (DEIM), and Gale Crater (GC) on Mars are the supply nodes (sources). While KSC can provide all the commodities in Eqs. (4.2), the other nodes can only provide resources such as hydrogen,

oxygen, and water. Surface manufacturing with in-situ resources has also been proposed but this case study only considers resource production [40, 44]. We assume that KSC has an infinite supply of all the commodities except for "crewRe". For the ISRU nodes, raw materials are infinitely available but the amount of resources produced depends on the capacity of the ISRU system. For this reason, we must enforce some constraint on this instead of setting the supply of resources to infinity. As explained earlier in Section 2.4.1, a facility is modeled as a loop edge. ISRU can be modeled in this way: when a plant of a mass of x is sent into a loop edge, it returns the flow that includes a resource of a mass of βx, where β is a proportional constant. There is an assumption behind this that the ISRU plant is linearly scalable. This is why we explicitly include "plant" in the decision variables. If we utilize the ISRU system somewhere, we can produce resources depending on the size of the plant but at the same time we must continuously supply the maintenance to the plant, which is also explicitly included in the variables. The details of the ISRU modeling is discussed later in Sections 4.2.4 and 4.2.5.

Defining the demand itself is essentially identical to defining the mission. If we have a demand of "plant" at LSP, it is a lunar mission to send a plant on the lunar south pole; if we have a demand of "crew" on Mars, it is a manned mission to Mars. In this thesis we choose human exploration of Mars as a case study and the demand is determined by reference to Mars DRA 5.0 [59]. While the mission objectives of Mars DRA 5.0 range from science such as search for life, current and ancient climate, geology and geophysics to engineering such as long-duration human spaceflight and sustained human presence on Mars, the mission from a logistics perspective is to send crew of six to Martian surface and to bring them back to Earth after about 500 days of stay on Mars. We have the demand of "crewRe" at PAC instead of having the demand of "crew" at GC (if we set the demand of "crew" at GC, it is interpreted as a one-way mission or the outbound portion of a decoupled problem). Therefore we do not have the demand of "crew" on Mars, but we must also deploy the surface habitat (SHAB) that supports the crew for the long stay on the surface of Mars. Unlike the crew, the SHAB would not be brought back to Earth or would even be useful for the subsequent human presence on Mars. Hence, we translate it into the demand of "habitat" at GC. Table A.1 in Appendix A provides a summary of the surface systems in the Mars DRA 5.0 scenario. The total mass of the surface systems amounts to 51,700 kg and we use this value in a lump as a demand of "habitat" on the surface of Mars. There

is no need to define other demands such as crew consumables or ISRU maintenance mass because these commodities are required or "consumed" through the requirement matrix $\boldsymbol{A}_{ij}^{\pm}$, transformation matrix $\boldsymbol{B}_{ij}$, and concurrency matrix $\boldsymbol{C}_{ij}^{\pm}$. All the orbital nodes (yellow nodes in Figure 4-3) are transshipment nodes and therefore we have $\boldsymbol{b}_i = \boldsymbol{0}$ for them.

4.2.4 Requirement Matrix $\boldsymbol{A}_{ij}^{\pm}$

The requirement matrix $\boldsymbol{A}_{ij}^{\pm}$ appears in the mass balance constraint:

$$\sum_{j:(i,j)\in\mathcal{A}} \boldsymbol{A}_{ij}^{+}\boldsymbol{x}_{ij}^{+} - \sum_{j:(j,i)\in\mathcal{A}} \boldsymbol{A}_{ji}^{-}\boldsymbol{x}_{ji}^{-} \leq \boldsymbol{b}_i \qquad \forall\ i \in \mathcal{N} \tag{4.4}$$

In this case, the requirement matrix $\boldsymbol{A}_{ij}^{\pm}$ is only used in one way: ISRU plant requiring maintenance mass. This involves a loop edge modeling facility and there is no requirement matrix for a regular edge.

ISRU Plant and Maintenance Mass

An ISRU system generally includes a power system, a tanker, and a terrain management vehicle as well as a plant. Once an ISRU system is deployed, the maintenance task arises. In this study we assume that the ISRU system is automated or can be teleoperated and that maintenance mass required is a linear function of the total ISRU system mass including ISRU plant and support elements. Hence, if a large ISRU system is deployed, it can produce a large amount of resources but at the same time it requires a large maintenance mass. If α is the proportional constant, then this can be written as:

$$\boldsymbol{A}_{ii}^{+}\boldsymbol{x}_{ii}^{+} = \begin{bmatrix} 1 & 0 \\ \alpha & 1 \end{bmatrix}_{ii}^{+} \begin{bmatrix} \text{plant} \\ \text{maintenance} \end{bmatrix}_{ii}^{+} \tag{4.5}$$

Note that only relevant variables are shown and the $\boldsymbol{A}_{ii}^{+}$ portion corresponding to the rest variables is an identity matrix. For the α value, we use 10% of the total ISRU system mass per year, which is a conservative assumption.

4.2.5 Transformation Matrix $\boldsymbol{B}_{ij}$

The transformation matrix $\boldsymbol{B}_{ij}$ literally models the flow transformation between commodities on an edge:

$$\boldsymbol{B}_{ij}\boldsymbol{x}_{ij}^{+} = \boldsymbol{x}_{ij}^{-} \qquad \forall\,(i,j) \in \mathcal{A} \tag{4.6}$$

In contrast to the $\boldsymbol{A}_{ij}^{\pm}$ matrix, the transformation matrix $\boldsymbol{B}_{ij}$ is used in many ways, a few of which has been presented in Section 2.3.3. They include propulsive burn, resource boil-off, crew consumables consumption and waste generation, ISRU resource production, electrolysis and synthesis of water, and Mars surface stay.

Propulsive Burn

As described in Section 2.3.3, this involves the propellant mass fraction:

$$\phi_{ij} = 1 - \exp\left(-\frac{\Delta V_{ij}}{I_{\mathrm{sp}} g_0}\right) \tag{4.7}$$

where ΔV_{ij} is the change in the vehicle's velocity on edge (i,j), I_{sp} is the specific impulse, and g_0 is the standard gravity. Since in this case study we consider chemical propulsion using LOX/LH_2 and NTR, it is suffice to include hydrogen and oxygen as a propellant. Let μ be the mixture ratio of oxidizer to fuel. Then we have

$$\boldsymbol{x}_{ij}^{\pm} = \begin{bmatrix} \text{dry mass} \\ \text{hydrogen} \\ \text{oxygen} \end{bmatrix}_{ij}^{\pm} \qquad \boldsymbol{B}_{ij} = \begin{bmatrix} 1 & 0 & 0 \\ -\dfrac{\phi}{1+\mu} & 1-\dfrac{\phi}{1+\mu} & -\dfrac{\phi}{1+\mu} \\ -\dfrac{\mu\phi}{1+\mu} & -\dfrac{\mu\phi}{1+\mu} & 1-\dfrac{\mu\phi}{1+\mu} \end{bmatrix}_{ij} \tag{4.8}$$

where `"dry mass"` includes the commodities other than hydrogen and oxygen.

We assume $I_{\mathrm{sp}} = 450$ [s] for LOX/LH_2 with the mixture ratio of $\mu = 6.0$ and $I_{\mathrm{sp}} = 900$ [s] for NTR. NTR only uses liquid hydrogen but Eq. (4.8) still holds by setting $\mu = 0$. The ΔV_{ij} value for each edge is listed in Figure A-1 in Appendix A [13, 61, 62].

Resource Boil-Off

The cryogenic propellant is lost to boil-off during transport or loiter time. Let r_{bo} be the boil-off rate per unit time. If Δt_{ij} is the duration of edge (i,j), then for any relevant

commodity,

$$(1 - r_{\text{bo}})^{\Delta t_{ij}}\, x_{ij}^{+} = x_{ij}^{-} \tag{4.9}$$

While the thermal environment varies in different locations, we use $r_{\text{bo}} = 0.127\%$ per day ($\simeq 3.81\%$ per month) for liquid hydrogen and $r_{\text{bo}} = 0.016\%$ per day ($\simeq 0.49\%$ per month) for liquid oxygen. The times of flight (TOFs) are provided in Figure A-2 in Appendix A.

Crew Consumables Consumption and Waste Generation

During spaceflight, consumables such as oxygen, water, and food are consumed and waste is generated by the crew. Let c and w be the consumables consumption and the waste generation per unit crew member per unit time, respectively. Then we have

$$\boldsymbol{x}_{ij}^{\pm} = \begin{bmatrix} \text{crew} \\ \text{consumables} \\ \text{waste} \end{bmatrix}_{ij}^{\pm} \qquad \boldsymbol{B}_{ij} = \begin{bmatrix} 1 & 0 & 0 \\ -c\Delta t_{ij} & 1 & 0 \\ w\Delta t_{ij} & 0 & 1 \end{bmatrix}_{ij} \tag{4.10}$$

While the net consumption of consumables depends on the ECLSS system and closure rate, we assume that each crew member consumes 0.88 kg of oxygen, 2.90 kg of water, and 1.83 kg of food, and generates 5.61 kg of waste a day. Since the total mass of consumables consumed is equal to the total mass of waste generated ($c = w$), mass is not lost in this transformation. Oxygen is also lost due to leakage from the vehicle. We assume that the spacecraft loses 0.000123 kg of oxygen per vehicle volume in cubic meters per day. These values were derived from the Jet Propulsion Laboratory (JPL) space logistics consumables model, in which the ECLSS closure rate is set to 90%.

ISRU Resource Production

ISRU resource production is modeled as a loop edge. Since we assume a linear scalability between the resource production and the ISRU system mass with a proportional constant β, then we have

$$\boldsymbol{x}_{ii}^{\pm} = \begin{bmatrix} \text{plant} \\ \text{resources} \end{bmatrix}_{ii}^{\pm} \qquad \boldsymbol{B}_{ij} = \begin{bmatrix} 1 & 0 \\ \beta & 1 \end{bmatrix}_{ii} \tag{4.11}$$

Putting this and Eq. (4.5) together, if an ISRU plant of a mass of x is deployed, it re-

quires maintenance mass of αx and produces resources of βx. For the β value, we assume an ISRU annual production rate of 10 kg per unit ISRU plant mass. For example, if we deploy an ISRU plant of 1,000 kg, it produces resources of 10,000 kg per year. However, this assumption might be somewhat optimistic even if expecting technological advancement in the future. Therefore, a lower ISRU production rate is also attempted later.

Electrolysis and Synthesis of Water

We also implement the water electrolysis capability using a loop edge. We know molecular masses of hydrogen, oxygen, and water are 1.00794, 15.9994, and 18.01528, respectively. Therefore, the water electrolysis can be expressed as:

$$\boldsymbol{x}_{ii}^{\pm} = \begin{bmatrix} \text{hydrogen} \\ \text{oxygen} \\ \text{water} \end{bmatrix}_{ii}^{\pm} \qquad \boldsymbol{B}_{ij} = \begin{bmatrix} 0.1119 & 0 & 0 \\ 0 & 0.8881 & 0 \\ 0 & 0 & 0 \end{bmatrix}_{ii} \tag{4.12}$$

which means unit mass of water is electrolyzed into 0.1119 of hydrogen and 0.8881 of oxygen. On the other hand, synthesis of water can also be modeled using $\boldsymbol{A}_{ii}^{+}$ and $\boldsymbol{B}_{ii}$ matrices. These capabilities of electrolysis and synthesis of water only give us an option and they are not necessarily used.

Mars Surface Stay

Lastly, Mars surface stay is implemented as a loop edge associated with the node of Gale Crater (GC). Since Mars DRA 5.0 assumes 500 days of surface stay, we set the duration of this loop edge to 500 days. Like other edges with duration, resource boil-off and crew consumables consumption/waste generation occur in this loop as well. The only difference with this loop is the transformation of `"crew"` into `"crewRe"`:

$$\boldsymbol{x}_{ii}^{\pm} = \begin{bmatrix} \text{crew} \\ \text{crewRe} \end{bmatrix}_{ii}^{\pm} \qquad \boldsymbol{B}_{ij} = \begin{bmatrix} 0 & 0 \\ 1 & 1 \end{bmatrix}_{ii} \tag{4.13}$$

Note that it does not represent any actual event or physical process but it just means that the crew is ready for return trip. It is rather a mathematical trick for modeling purposes, serving as a `"switch"`. As stated in Section 4.2.3, there is a demand of `"crewRe"` at PAC.

In order to satisfy this demand, "crew" must first go to Mars, stay there for 500 days to switch to "crewRe", and come back to Earth. This is the reason why we define "crew" and "crewRe" separately. Without this distinction and a "switch" loop, it would end up satisfying this demand with merely "a round trip to LEO". By implementing this switch at a specific node, we can model a round trip mission to that node.

As discussed in Section 2.3.3, when there are multiple flow transformation events on a single edge, $\boldsymbol{B}_{ij}$ is expressed as the product of multiple matrices, in which the subsequent transformation matrix is multiplied from the left.

$$\boldsymbol{B}_{ij} = \boldsymbol{B}_{ij}^{(n)} \cdots \boldsymbol{B}_{ij}^{(2)} \boldsymbol{B}_{ij}^{(1)} \tag{4.14}$$

In general, a non-diagonal matrix is not commutative. Therefore, if there are interactions between different commodities, that is, $\boldsymbol{B}_{ij}$ matrices have off-diagonal entries, then the order of matrix multiplication must be exactly the sequence of transformation events.

4.2.6 Concurrency Matrix $\boldsymbol{C}_{ij}^{\pm}$

The concurrency matrix $\boldsymbol{C}_{ij}^{\pm}$ represents the constraint between commodities within an edge in the form:

$$\boldsymbol{C}_{ij}^{+}\boldsymbol{x}_{ij}^{+} \leq \boldsymbol{0} \quad \text{and} \quad \boldsymbol{C}_{ij}^{-}\boldsymbol{x}_{ij}^{-} \leq \boldsymbol{0} \qquad \forall\,(i,j) \in \mathcal{A} \tag{4.15}$$

The concurrency matrix $\boldsymbol{C}_{ij}^{+}$ is used in three ways: crew transfer vehicle, structural mass for propellant, and aeroshell.

Crew Transfer Vehicle

When the crew transfers from node to node, a vehicle to shelter them must travel along with them. Especially for a long-duration interplanetary transfer, they need a "transit habitat" with the appropriate ECLSS system. If we define a minimum vehicle mass per crew member (denoted γ), then we have

$$[\gamma m_{\text{crew}}]_{ij}^{\pm} \leq [m_{\text{vehicle}}]_{ij}^{\pm} \tag{4.16}$$

This can be rewritten in the form of $\boldsymbol{C}_{ij}^{\pm}$ as:

$$\boldsymbol{x}_{ij}^{\pm} = \begin{bmatrix} \text{crew} \\ \text{vehicle} \end{bmatrix}_{ij}^{\pm} \qquad \boldsymbol{C}_{ij}^{\pm} = \begin{bmatrix} \gamma & -1 \end{bmatrix}_{ii} \tag{4.17}$$

Table A.2 in Appendix A provides a summary of Mars transit habitat (MTH) in the Mars DRA 5.0 scenario. The total mass of MTH amounts to 37,540 kg and we use this value in a lump as a minimum vehicle mass when the crew transfers on an in-space edge. For other transfer edges such as launch, entry, descent, and ascent, we assume that the crew at least needs the crew exploration vehicle (CEV) that weighs 10,000 kg. The MTH and CEV are designed to accommodate crew of six.

Structural Mass for Propellant

Likewise, propellant cannot travel by itself; it needs "structure". The ratio of structure mass to propellant mass is defined using the inert mass fraction:

$$\eta \equiv \frac{m_{\text{st}}^{+}}{m_{\text{pr}}^{+}} = \frac{f_{\text{inert}}}{1 - f_{\text{inert}}} \tag{4.18}$$

If we have 1 unit of propellant, we must carry at least η units of structure along with it. Then we have

$$\boldsymbol{x}_{ij}^{+} = \begin{bmatrix} \text{propellant} \\ \text{inert} \end{bmatrix}_{ij}^{+} \qquad \boldsymbol{C}_{ij}^{+} = \begin{bmatrix} \eta & -1 \end{bmatrix}_{ij}^{+} \tag{4.19}$$

which is equivalent to

$$[\eta m_{\text{pr}}]_{ij}^{+} \leq [m_{\text{st}}]_{ij}^{+} \tag{4.20}$$

We handle inert mass for LOX/LH_2 and NTR separately because these two different propulsion systems cannot share the same structure. In this case study, we assume $f_{\text{inert}} = 0.08$ for LOX/LH_2 (0.15 for ascent/descent) and $f_{\text{inert}} = 0.30$ for NTR.

Aeroshell

For Mars arrival or Earth arrival, aerobraking is available with an aeroshell. Since aerobraking is an option, this is modeled as a parallel edge separately from an transfer edge without aerobraking. In total, there are 4 parallel edges between the same end nodes: LOX/LH_2 with/without aerobraking and NTR with/without aerobraking. Let θ denote the aeroshell

mass fraction, meaning that when a spacecraft with a mass of 1 performs aerobraking, it must have an aeroshell with a mass of θ. Then we have

$$\boldsymbol{x}_{ij}^{-} = \begin{bmatrix} \text{spacecraft} \\ \text{aeroshell} \end{bmatrix}_{ij}^{-} \qquad \boldsymbol{C}_{ij}^{-} = \begin{bmatrix} \theta & -1 \end{bmatrix}_{ij}^{-} \tag{4.21}$$

which is equivalent to

$$[\theta m_{\text{sc}}]_{ij}^{-} \leq [m_{\text{as}}]_{ij}^{-} \tag{4.22}$$

We assume that when performing aerobraking, spacecraft needs aeroshell with a mass of about 15% of the total mass being braked. Note that aerobraking is performed at arrival so that this is an "inflow" concurrency constraint (with a superscript of "$-$").

All we need for implementing the GMCNF model has been presented up to this point. The following section discusses the optimization results.

4.3 Optimization Results and Discussions

This section presents the optimizations results, followed by the discussions. First we solve the baseline problem and compare the result with the Mars DRA 5.0 scenario, focusing on the difference in the initial mass in low-Earth orbit (IMLEO) and the utilization of infrastructure network. Then we change the problem settings, assumptions, and conditions and perform a sensitivity analysis to find the key drivers and thresholds.

As described in Chapter 3, in this case study the GMCNF LP problem is solved using the CPLEX `cplexlp` function within MATLAB. Unlike the MILP problem presented in Chapter 5, the LP problem does not need much computational effort in general. Using a normal store-bought laptop computer with average specs as of 2013, one instance can be solved within 10 seconds. Therefore it is easy to try many different instances, which greatly helps us in debugging, tuning the problem settings, and performing a sensitivity analysis.

4.3.1 Baseline Problem

In the baseline problem we use the same problem setting as the Mars DRA 5.0 scenario. Again the mission objective of Mars DRA 5.0 in a logistics language is to send crew of six and the surface systems presented in Table A.1 to the Martian surface and to bring the crew back to Earth after 500 days of surface stay. We translate this objective into the demand for "habitat" of 51,700 kg at GC and "crewRe" of 600 kg at PAC (assuming 100 kg per crew member). The supply of each commodity is set to infinity at KSC except for "crewRe". In order to make a fair comparison with the Mars DRA 5.0 scenario, we impose an additional condition that we can only use LOX/LH_2 for launch to LEO. In other words, NTR is only allowed in space, which somewhat reflects the political concern about nuclear propulsion.

One important thing to note about this model is that it simulates a static network flow. It does not consider the time evolution of the network flow or the network topology. Therefore, for example, if we obtain the optimization result that utilizes ISRU systems, it assumes that the ISRU system is already deployed and ready to produce resources from the beginning. In other words, it is equivalent to computing a network flow in the "post-deployment" phase. While this model does not consider time evolution, we can arbitrarily define the scope of problem, that is, the time period to be considered. By defining a time

period for a network flow, the network flow actually represents the flow rate. If the time period is one day, the network flow is a daily flow; if the time period is one year, the network flow is an annual flow. This can be different from the mission duration, which is about 860 days (180 days on the outbound leg + 500 days on Mars + 180 days on the return leg). While we can choose any length of time for the scope of the problem, it is reasonable to use the lifetime of the ISRU system because we can easily evaluate the life-cycle cost performance of the ISRU system.

Then the question is how long the lifetime of the ISRU system is. It is unlikely that the ISRU system would last for 10 years because, for example, with each passing year, the local ice field around the plant is getting depleted and the rovers transporting regolith to the processing unit must travel greater distances. It might be difficult to keep the constant resource production rate for a long time. Also these working rovers are constantly excavating and transporting regolith and are likely to be worn out quickly. Thus we assume 5 years as the lifetime of the ISRU system, or a reasonable length of time during which the ISRU plant keeps the same pace of resource production.

The network graph (Figure 4-3) consists of 16 nodes and 357 directed edges including 9 loops in total. There are 14 types of commodities as in Eqs. (4.2). Using the notations in the previous chapters, we have the number of nodes ($n = 16$), the number of edges ($m = 357$), the number of types of commodities ($k = 14$), and the maximum number of concurrency constraints ($l = 2$). Hence, this problem has 9996 variables, 1652 inequality constraints, and 4998 equality constraints, in addition to 9996 nonnegativity constraints. Again the objective function is the total mass to be launched from Earth (KSC). Since it includes the ISRU plant and maintenance mass (not only the portion for a crew mission to Mars), it serves as a comprehensive performance indicator. Table 4.1 summarizes the assumptions that have been presented in the previous sections. All the parameter values used in the analysis are presented in Figures A-1 and A-2 as well as Table 4.1.

After about 10 seconds of computation, the problem is successfully solved and the optimal solution turns out to be 2,377,746 kg. The corresponding total IMLEO is 276.0 t. In the Mars DRA 5.0, two reference scenarios are presented: NTR vs. chemical/aerocapture option for in-space transportation [59]. The estimated total IMLEOs are 848.7 t for reference NTR and 1,251.8 t for reference chemical/aerocapture, respectively. The former is equivalent to 9 Ares V launches while the latter is equivalent to 12 Ares V launches. If

Table 4.1: Summary of assumptions used in the analysis

Parameter	Assumed Value
Scope of problem	5 years
Mission data	
Number of crew	6
Mass per crew member	100 [kg]
Mars Transit Habitat (MTH)	27,540 [kg]
Crew Exploration Vehicle (CEV)	10,000 [kg]
Surface Habitat (SHAB)	51,700 [kg]
Propulsion system	
Chemical rocket (LOX/LH_2)	
Specific impulse I_{sp}	450 [s]
Mixture ratio μ	6.0
Inert mass fraction f_{inert}	0.08 (0.15 for descent/ascent)
Nuclear thermal rocket (NTR)	
Specific impulse I_{sp}	900 [s]
Inert mass fraction f_{inert}	0.30
Boil-off rate r_{bo}	
Hydrogen	0.127% per day ($\simeq$ 3.81% per month)
Oxygen	0.016% per day ($\simeq$ 0.49% per month)
Aeroshell mass fraction θ	15% of total mass being braked
Crew consumables consumption	
Oxygen	0.88 [kg] per crew member per day
Water	2.90 [kg] per crew member per day
Food	1.83 [kg] per crew member per day
Waste generation	5.61 [kg] per crew member per day
Oxygen leakage from vehicle	0.000123 [kg] per vehicle volume per day
ISRU system	
Resource production rate	10 [kg] per plant mass per year
Maintenance mass required	10% of plant mass per year

we simply compare the total IMLEOs, the optimal solution saves 67.5% from the reference NTR scenario and 78.0% from the reference chemical/aerocapture scenario. Figure 4-4 shows the major flows of any of the 14 types of commodities of the baseline solution in bold lines on a single network graph. Table 4.2 lists the amount of each commodity on the edges used in the baseline solution (bold lines in Figure 4-4). Putting aside the actual feasibility, it is interesting that the resources produced on Deimos are delivered back to LEO, GTO, and EML2 to be used in the cislunar system. This is probably because Deimos is a little closer to part of the cislunar system than the lunar surface in terms of ΔV (see Figure A-1). Let us investigate the flows of `"crew"`, `"crewRe"`, and `"plant"` separately.

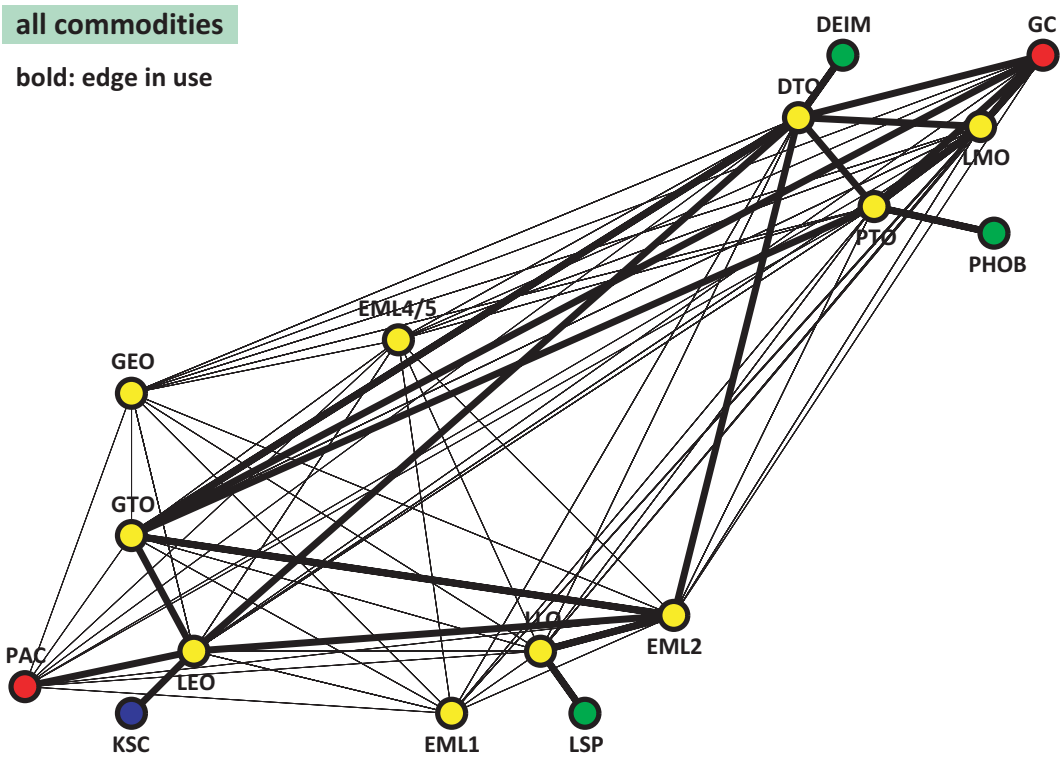

Figure 4-4: Flows of all commodities of the baseline solution

Table 4.2: Commodity delivered through each edge in the baseline solution

from	to	prop.	aero?	vehicle	habitat	crew	crewRe	hydrogen	oxygen	water	food	waste	inertLOX	inertNTR	aeroshell	plant	mainte.
KSC	LEO	LOX/LH_2	NO	10000	51700	600	0	0	0	0	9509	34	182561	0	1768	13239	6619
LEO	GTO	LOX/LH_2	NO	37540	51700	600	0	0	0	0	9487	34	16648	0	27977	13239	6619
LEO	PAC	LOX/LH_2	YES	10000	0	0	600	0	0	0	0	34	2	0	1595	0	0
GTO	EML2	LOX/LH_2	NO	0	0	0	0	0	0	0	0	0	1589	0	2936	4821	2411
GTO	DTO	LOX/LH_2	YES	37540	0	600	0	0	0	0	1987	6059	15963	0	25445	4856	2428
GTO	PTO	LOX/LH_2	YES	0	45565	0	0	0	0	0	5523	0	7196	0	9306	2504	1252
GTO	GC	LOX/LH_2	YES	0	6135	0	0	0	0	0	0	0	279	0	1200	1057	529
LSP	LLO	LOX/LH_2	NO	0	0	0	0	23550	11142	0	0	0	10312	0	0	0	0
LLO	LSP	LOX/LH_2	NO	0	0	0	0	0	0	0	0	0	10322	0	0	4821	2411
LLO	EML2	LOX/LH_2	NO	0	0	0	0	21665	0	0	0	0	2209	0	0	0	0
EML2	LEO	LOX/LH_2	YES	0	0	0	0	17843	0	0	0	0	1710	0	2933	0	0
EML2	GTO	LOX/LH_2	NO	0	0	0	0	3137	0	0	0	0	345	0	0	0	0
EML2	LLO	LOX/LH_2	NO	0	0	0	0	0	0	0	0	0	2231	0	0	4821	2411
DTO	LEO	LOX/LH_2	YES	37540	0	0	600	0	107070	35	0	6059	14707	0	24902	0	0
DTO	GTO	LOX/LH_2	YES	0	0	0	0	6000	55799	3132	0	0	8059	0	10948	0	0
DTO	EML2	LOX/LH_2	NO	0	0	0	0	0	3473	0	0	0	493	0	0	0	0
DTO	DEIM	LOX/LH_2	NO	0	0	0	0	0	0	0	0	0	42847	0	0	4856	2428
DTO	LMO	LOX/LH_2	YES	27540	0	0	0	0	0	0	0	0	1	0	4131	0	0
DTO	GC	NTR	YES	10000	0	600	0	0	0	0	0	34	0	8	1596	0	0
DEIM	DTO	LOX/LH_2	NO	0	0	0	0	20450	174080	6316	0	0	42804	0	0	0	0
PTO	DTO	LOX/LH_2	NO	37540	0	0	600	0	75551	0	0	34	7405	8	16174	0	0
PTO	PHOB	LOX/LH_2	NO	0	0	0	0	0	0	0	0	0	22094	0	0	2504	1252
PTO	LMO	LOX/LH_2	YES	0	0	0	0	1848	0	17	11	0	162	0	306	0	0
PTO	LMO	NTR	YES	0	0	0	0	0	11092	0	0	0	0	1	1664	0	0
PTO	GC	LOX/LH_2	YES	0	45565	0	0	8049	0	0	5501	0	701	0	8972	0	0
PHOB	PTO	LOX/LH_2	NO	0	0	0	0	11737	97618	35	0	0	22072	0	0	0	0
LMO	PTO	LOX/LH_2	NO	37540	0	0	600	0	0	0	0	34	1125	9	17837	0	0
LMO	GC	LOX/LH_2	YES	0	0	0	0	0	0	0	0	0	7762	0	1164	0	0
GC	LMO	LOX/LH_2	NO	10000	0	0	600	0	0	0	0	34	8733	8	12920	0	0

Figures 4-5 shows the flow of "crew" and Figure 4-6 shows the flow of "crewRe". The flow of crew represents the route that the crew takes in the network. Since we have implemented the concurrency constraint that the vehicle must travel along with the crew, then the route that the crew takes is identical to the route that the vehicle takes. Therefore these figures can simply be interpreted as how the crew goes to Mars and comes back to Earth. Since the crew vehicle headed for Mars is called the Mars transfer vehicle (MTV) in Mars DRA 5.0, it is referred to as the MTV hereafter.

As also noted in the figure, the red line represents transport using LOX/LH_2, the blue line represents transport using NTR, and the dashed line represents transport using aerobraking at arrival. In Figure 4-5, for example, the solid red line from LEO to GTO represents crew transport from LEO to GTO using LOX/LH_2 (all-propulsive) while the dashed blue line from DTO to GC represents crew transport from DTO to GC using NTR with aerobraking at arrival.

For the outbound leg in Figure 4-5, after launch to low-Earth orbit (LEO), the MTV first stops by at geostationary transfer orbit (GTO) and then is injected into the trans-Mars trajectory. At Mars arrival, the MTV also stops by at Deimos transfer orbit (DTO), followed by atmospheric entry. The crew spends 500 days on the surface. On the other hand, the crew vehicle returning to Earth is called the Earth return vehicle (ERV). For the return leg in Figure 4-6, after ascent to low Mars orbit (LMO), the ERV stops by at Phobos transfer orbit (PTO) and DTO like a "local train". Then the ERV is injected to trans-Earth trajectory to LEO, followed by atmospheric reentry and Pacific Ocean splashdown. As for the propulsion system, NTR is used only for the entry, descent, and landing (EDL) to GC and the rest uses LOX/LH_2. Also, aerobraking is used for orbit capture in DTO and entry to Martian atmosphere for the outbound leg, and for orbit capture in LEO and reentry to Earth atmosphere for the return leg. Therefore it turns out that except for EDL to GC, LOX/LH_2 is used throughout the mission.

It is also interesting to look at the flow of "plant", which is shown in Figure 4-7. We can see the ISRU plant is carried to all the surface nodes, which means that the ISRU plant is deployed in all the ISRU candidate locations. Table 4.3 lists the result of ISRU at each surface node. Note that we assume that water ice is available on the Moon, Deimos, and Phobos while oxygen is produced via Sabatier reaction on Mars. Putting aside the actual resource availabilities in these locations, it turns out that the largest ISRU plant is deployed

Table 4.3: ISRU at each surface node

	LSP	**DEIM**	**PHOB**	**GC**
ISRU plant deployed	4,821 [kg]	4,856 [kg]	2,504 [kg]	1,057 [kg]
Resources produced (5 years)	241,074 [kg]	242,799 [kg]	125,197 [kg]	52,858 [kg]
Maintenance required (5 years)	2,411 [kg]	2,428 [kg]	1,252 [kg]	529 [kg]

on Deimos, weighing 4,856 kg, the second largest is on the Moon, weighing 4,821 kg, the third largest is on Phobos, weighing 2,504 kg, and lastly the smallest is deployed on Mars, weighing 1,057 kg. The total amount of resources produced and maintenance mass required for 5 years are also listed in the table. Again, this production rate might be too aggressive. Other instances with lower production rates are described later in the next section. One interesting thing is that since all the ISRU plants are delivered through GTO, it serves as a hub in the network. This, along with the fact that the MTV's long trip to Mars also starts out from GTO, implies the importance of GTO in the network.

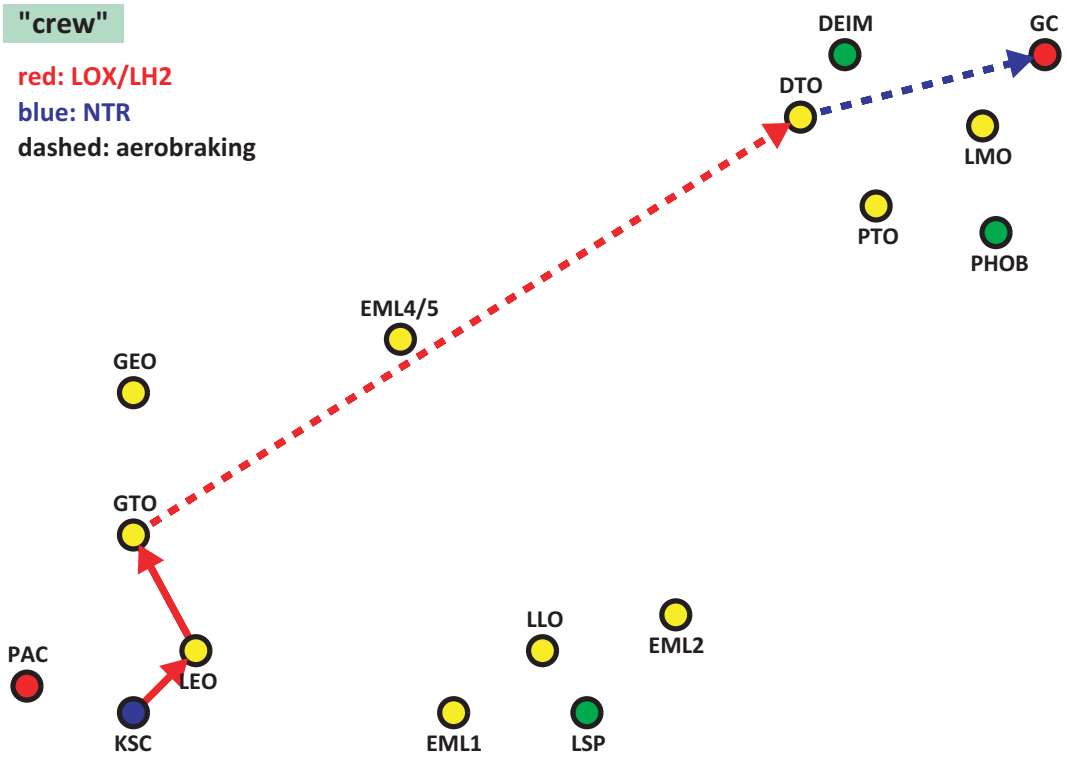

Figure 4-5: Flow of "crew" of the baseline solution

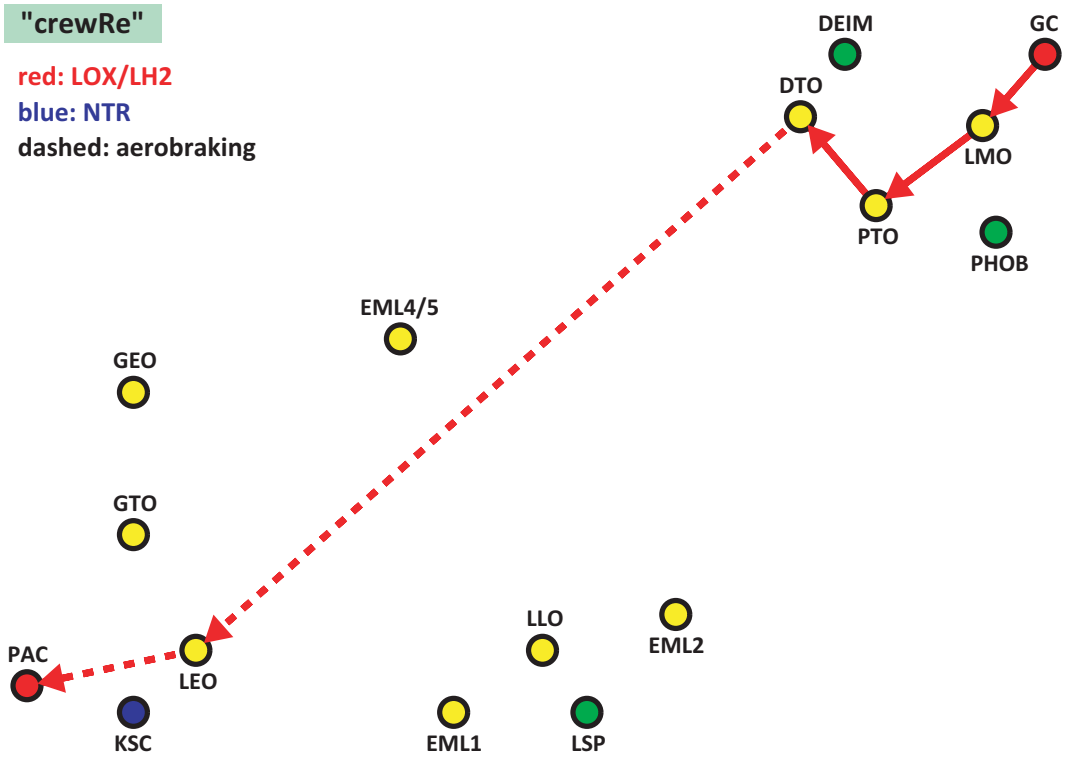

Figure 4-6: Flow of "crewRe" of the baseline solution

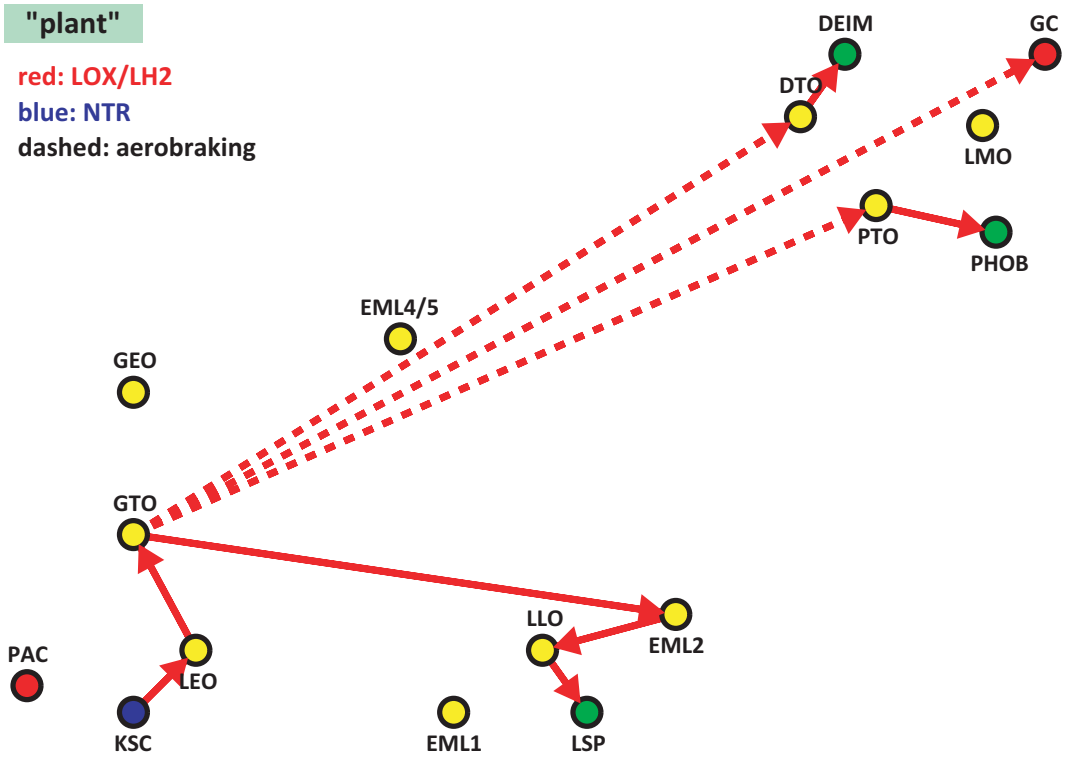

Figure 4-7: Flow of "plant" of the baseline solution

To summarize, it is found that the optimal solution makes the most use of ISRU in all the candidate locations. The ISRU plants are delivered to those locations as in Table 4.3, and in turn the resources produced are delivered to orbital nodes. The MTV stops by at each orbital node to refuel itself, instead of directly flying to Mars and back to Earth. One thing to note is that the solution is just a network flow and it does not indicate any concrete operation such as depots. The flow just converges and diverges at each node. Nodes at which the flow merges do not necessarily suggest fuel depots. Another interpretation of flow convergence and divergence could be that two vehicles rendezvous, fly together to some point, and separate. This is a "pickup bus" style.

One possible scenario that can be built from the flow information is shown in Figure 4-8. There are two resource depots in this scenario: one at GTO and the other at DTO. First the MTV is launched from KSC to LEO using NTR and rendezvous with an orbital transfer vehicle (OTV) at LEO. The OTV takes the MTV to a resource depot at GTO and the MTV refuels itself at the depot. This OTV and depot are maintained with the lunar resources produced at LSP as well as the Deimos resources produced at DEIM. Then the MTV is injected into trans-Mars trajectory and after 180 days it uses aerocapture to insert

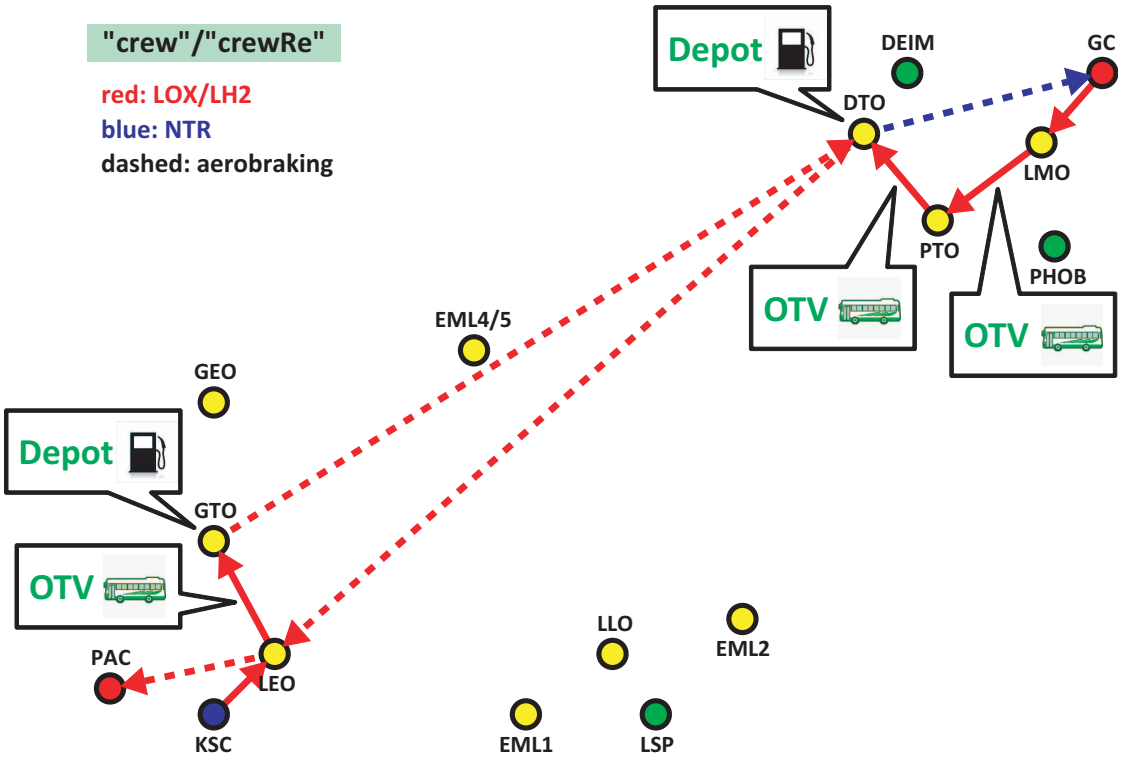

Figure 4-8: Example scenario for the baseline solution

itself into DTO to rendezvous with the other resource depot. This depot is supplied by Deimos and Phobos resources. Having refueled at the depot, the CEV performs EDL to GC using NTR with aerobraking. For the return leg, the crew ascends to LMO and gets aboard the ERV. Then another OTV takes the ERV to PTO. At PTO, the OTV refuels itself by Phobos resources or the ERV switches to yet another OTV. This is still disputable but the ERV somehow utilizes Phobos resources to get to the DTO depot, which is the same one as used in the outbound leg. Having refueled at this depot, the ERV is injected into trans-Earth trajectory and after 180 days it uses aerocapture to insert itself into LEO. Finally the crew aboard the CEV performs a reentry and splashes down in the Pacific Ocean (PAC). This is one example scenario that represents the network flow result of the baseline solution.

In Mars DRA 5.0, the reference NTR scenario is much better than the reference chemical/aerocapture scenario in terms of IMLEO, whereas in the optimal solution, while the chemical (LOX/LH_2) rocket is mainly used, the IMLEO is cut as much as 67.5% from the DRA 5.0 NTR scenario. As we have seen, the biggest reason is obviously ISRU. Since ISRU provides much oxygen and some hydrogen, it can be inferred that LOX/LH_2 is likely to

take advantage of ISRU because it heavily uses oxygen.

This is the baseline solution to the problem with the Mars DRA 5.0 demand. In the next section, we solve variant problems with different settings to investigate the effect of each factor.

4.3.2 Variant Problems

This section attempts several different settings and parameters. Based on the baseline problem presented in the previous section, we solve variant problems that have different settings or parameters in:

- Propulsion system
- ISRU availability
- Boil-off rate
- ISRU system lifetime
- ISRU resource production rate

We especially focus on how the total mass to be launched from KSC and the network topology vary with these factors.

Propulsion System

First we solve the problems with some limitations on propulsion systems. The two reference scenarios in Mars DRA 5.0 do not allow the combination use of chemical and nuclear thermal propulsions while the baseline solution in the previous section uses both. Therefore, we look at three cases: (1) LOX/LH_2 only with aerobraking option, (2) NTR only with aerobraking option, and (3) LOX/LH_2 and NTR without aerobraking option. Note that other parameters and assumptions remain the same.

Table 4.4 compares the results of these variants with the baseline solution. These variants are essentially the problems with limited options on propulsion systems so that the results never improve. As opposed to the Mars DRA 5.0 scenarios in which NTR is preferred to chemical, it turns out that the second best is (1) LOX/LH_2 with aerobraking. This is probably because ISRU can provide much oxygen, which greatly reduces the propellants that must be brought from Earth. NTR is two times better than LOX/LH_2 in specific impulse (I_{sp}) and this is the primary reason why NTR is preferred in Mars DRA 5.0. However, this result shows that ISRU oxygen production helps reduce the initial mass

Table 4.4: Comparison between different propulsion system settings

Scenario	Initial Mass at KSC ($\mathcal{J}$)	ISRU Plant			
		LSP	DEIM	PHOB	GC
Baseline Scenario	2,377,746 [kg]	4,821 [kg]	4,856 [kg]	2,504 [kg]	1,057 [kg]
(1) Chemical/Aerobrake	2,378,368 [kg]	4,822 [kg]	4,857 [kg]	2,510 [kg]	1,057 [kg]
(2) NTR/Aerobrake	3,797,386 [kg]	0 [kg]	27,088 [kg]	12,711 [kg]	208 [kg]
(3) Chemical/NTR	5,232,681 [kg]	27,794 [kg]	52,315 [kg]	8,272 [kg]	806 [kg]

at KSC more. On the other hand, the third variant without aerobraking option has the largest initial mass, which is more than twice that of the baseline scenario. In other words, the aerobraking option makes the most important contribution in saving the initial mass at KSC.

Table 4.4 also shows the size of ISRU plant deployed at each node. The first scenario with chemical/aerobrake results in almost the same allocation of the ISRU plants as in the baseline scenario, which makes sense because the baseline scenario relies mostly on LOX/LH_2 and ISRU oxygen. Figure 4-9 shows the path that the crew takes to Mars and back to Earth, which is nearly the same as the one in the baseline (Figure 4-8). The second scenario with NTR/aerobrake does not utilize the lunar resources while it heavily relies on Phobos and Deimos ISRU. Figure 4-10 illustrates the crew's route. This scenario tends to take a straightforward route except for a "local train" refueling in the Martian system. Lastly, the third scenario without aerobraking option turns out to heavily utilize the ISRU resources, especially from the lunar and Deimos surfaces. The outbound and return routes are illustrated in Figure 4-11, which is somewhat different from the previous ones. For the outbound leg, the MTV transfers from GTO to EML2 before injection into trans-Mars trajectory. In this scenario, a resource depot should be located in EML2 instead of GTO. It appears to be a detour but it actually is not as costly as it looks because the Oberth maneuver is available for trans-Mars injection from EML2.

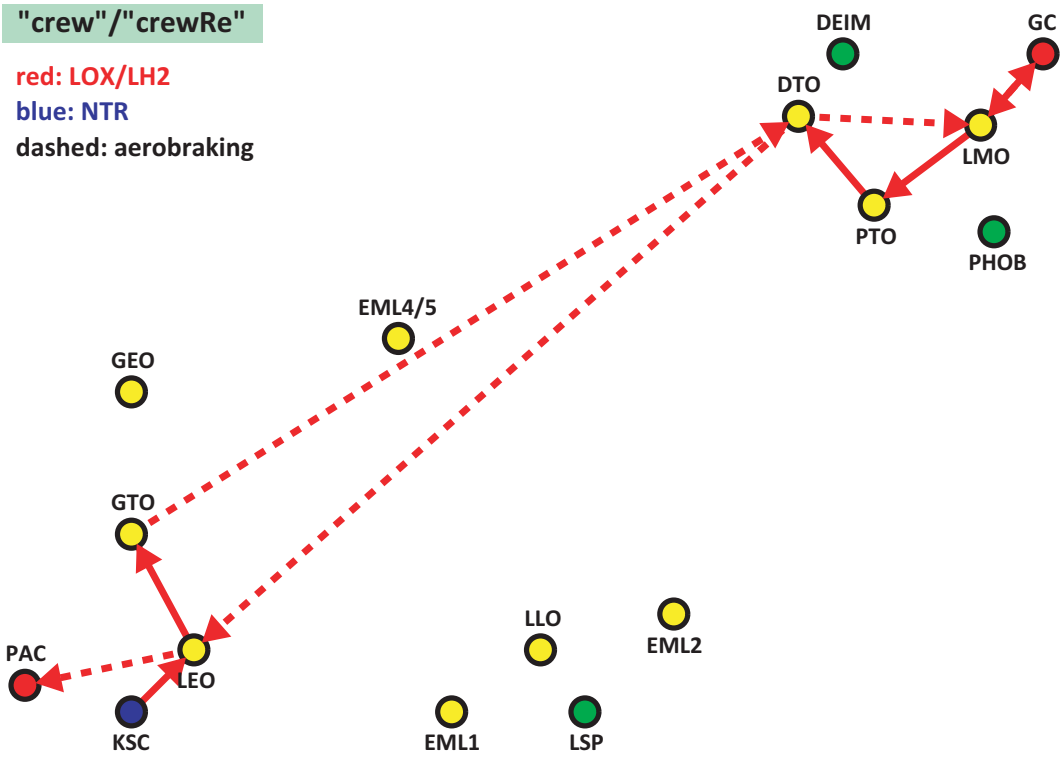

Figure 4-9: (1) LOX/LH_2 only with aerobraking option

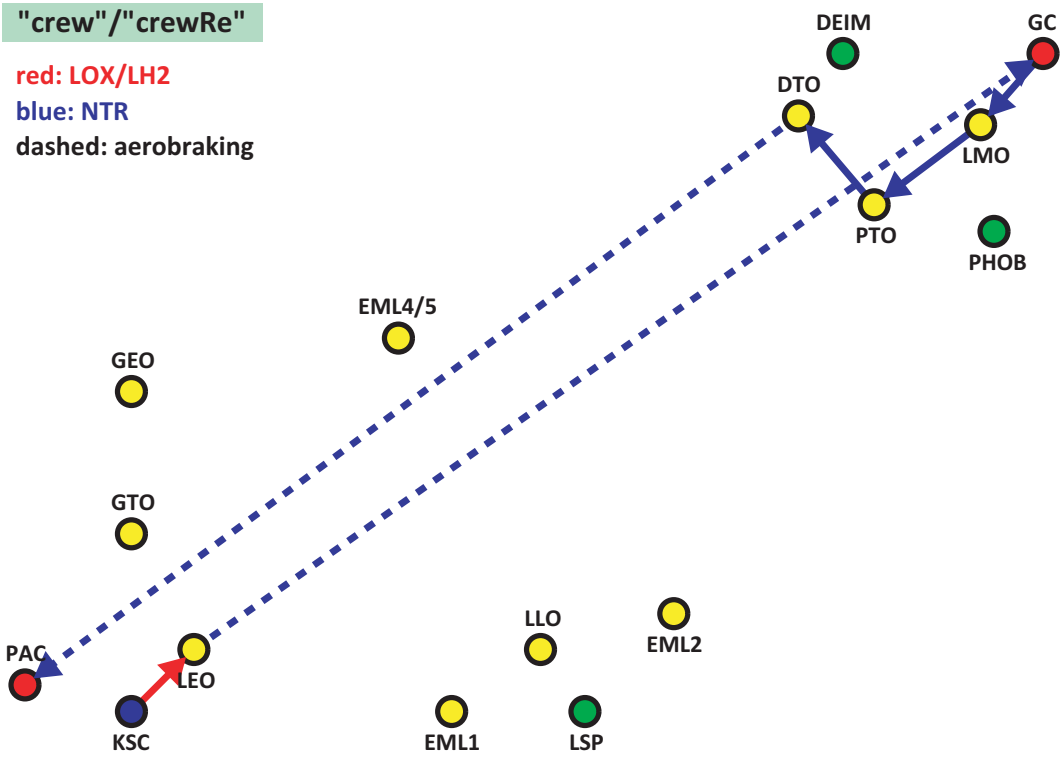

Figure 4-10: (2) NTR only with aerobraking option

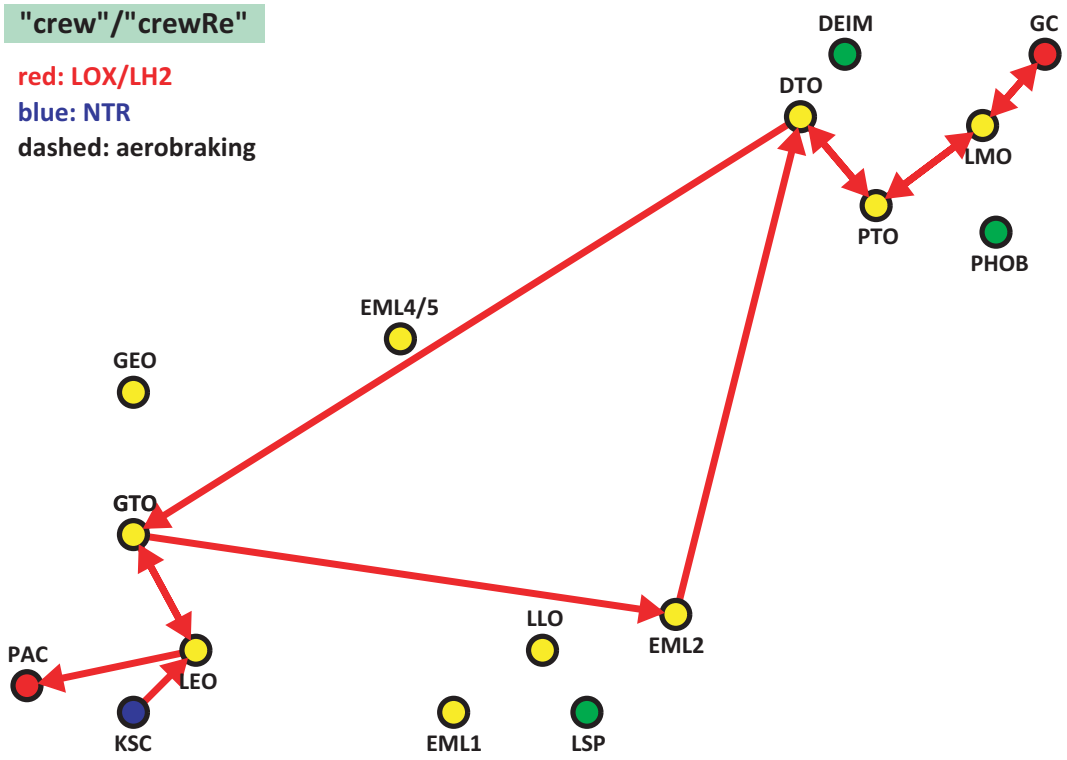

Figure 4-11: (3) LOX/LH_2 and NTR without aerobraking option

ISRU Availability

In the baseline problem, we assume that ISRU is available on the Moon, Deimos, Phobos, and Mars. However, the resource availability is not guaranteed in all these locations. Especially, ISRU on Phobos and Deimos is controversial although the evidence that there is likely to be water ice in the interior of Deimos and/or Phobos is provided in the literature [49]. Another story leading to poor ISRU availability is that the ISRU technology including excavating and transporting raw materials is not as effective as expected or even infeasible so that we cannot greatly rely on ISRU. This section examines the following three cases: (4) ISRU available on the Moon and Mars, (5) ISRU available on the Moon only, (6) ISRU available on Mars only, and (7) ISRU not available. Again note that other parameters and assumptions are not changed from the baseline problem.

Likewise, Table 4.5 compares these three scenarios with the baseline. Again these variants limit the ISRU availabilities so that the results never improve. In scenario (4) in which ISRU is available on the Moon and Mars and scenario (5) in which ISRU is only available on the Moon, the initial mass at KSC does not degrade very much despite the fact that the baseline scenario uses a substantial amount of Deimos and Phobos resources. Instead, the

Table 4.5: Comparison between different assumptions in ISRU availabilities

Scenario	**Initial Mass at KSC ($\mathcal{J}$)**	**ISRU Plant**			
		LSP	**DEIM**	**PHOB**	**GC**
Baseline Scenario	2,377,746 [kg]	4,821 [kg]	4,856 [kg]	2,504 [kg]	1,057 [kg]
(4) ISRU on Moon/Mars	2,721,529 [kg]	21,138 [kg]	0 [kg]	0 [kg]	1,057 [kg]
(5) ISRU on Moon only	2,912,353 [kg]	27,161 [kg]	0 [kg]	0 [kg]	0 [kg]
(6) ISRU on Mars only	5,562,650 [kg]	0 [kg]	0 [kg]	0 [kg]	910 [kg]
(7) No ISRU	6,564,098 [kg]	0 [kg]	0 [kg]	0 [kg]	0 [kg]

lunar ISRU plant is much upgraded so as to compensate the loss of Deimos and Phobos contributions. Figure 4-12 and 4-13 illustrate the same route except that LOX/LH_2 is used for Mars ascent in scenario (4). Similarly to scenario (3) in Figure 4-11, the outbound leg passes through EML2. This implies that EML2 could be an alternative to GTO as a cislunar gateway. NASA has been focusing on the Flexible Path idea and exploration platform at EML2 and interestingly this result is consistent with that idea while it is merely a result that automatically comes out from optimization. In scenario (6) in which ISRU is only available on Mars and scenario (7) in which no ISRU is available, the initial mass at KSC drastically increases. Figures 4-14 and 4-15 illustrate the same route except that LOX/LH_2 is used for Mars ascent in scenario (6). As can be easily understood, as the ISRU availability decreases, the complexity of network flow decreases and the path becomes more "direct" and tends toward NTR. This makes intuitive sense because oxygen-rich ISRU helps make LOX/LH_2 more effective than NTR. To summarize, it is found that ISRU availability is one of the key drivers to improve the initial mass at KSC.

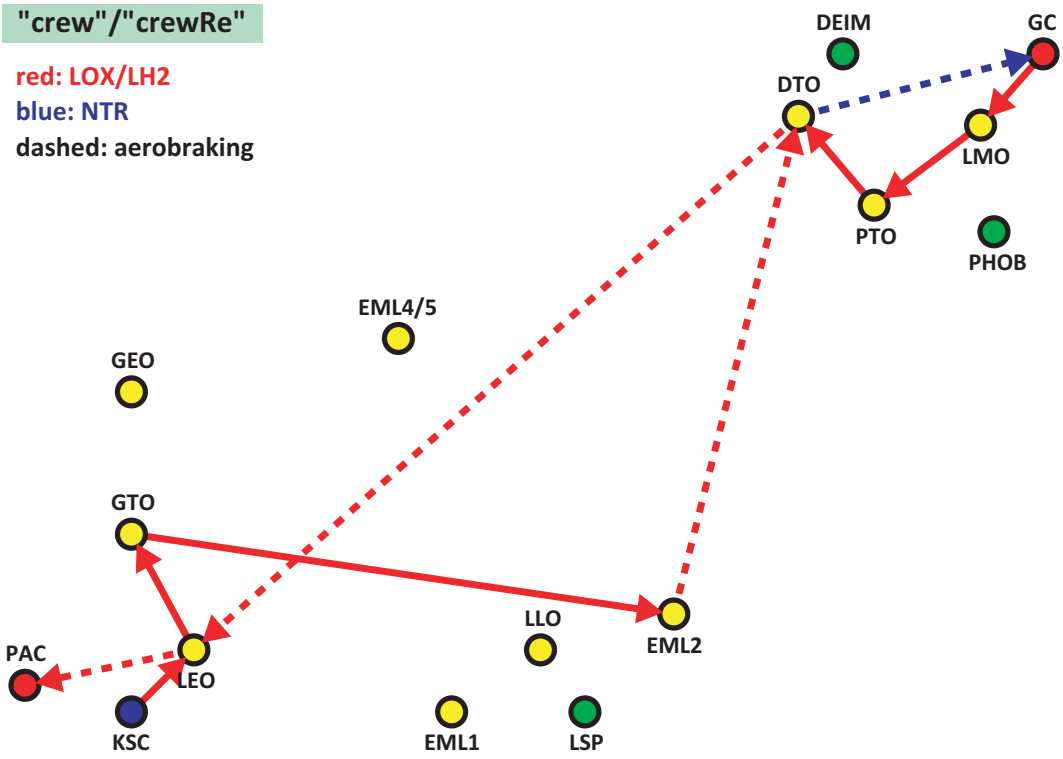

Figure 4-12: (4) ISRU available on the Moon and Mars

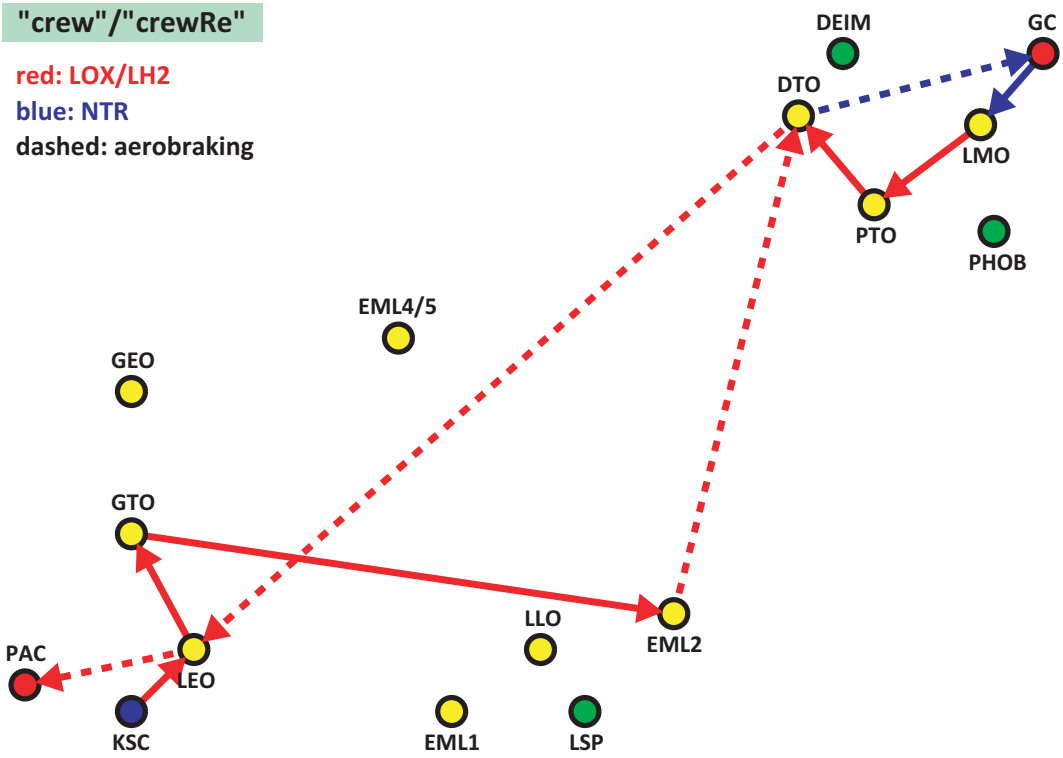

Figure 4-13: (5) ISRU available on the Moon only

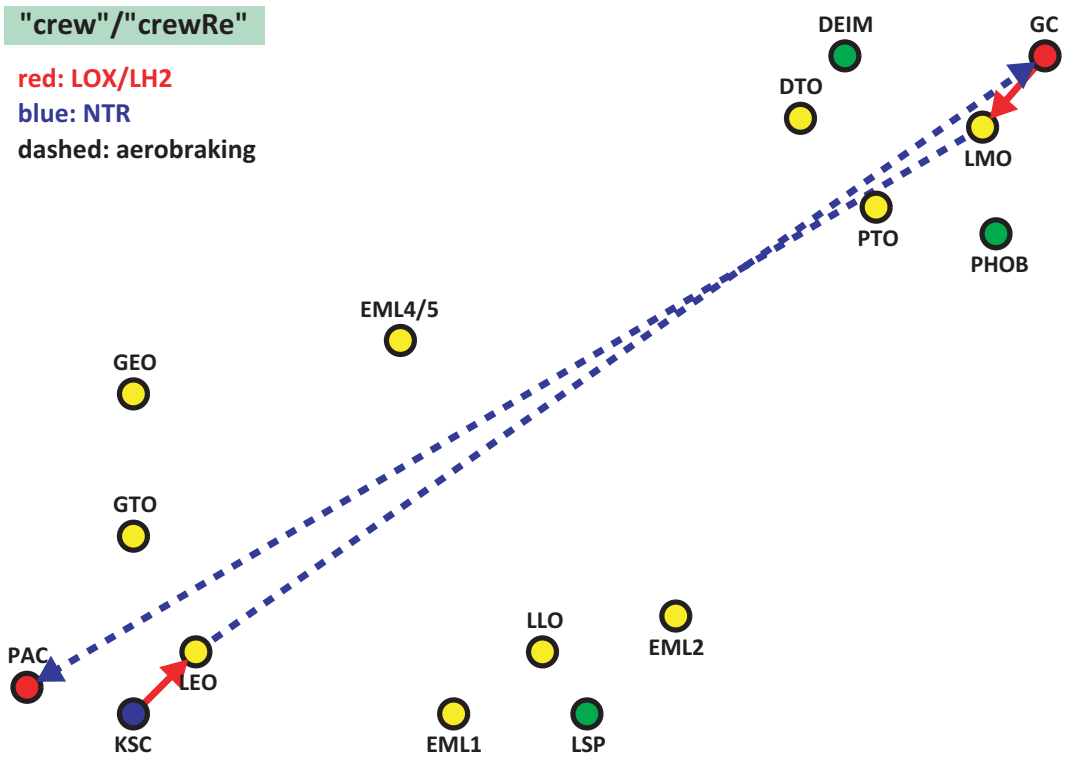

Figure 4-14: (6) ISRU available on Mars only

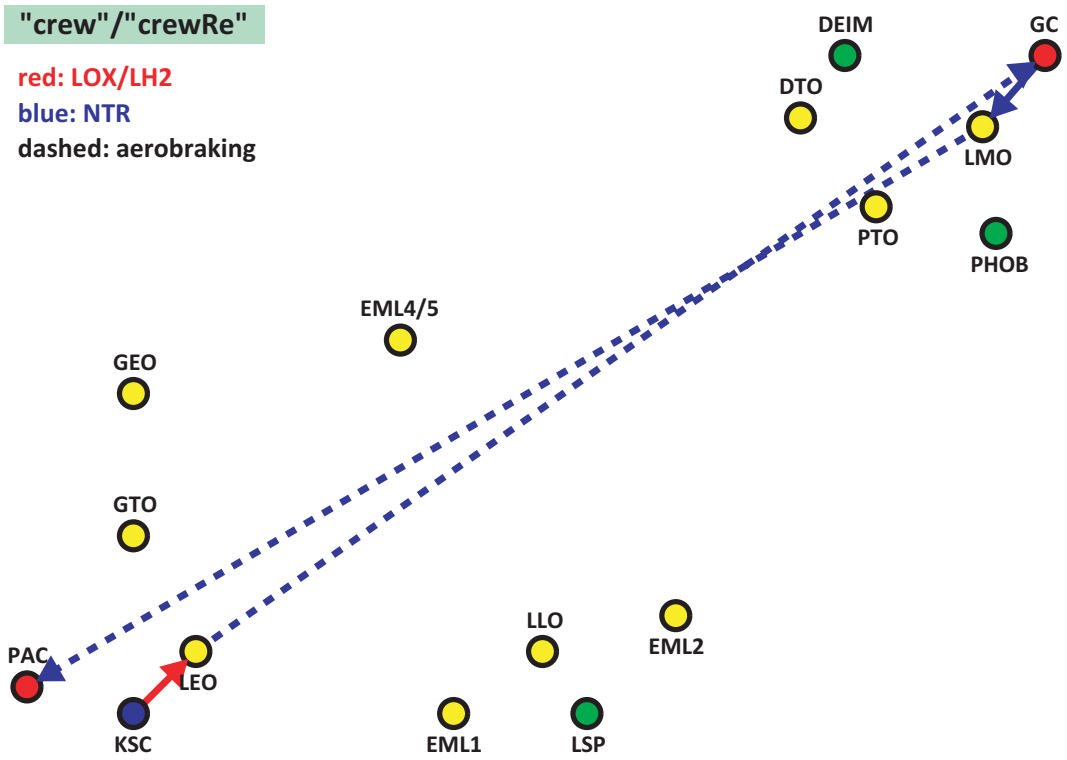

Figure 4-15: (7) ISRU not available

Table 4.6: Comparison between the baseline and zero boil-off (ZBO) scenarios

Scenario	Initial Mass at KSC ($\mathcal{J}$)	ISRU Plant			
		LSP	DEIM	PHOB	GC
Baseline Scenario	2,377,746 [kg]	4,821 [kg]	4,856 [kg]	2,504 [kg]	1,057 [kg]
(8) Zero boil-off	2,331,486 [kg]	0 [kg]	6,796 [kg]	4,174 [kg]	1,057 [kg]

Boil-Off Rate

In the baseline problem, we assume that for liquid hydrogen the boil-off rate is 0.127% per day (3.81% per month) while that of liquid oxygen is 0.016% per day (0.49% per month). Boil-off of cryogenic propellants in space is caused by heating from solar and other sources. This could be mitigated by technological solutions as well as system-level planning solutions. One system-level solution is reductions in the standby time of the cryogenic storage by a just-in-time (JIT) delivery to a customer. However, when it comes to Mars exploration, we cannot avoid a long-duration expedition. For example, if we need to carry hydrogen along with the 180-day interplanetary flight, the boil-off would be over 20%. Therefore planning solutions would not replace the need for efficient technological storage solutions. While a passive insulation system to effectively store cryogenic fluids could mitigate the boil-off, it is possible to achieve zero boil-off (ZBO) using an active thermal control system. Thus we look at the ZBO scenario, in which we assume an ideal 0% boil-off rate for both hydrogen and oxygen.

Table 4.6 compares the zero boil-off (ZBO) scenario with the baseline. It turns out that the initial mass at KSC improves 2% from the baseline. This improvement is not very big but the network topology changes; the lunar ISRU is not utilized at all and instead the plants on Deimos and Phobos are upgraded. As far as this result is concerned, the zero boil-off technology does not make a big difference in the initial mass at KSC. However, in this model we do not consider the standby time of the cryogenic storage, that is, we assume a just-in-time delivery. This assumption might make the objective function somewhat less sensitive to boil-off rate.

ISRU System Lifetime

In the baseline problem we make an arbitrary assumption that the ISRU system lifetime

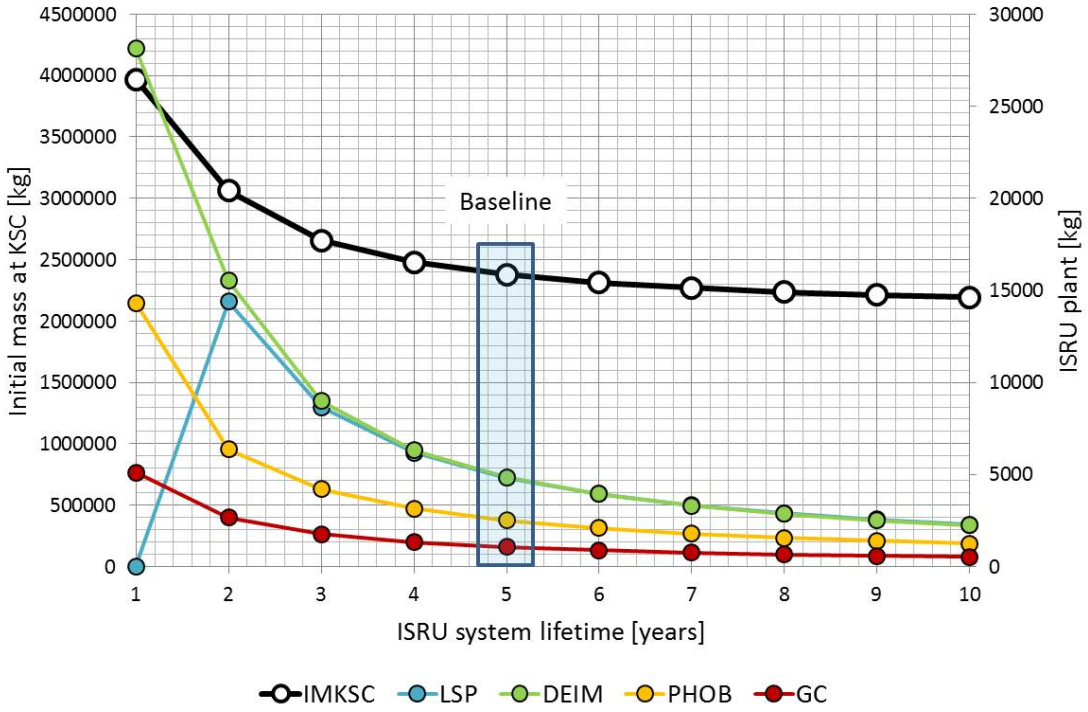

Figure 4-16: Initial mass at KSC and ISRU plant with respect to ISRU lifetime

(during which the ISRU plant keeps the constant resource production rate) is 5 years. However, if it is shorter/longer, that might be a different story. For example, if the lifetime is very short, the amount of the total resources produced will be low with respect to the ISRU plant mass, which implies that it is not worth the investment. Therefore we change the ISRU lifetime between 1 and 10 years and look at how the initial mass at KSC and the ISRU plant mass in each location vary with the lifetime.

Figure 4-16 plots the initial mass at KSC (to the left axis) and the ISRU plant mass in each location (to the right axis) with respect to the assumed ISRU system lifetime. If the ISRU system only lasts for a year, the lunar ISRU is not invested at all while the other three locations should be utilized. If the ISRU system lasts for two years, the lunar ISRU starts to be used and the flow network topology changes. If the ISRU lifetime is longer than two years, as the lifetime gets longer, the initial mass at KSC goes down, converging to around 2,200,000 kg. This is apparent because as the lifetime gets longer, the amount of lifecycle resource production increases with respect to the same plant mass to be delivered. The plant mass in each location also decreases. However, it does not mean a reduction in investments. Since the ISRU plant produces more resources if it lasts longer, a smaller plant

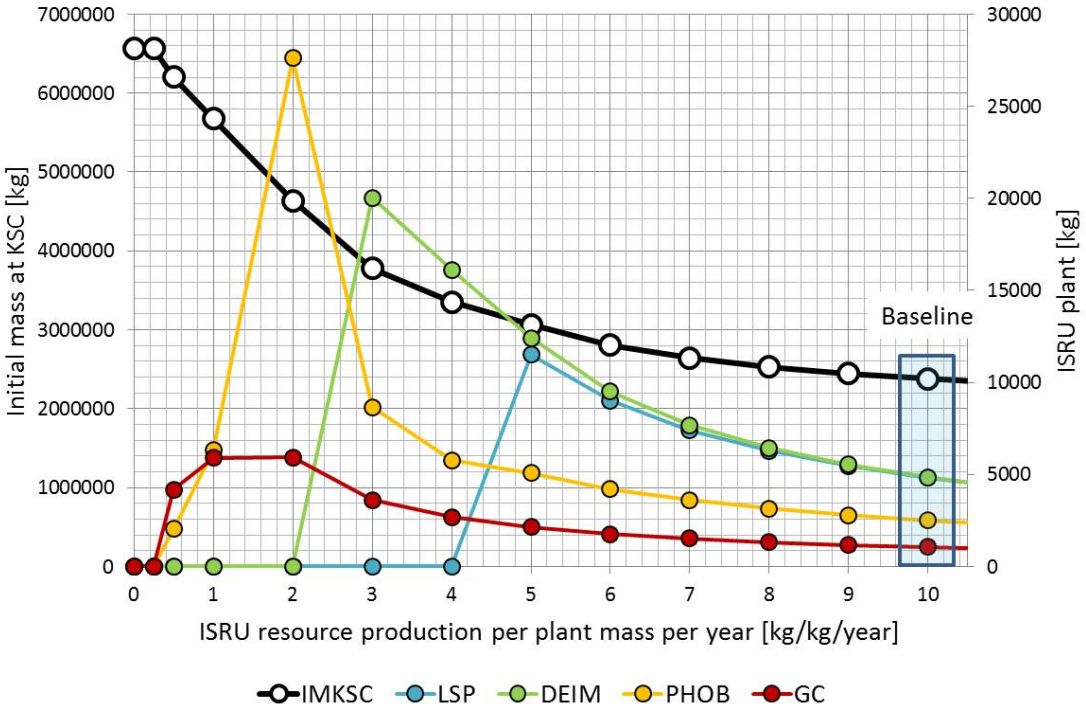

Figure 4-17: Initial mass at KSC and ISRU plant with respect to ISRU production rate

can keep the same amount of resource supply and the network topology does not basically change. To summarize, unless the lifetime is very short, ISRU can provide great value.

ISRU Resource Production Rate

Lastly, we vary the ISRU resource production rate. In the baseline problem we assume an ISRU annual production rate of 10 kg per unit plant mass. However, we should know how sensitive the result is to the production rate, particularly in the case of a lower productivity for some reason. It is easy to imagine that if the production rate is below a certain threshold, ISRU is no longer beneficial and we should rather go without ISRU. We change the ISRU annual resource production per plant mass between 0 and 10 kg. Obviously a production rate of 0 converges to scenario (7), in which no ISRU is allowed. Also, since a low production rate is equivalent to a short lifetime in the context of this model, we can expect that the result shows a similar trend to the previous case.

Figure 4-17 plots the initial mass at KSC (to the left axis) and the ISRU plant mass in each location (to the right axis) with respect to the annual resource production per plant mass. For the annual production rates between 5 and 10, the results are straightforward;

the initial mass at KSC simply increases and the ISRU plant in each location becomes upgraded while keeping the same network topology. At the annual production rate of 4, the lunar ISRU discontinuously drops to zero, meaning that if the production rate is below a certain threshold between 4 and 5, the lunar ISRU should not be used at all. Similarly, if the annual production rate falls below another threshold between 2 and 3, ISRU on Deimos becomes worthless while the resulting network highly relies on Phobos ISRU. For the annual production rate below 2, both Phobos and Mars ISRU become downgraded and finally at some point between 0.25 and 0.5, the cost exceeds the benefit. As for the propulsion system, LOX/LH_2 is still mainly used at a production rate of 4 where the lunar ISRU drops to zero while the main propulsion system is switched to NTR at a production rate of 2 where the Deimos ISRU drops to zero and the crew path becomes more direct, which is very intuitive because as the ISRU resources we can utilize decrease, it makes sense to go straight to the destination and come straight back home using a rocket with a higher I_{sp}.

To summarize, as the ISRU resource production rate decreases from 10 kg/kg/year of the baseline, the initial mass at KSC monotonically increases as a matter of course whereas the ISRU plant mass in each location discontinuously drops to zero at a certain threshold, meaning that below the threshold the cost exceeds the benefit. With the other settings and assumptions of the baseline problem, the lunar ISRU is worth the investment for the production rate of 5 or greater, the Deimos ISRU for 3 or greater, and the Phobos and Mars ISRU for 0.5 or greater.

4.3.3 Discussions

This section summarizes the key results and discusses the limitations of the GMCNF model used in the analysis.

Summary of Key Results

First we solved the baseline problem with settings and assumptions presented in Figures A-1 and A-2 as well as Table 4.1. The baseline solution turns out to save 67.5% from the Mars DRA 5.0 reference NTR scenario in terms of the initial mass in LEO (IMLEO). In the baseline solution, all the four ISRU candidates are utilized and as opposed to the reference NTR scenario, the LOX/LH_2 propulsion is mainly used throughout the mission, taking maximum advantage of oxygen-rich ISRU. One possible scenario that can be built from the

Table 4.7: Summary of the solutions with various settings

Scenario	Initial Mass at KSC ($\mathcal{J}$)	ISRU Plant LSP	DEIM	PHOB	GC
Baseline Scenario	2,377,746 [kg]	4,821 [kg]	4,856 [kg]	2,504 [kg]	1,057 [kg]
Propulsion System					
(1) Chemical/Aerobrake	2,378,368 [kg]	4,822 [kg]	4,857 [kg]	2,510 [kg]	1,057 [kg]
(2) NTR/Aerobrake	3,797,386 [kg]	0 [kg]	27,088 [kg]	12,711 [kg]	208 [kg]
(3) Chemical/NTR	5,232,681 [kg]	27,794 [kg]	52,315 [kg]	8,272 [kg]	806 [kg]
ISRU Availability					
(4) ISRU on Moon/Mars	2,721,529 [kg]	21,138 [kg]	0 [kg]	0 [kg]	1,057 [kg]
(5) ISRU on Moon only	2,912,353 [kg]	27,161 [kg]	0 [kg]	0 [kg]	0 [kg]
(6) ISRU on Mars only	5,562,650 [kg]	0 [kg]	0 [kg]	0 [kg]	910 [kg]
(7) No ISRU	6,564,098 [kg]	0 [kg]	0 [kg]	0 [kg]	0 [kg]
Boil-Off Rate					
(8) Zero boil-off	2,331,486 [kg]	0 [kg]	6,796 [kg]	4,174 [kg]	1,057 [kg]

result is given in Figure 4-8, in which two resource depots are located at GTO and DTO as gateways of the cislunar and Martian systems, respectively, and orbital transfer vehicles (OTVs) run in each system like a pickup bus.

Based on this baseline solution, we conducted several what-if analyses with different settings to see the effect of each factor. Table 4.7 summarizes the results of theses variants as well as the baseline solution. The first three scenarios investigated different propulsion system options. Since oxygen is assumed to be available from ISRU, LOX/LH_2 turns out to be preferred to NTR. Also it is found that the aerobraking option makes a great contribution in reducing the initial mass at KSC. The second four variants attempted different ISRU availabilities. As long as the lunar ISRU is available, the initial mass at KSC does not degrade very much while in the cases of ISRU only available on Mars and of no ISRU, the initial mass is drastically increased, which obviously means that ISRU on the Moon greatly helps to reduce the launch requirement. As the ISRU availabilities decrease, the network complexity decreases concurrently. For the zero boil-off scenario, we did not see a big improvement in the initial mass within the scope of this case study. Also we can see from Figures 4-16 and 4-17 that as the ISRU resource production increases/decreases, the network topology changes at several thresholds.

Limitations

The limitations of the GMCNF LP model primarily arise in three areas: risk analysis, model linearity, and time evolution of network flow/topology. The current model assumes that all transports occur with certainty and all demands are purely deterministic. The risks of node and edge failures are not treated in the model. Robustness optimization needs to be implemented to take into account those risks.

The second limitation of the model is model linearity. In the GMCNF model developed in this study, both the objective function and the constraints are all written in the linear form. While nonlinearity in the predetermined parameters can be built in such as ΔV and TOF, nonlinear objective function or constraints on the flow cannot be handled in this model. For example, we assume a linear scalability between the size of an ISRU plant and the amount of resources produced. If we perform subsystem-level detailed design and planning, we would need a high fidelity model. At the same time, however, there is a great advantage in linear formulation, that is, LP problems can be solved quickly so that we can solve many instances, which helps make trade studies more efficient.

The third limitation of the model is time evolution of network flow/topology. This model simulates a static network flow for a given snapshot of supply/demand and therefore it does not consider the time evolution of the network flow or the network topology. It determines the optimal flow such that it only satisfies the mass balance at each node. Hence, it cannot capture literally the "flow" of events. For example, when the ISRU plant is delivered to the lunar surface at the beginning, obviously we cannot utilize the lunar resources. However, this model does not know that the deployment of the plant must happen before the lunar resources become available so that the contradiction is inherent in the model that the delivery of the lunar plant utilizes the resources produced by itself. Therefore, one possible future work is to implement the "assembly" phase optimization in the model. Considering these two limitations, this model is probably more useful for high level system trades such as mission architectures and infrastructure concepts.

Chapter 5

Case Study II: Complex Infrastructure Systems

This thesis research originally started for the purpose of the space application described in Chapter 4. For this reason, Introduction in Chapter 1 laid primary emphasis on space exploration logistics. Meanwhile, the Center for Complex Engineering Systems (CCES) at King Abdulaziz City for Science and Technology (KACST) in Riyadh, Saudi Arabia, and Massachusetts Institute of Technology (MIT) embarked on a research project called the Sustainable Infrastructure Planning System (SIPS) project and we have also made an attempt to apply the generalized multi-commodity network flow model to this project. This chapter presents the GMCNF mixed integer linear programming formulation in the context of this project as a terrestrial application.

5.1 Introduction

The Kingdom of Saudi Arabia (KSA) has been the largest producer of petroleum in the world and is experiencing rapid population growth at the same time. The current population is approaching 30 million residents and demand for resources such as clean water and electricity is increasing at a rate of approximately 7% per year. Saudi Arabia is investing heavily in new infrastructure projects to meet current and future demands that require substantial capital investment and will consume natural resources. Satisfying these demands requires a robust set of linked infrastructures that should be of comparable quality and availability across the 13 regions of the Kingdom.

The Sustainable Infrastructure Planning System (SIPS) project aims to develop new frameworks and software tools for analyzing and optimizing multi-domain infrastructure investments in an integrated way taking into account the couplings that exist particularly between water and energy. The initial emphasis of the project is on the water infrastructure and the objective is to develop a system dynamics (SD) model as well as an agent-based model (ABM) combined in a hybrid approach to model water supply and demand at the macro scale. At the micro scale, a facility-based multi-commodity network flow (MCNF) model is implemented. To assess the sustainability of the different decisions and their effects to the complex system, multiple sustainability key performance indicators (KPIs) are developed. Furthermore, multiple methodologies and techniques such as stochastic simulation are utilized to simulate uncertainty and evaluate possible decision impacts and possible future scenarios. Finally, a web-based collaborative planning interface (CPI) is used to allow stakeholders to interact with different decision variables and to analyze and visualize the different KPIs resulting from the simulation.

Thus, multiple modules are running concurrently within the SIPS project. This chapter is focused on the micro model, a facility-based multi-commodity network flow, and presents how the MILP model works in this context.

5.1.1 Motivation

Over the past four decades the Kingdom of Saudi Arabia (KSA) has achieved high rates of economic growth with the GDP increasing by over 4.6 fold and reaching a total of 1,679.25 billion SR in 2010 [63]. Consequently, significant achievements have been made in the provision of public services and infrastructures such as education, health care, clean drinking water, electricity, roads, transport, and communications, which has contributed significantly towards raising the standard of living and improving the quality of life. Demand for infrastructure is set to continue expanding significantly in the decades ahead, driven by national economic growth, urbanization, and technological progress. However, challenges to maintain and expand these infrastructure systems in a sustainable manner are numerous. The major challenges Saudi Arabia faces include (1) increased demand for infrastructure development, (2) disparities in regional development, (3) massive financial resources requirements, and (4) ecological footprint. Currently Saudi Arabia is releasing about 0.8 kg of CO_2 per USD of GDP generated, making it one of the most carbon-intensive economies in the world.

The infrastructure challenges in the Kingdom mentioned above constitute our motivation to develop a Sustainable Infrastructure Planning System (SIPS). Within SIPS, infrastructure elements and projects will be viewed as a system of systems modeled as networks where both individual infrastructure systems and the synergies between them are analyzed to achieve a holistic approach to sustainability [64]. SIPS will incorporate a decision support system (DSS) and benefit from adoption of sustainability standards and key performance indicators (KPIs) for large-scale developments and infrastructure. SIPS will deal with the larger question of framing the problem so that it is useful for policy-makers and provides a framework for gauging the sustainability and livability of infrastructure systems and projects in Saudi Arabia. One of the key contributions of SIPS is the quantification of positive or negative correlation of infrastructure investments and policies of different type across domains such as water, energy, transportation, sanitation, agriculture, and so forth. In the early phase of the project, the emphasis of SIPS has been on modeling the water system and its connections with the energy system.

5.1.2 Integrated Modeling Framework

The Sustainable Infrastructure Planning System (SIPS) project takes an integrative view of the Kingdom-wide system of infrastructure systems. As a system-of-systems (SoS), the constituent systems have operational and managerial independence across various ministries and stakeholders in Saudi Arabia [65]. Traditionally each of the infrastructure systems would be designed independently, potentially leading to unexpected emergent behaviors. A key motivation of the SIPS project is to solicit explicit cooperation and careful coordination of decisions across infrastructure systems to create conditions for sustainable performance. Thus, the integrated perspective is necessary to resolve the time-varying interdependencies and align interests across constituent systems to achieve a Kingdom-wide objective of sustainable development.

The integration framework of SIPS, illustrated in Figure 5-1, interweaves infrastructure system interdependencies with multiple aspects of sustainability over spatial and temporal dimensions. Four aspects of sustainability (economic, environmental, social, and technical) are identified with the recognition that all are necessary to achieve sustainable development. Each infrastructure system intersects with the sustainability aspects. At present, SIPS focuses on water and energy due to their overall importance to the Kingdom, though future

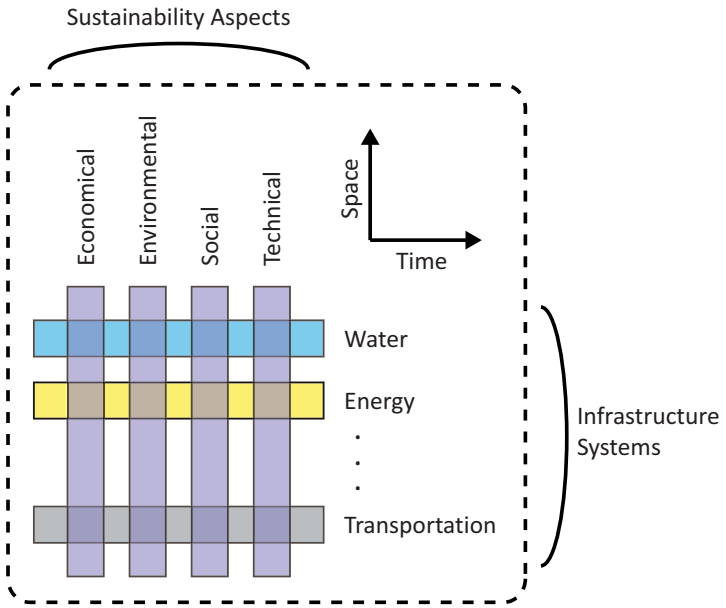

Figure 5-1: Integrative view of SIPS

efforts may integrate other hard infrastructure such as transportation and communication as well as consider the water-energy nexus implications of agriculture.

Aspects of sustainability and the constituent infrastructure systems are investigated in both space and time. The spatial dimension reflects the unique geographical features within the Kingdom, where infrastructure systems located in one region may supply resources to physically distant cities connected with distribution networks. The temporal dimension reflects both the cumulative lifecycle effects of operation and uncertainties involved with long-lived interdependent infrastructure in a changing world.

5.1.3 Micro Modeling

The mathematical modeling components include a number of models operating at multiple levels of fidelity focusing on particular perspectives on the integrative framework. The two core classes of models include macro-level models, which operate in aggregate for the entire Kingdom, and micro-level models, which investigate individual resource flows between infrastructure elements. An intermediate macro-micro model also seeks to combine the two perspectives at the regional level. In addition to the differing levels of fidelity, particular modeling applications capture the spatial and temporal aspects of the integrative framework including the impact of spatial location in resource production, distribution, and

consumption, and incorporating uncertainty in temporal processes via scenarios and what-if analysis.

The macro-level model investigates a system dynamics (SD) both on the supply side and demand side for the entire Kingdom, incorporating parametric uncertainties. On the other hand, the micro-level model wishes to look at how all the demands are satisfied for a given set of supplies and demands at the facility level. While decisions in the temporal context must take into consideration uncertainties in demands, the spatial aspect can be quantitatively handled by the graph-theoretic approach. The objective of the infrastructure modeling is to represent the infrastructure systems as a set of interconnected elements supplying resources or providing services to society. The infrastructure systems targeted within SIPS are all realized as large physical networks of interrelated components, suggesting a natural modeling approach may leverage graph-theoretic principles.

In the framing of infrastructure systems as a network (graph), nodes correspond to infrastructure elements that produce or consume resources such as desalination plants, power plants, and urban centers, and edges correspond to infrastructure connections such as water pipelines, electricity transmission lines, and roads. Models of infrastructure elements (nodes) include geographical location, state of operation, governing equations related to that element, and data related to the values of variables within those equations. Models of infrastructure connections (edges) include similar information as nodes pertaining to geographic locations, state of operation, and governing equations, but also specify the origin and destination nodes for resource flows.

One advantageous aspect of the graph-theoretic approach is that it works well at multiple levels of aggregation (the degree of resolution to which infrastructure is modeled). For example, at a higher level of aggregation than individual infrastructure elements, nodes could represent a geographical area that contains multiple infrastructure elements (such as a municipal zone), and edges represent composite connections between geographical areas. At an even higher level of aggregation, nodes could correspond to entire cities or regions (when regional dimension aggregation is needed). As the level of aggregation increases, detail is lost to the specifics of individual infrastructure operation, but at the same time data requirements are reduced to manageable levels to perform analysis on the entire Kingdom.

Another aspect of the infrastructure model is that it captures behaviors and interactions between infrastructure elements and dependencies between systems. Examples of these

Table 5.1: Example model functions for various infrastructure system elements

Infrastructure System	Example Elements	Model Functions
Water	Desalination Plant	Transform seawater and electricity to freshwater
	Freshwater Pipeline	Transport freshwater, consume electricity (pumping)
Energy	Natural Gas Power Plant	Transform natural gas to electricity and carbon dioxide
	High Voltage AC Line	Transport electricity, consume electricity (resistance)
Transportation	Highway	Transport people, transform petroleum to carbon dioxide
	Freight Rail Line	Transport goods, transform petroleum to carbon dioxide

behaviors and interactions are listed in Table 5.1. As shown in Figure 5-2, the interactions (interdependencies) between infrastructure systems exist so that multiple layers of networks interact with each other, which can be translated as multiple interacting "commodities" sharing the network. For this reason, the problem can be modeled as a multi-commodity network flow (MCNF) problem and the decision variable vector includes these infrastructure dimensions:

$$\boldsymbol{x}_{ij}^{\pm} = \begin{bmatrix} \text{Water} \\ \text{Energy} \\ \text{Transportation} \end{bmatrix}_{ij}^{\pm} \tag{5.1}$$

For a given snapshot of supplies and demands, the MCNF model can optimize the flow in the network with respect to a specific objective function. However, the commodities are not only consumed at demand nodes (sinks), but also can be lost, consumed, or transformed into another form on edges, which cannot be handled by the classical MCNF formulation as described in Section 2.2.2. Therefore, the generalized multi-commodity network flow (GMCNF) formulation presented in Section 2.3 was developed and applied to this context.

The research questions that the GMCNF model wishes to address are:

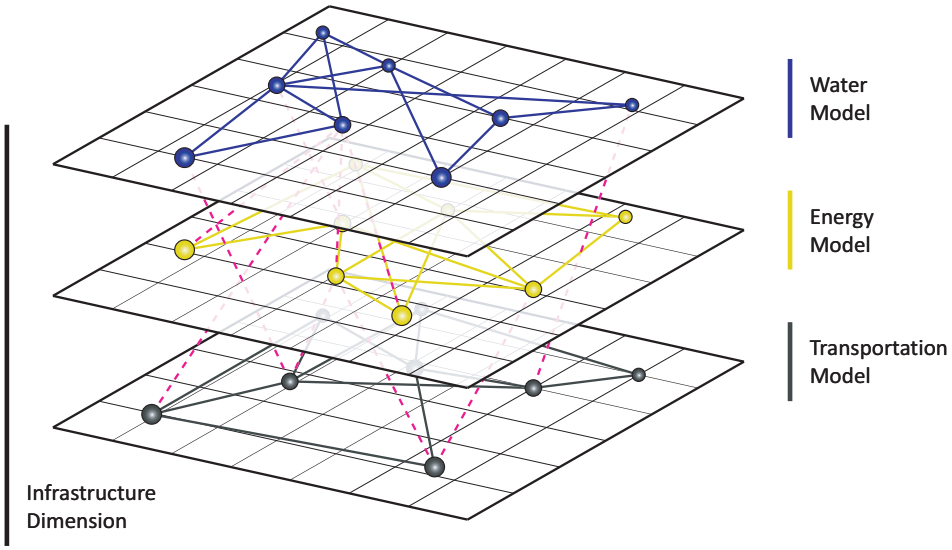

Figure 5-2: Example of the infrastructure dimension of the Kingdom

- With the current infrastructure systems in place, is the current network flow optimal? If it is not optimal, what is the optimality gap?
- Given a change in supply/demand, what will be the subsequent optimal network flow?
- Is it worth investing in the new infrastructure at a specific location?
- What is the impact of losing a specific infrastructure due to outage or retirement?
- What infrastructure element is the key driver?

For example, if we focus on a specific city and see how its demand for water is satisfied, this model would be able to perform a trade-off analysis between desalination water, ground water, and recycled water.

Figure 5-3 shows a minimum network including all the building blocks in this study. Supply nodes include desalination plants (blue) and power plants (yellow). Desalination/power plants can provide both potable water and electricity. Demand nodes are cities (red and green), some of which have waste water treatment capability. Edges represent water pipelines or powerlines while loops represent water production at desalination plants, electricity generation at power plants, or waste water treatment at cities. Since the initial emphasis of the SIPS project is on the water infrastructure, this case study is focused on water and therefore "supply/demand" is defined in terms of water. It is obvious that cities also demand electricity, but this case study only considers electricity used to produce, recycle, or transport water.

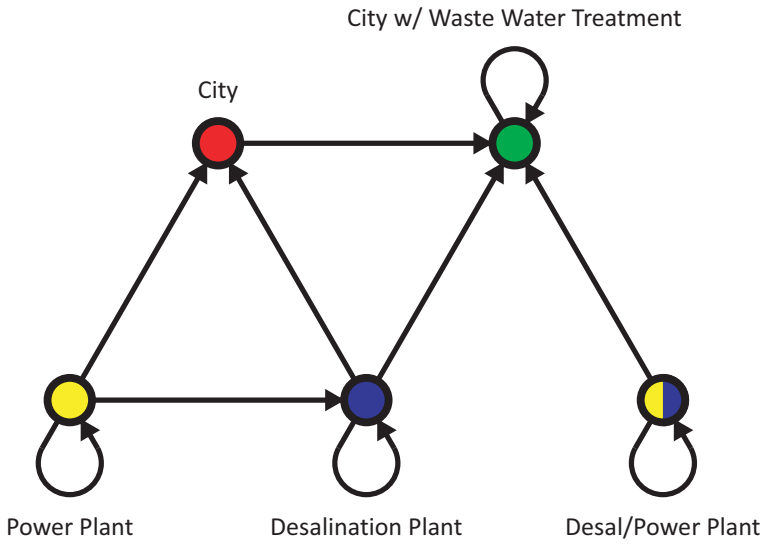

Figure 5-3: Building blocks of SIPS network

5.1.4 Why MILP?

While we solved LP problems in the space application in Chapter 4, why do we solve MILP problems in this application? The reason can be explained using a simple toy problem with 3 nodes and 2 edges in Figure 5-4. The left node represents an existing desalination/power plant A, whose desalination technology is multi-stage flash distillation (MSF) and primary fuel is oil. The right node represents a potential new desalination/power plant B, assuming reverse osmosis (RO) for desalination technology and natural gas for primary fuel. Note that plant B does not exist yet; it is to be constructed if we decide to need it. The node in the middle is city C, demanding 10,000 m^3/day of potable water from either of the two plants. Edge AC represents a 30-km existing pipeline connecting plant A and city C while edge BC represents a 60-km potential new pipeline connecting plant B and city C.

Suppose we wish to minimize the total cost as well as the total CO_2 emission. In this study, the total cost is defined as the sum of capital expenditures (CAPEX) and operational expenditures (OPEX). CAPEX is a cost for developing or providing non-consumable parts for a product or system while its counterpart, OPEX, is an ongoing cost for running a product, business, or system. CAPEX is incurred when a business spends money either to acquire fixed assets or to upgrade existing fixed assets.

Let us compare the following two scenarios. In scenario A, all the water demanded by city C is produced at plant A and transported through pipeline AC. All the electricity

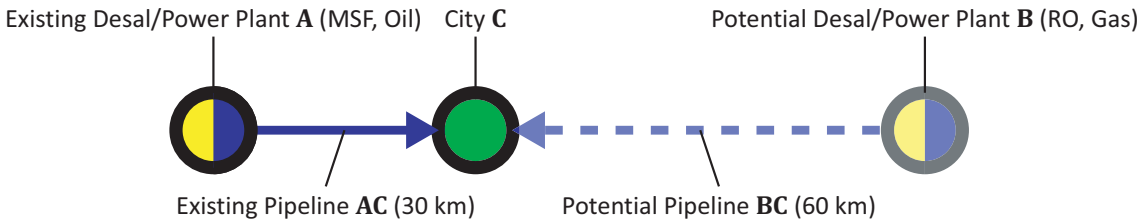

Figure 5-4: A toy MILP problem with 3 nodes and 2 edges

Table 5.2: Comparison between scenarios A and B in the toy MILP problem

	Scenario A	**Scenario B**
Plant:	**A**	**B**
Desalination technology	Multi-stage flash (MSF)	Reverse osmosis (RO)
Primary fuel	Crude oil	Natural gas
Water production	10,152 [m^3/day]	10,309 [m^3/day]
Electricity generation	136,210 [kWh/day]	57,045 [kWh/day]
for desalination	131,980 [kWh/day]	48,454 [kWh/day]
for pumping	4,230 [kWh/day]	8,591 [kWh/day]
CAPEX	0 [USD/year]	47,538 [USD/year]
OPEX	10,530,034 [USD/year]	7,726,460 [USD/year]
CO_2 emission	125,427 [mt/year]	15,922 [mt/year]
Pipeline:	**AC**	**BC**
Distance	30 [km]	60 [km]
CAPEX (fixed)	0 [USD/year]	2,400,000 [USD/year]
OPEX (fixed)	1,095,000 [USD/year]	2,190,000 [USD/year]
Total:		
Cost	**11,625,034 [USD/year]**	**12,363,999 [USD/year]**
CO_2 emission	**125,427 [mt/year]**	**15,922 [mt/year]**

needed for desalination as well as pumping is also generated at plant A. Both the plant and pipeline used in this scenario are already existing so that no CAPEX is incurred. In scenario B, on the other hand, all the water demanded by city C is produced at plant B and transported through pipeline BC. All the electricity needed for desalination as well as pumping is also generated at plant B. As opposed to scenario A, both the plant and pipeline used in this scenario do not exist yet and therefore we have to construct them, which incurs CAPEX. At the cost of CAPEX, however, this scenario is expected to reduce CO_2 emission because reverse osmosis and natural gas emit less amount of carbon dioxide when compared to multi-stage flash distillation and oil, respectively. The detailed comparison between these two scenarios is listed in Table 5.2 while the assumptions behind it is discussed later.

Scenario A costs about 11.6 million USD per year while scenario B costs about 12.4 million USD per year. Scenario B costs 6.4% more due to the CAPEX contribution. But in terms of CO_2 emission, scenario B is much better, emitting only one-eighth of that of scenario A. This obviously implies that a potential investment in scenario B is more than worth considering if we are interested even a little bit in reducing the CO_2 emission. Since these two scenarios are not dominated by each other, they are on the Pareto front with respect to those two objective functions (total cost and CO_2 emission) and there exists a trade-off between the two scenarios.

In scenario B, we assume CAPEX for plant B is proportional to capacity to be built while CAPEX for pipeline BC is a fixed cost. Hence, using the notations in Section 3.2.2, CAPEX for plant B involves $\boldsymbol{y}_{BB}$ while CAPEX for pipeline BC involves $\boldsymbol{z}_{BC}$. This way $\boldsymbol{y}$ and $\boldsymbol{z}$ can capture investments in potential infrastructure and the GMCNF MILP model is expected to work in this context.

5.2 GMCNF Model for SIPS

5.2.1 KSA Map and Network Graph

As shown in Figure 5-3, building blocks of the network are cities, desalination plants, and power plants. There are indeed so many cities, desalination plants, and power plants in the Kingdom of Saudi Arabia and we need to be selective to some extent in creating a network on which the GMCNF MILP problem is solved. It is reasonable to filter them by size such as population for cities and capacity for plants. The KSA Central Department of Statistics and Information provides city population as of 2010 [66]. As a basis for selecting the cities to be considered in the model, we use a minimum population of 20,000. We also include a few small cities of less than 20,000 inhabitants because they are on the major pipeline networks. As a result, 97 cities are selected, covering 78% of the total population in Saudi Arabia. Desalination plants are selected by water production capacity using the information provided by DesalData.com [67]; 47 existing plants (online and presumed online) and 10 future plants (planned and construction) are included in the model, totaling about 5.43 million cubic meters per day. We only consider desalination plants for municipalities as drinking water and therefore desalination plants for other customer types such as industry, irrigation, and military are not included. Power plants are selected by electricity generation

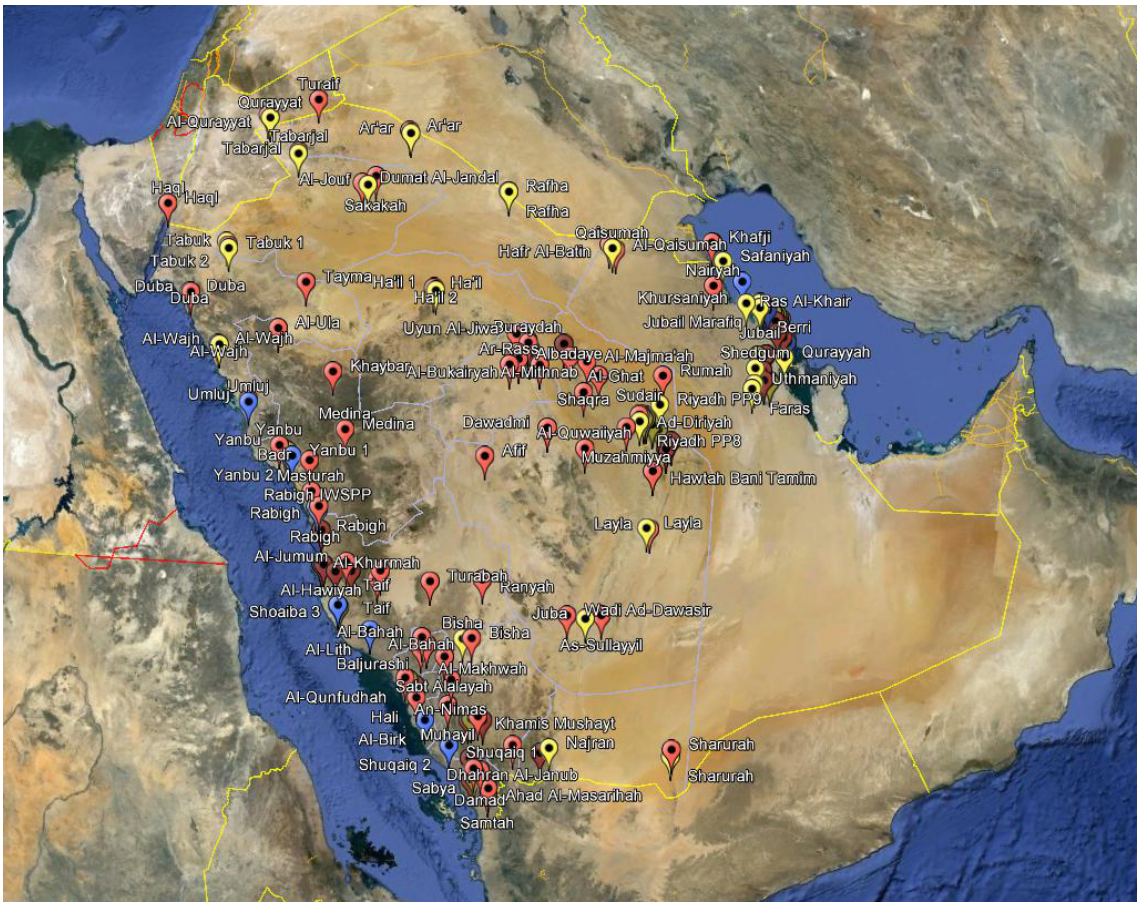

Figure 5-5: KSA map with 97 cities (red), 57 desalination plants (blue), and 69 power plants (yellow)

capacity; 69 power plants and 16 desalination/power plants are included, totaling about 60.0 gigawatts. Figure 5-5 shows the KSA map with red pins for cities, blue pins for desalination plants, and yellow pins for power plants, created using Google Earth. Note that some pins are aggregate nodes representing nearby facilities. The GPS coordinates (latitude and longitude) and elevation are identified using Google Earth.

This map is translated into a network graph in Figure 5-6, which includes 97 city nodes in red and green, 42 desalination plant nodes in blue (some are aggregate nodes), and 69 power plant nodes in yellow. The size of each node represents the city population or plant capacity. The blue lines are the working pipelines of the Saline Water Conversion Corporation (SWCC). Major pipeline networks include the Yanbu-Medina network, Rabigh network, Shoaibah-Jeddah network (also supplying water to Mecca and Taif), Qunfudhah network, and Asir network (supplying water to Abha, Khamis Mushayt, Ahad Rafidah,

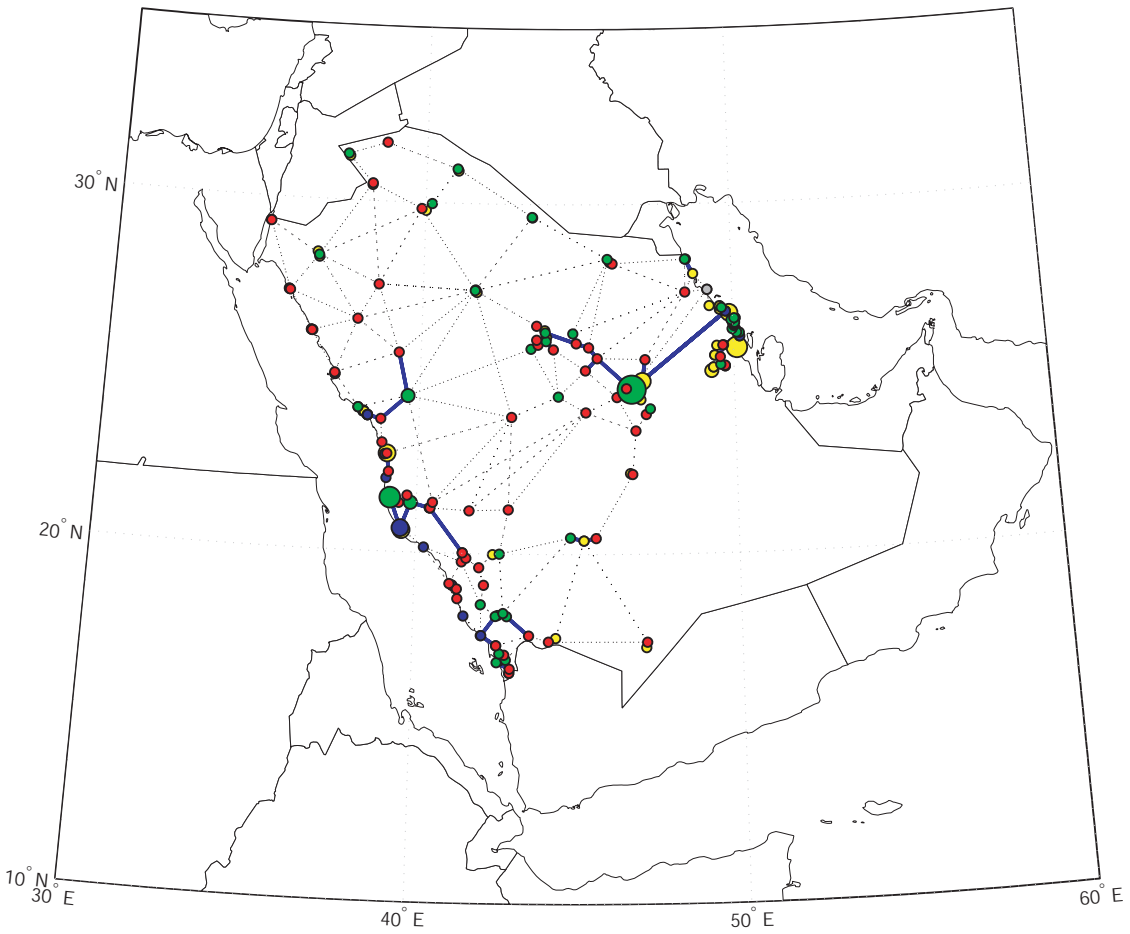

Figure 5-6: Network graph with 208 nodes and 812 edges (including 208 loops)

etc.) along the Red Sea coast (west coast), and the Khafji network, Jubail network, Eastern province network (supplying water to Dammam, Dhahran, Qatif, Saihat, Safwa, Ras Tanura, etc.), and Khobar-Abqaiq-Hofuf network along the Persian Gulf coast (east coast). They also include long-distance pipelines from Jubail to Riyadh and the Riyadh-Qassim network supplying water up to Qassim cities. The dotted lines represent the potential connections that do not exist yet but are considered in the optimization (like edge BC in Figure 5-4). All the edges are drawn straight but this is because it is a notional network graph and of course the actual connections are not necessarily straight. There are 302 connections in total. Since the GMCNF model uses a directed graph and one connection has a possibility of both directions, 604 directed edges are defined. To summarize, there are 208 nodes and 812 edges (including 208 loops) in the network graph.

5.2.2 Decision Variables and Objective Functions

As stated earlier, this case study is focused on water supply and demand. Electricity is only demanded in producing and transporting potable water and treating waste water. Since recycled waste water is not for drinking, we also define it as non-potable water. Hence, the decision variable vector used in this analysis is defined as:

$$\boldsymbol{x}_{ij}^{\pm} = \begin{bmatrix} \text{feed water} \\ \text{potable water} \\ \text{non-potable water} \\ \text{waste water} \\ \text{power resource} \\ \text{electricity} \end{bmatrix}_{ij}^{\pm} \tag{5.2}$$

where the first four variables are related to water and the last two are related to electricity. A capacity expansion $\boldsymbol{y}_{ij}^{\pm}$ and a decision binary $\boldsymbol{z}_{ij}$ are also defined in the same way. Since the number of commodities to be considered is 6, the $\boldsymbol{A}_{ij}^{\pm}$ and $\boldsymbol{B}_{ij}$ matrices are 6-by-6 square matrices. Note that the $\boldsymbol{C}_{ij}^{\pm}$ matrix is not relevant in this case study because these commodities do not have a concurrency constraint between each other.

Using the notations in the previous chapters, now we have the number of nodes ($n = 208$), the number of edges ($m = 812$), and the number of types of commodities ($k = 6$). Hence, this problem has 24360 variables, 4872 of which are binary, 20736 inequality constraints, and 4872 equality constraints, in addition to 24360 nonnegativity constraints.

While we could choose any objective function with respect to which the network flow is optimized, we use the following two: the total cost (= CAPEX + OPEX) and the total CO_2 emission. These objective functions are defined in the same way as described in the toy problem in Section 5.1.4.

CAPEX is incurred for the construction of a new infrastructure (plant or pipeline) and the capacity expansion of the existing facility. We assume that CAPEX for a new plant or capacity expansion is proportional to the newly built capacity ($\boldsymbol{y}_{ij}^{\pm}$) and that CAPEX for a new pipeline is a fixed cost, which can be predefined from the pipeline distance and therefore is a binary cost ($\boldsymbol{z}_{ij}$). Hence, the total CAPEX can be written in the form:

$$\text{CAPEX} = \sum_{(i,j)\in\mathcal{A}} \left({\boldsymbol{c}_{ij}^{y^+}}^{\mathrm{T}} \boldsymbol{y}_{ij}^{+} + {\boldsymbol{c}_{ij}^{y^-}}^{\mathrm{T}} \boldsymbol{y}_{ij}^{-} + {\boldsymbol{c}_{ij}^{z}}^{\mathrm{T}} \boldsymbol{z}_{ij} \right) \tag{5.3}$$

On the other hand, OPEX is incurred for desalination, ground water processing, and waste water treatment as well as electricity generation. For this type of OPEX, we assume a cost proportional to the amount of water produced or electricity generated ($\boldsymbol{x}_{ij}^{\pm}$). OPEX also includes the operation and maintenance cost for pipelines and powerlines, which is a fixed cost ($\boldsymbol{z}_{ij}$) defined in the same manner as CAPEX. Hence, the total OPEX can be written in the form:

$$\text{OPEX} = \sum_{(i,j)\in\mathcal{A}} \left({\boldsymbol{c}_{ij}^{x^+}}^{\mathrm{T}} \boldsymbol{x}_{ij}^{+} + {\boldsymbol{c}_{ij}^{x^-}}^{\mathrm{T}} \boldsymbol{x}_{ij}^{-} + {\boldsymbol{c}_{ij}^{z}}^{\mathrm{T}} \boldsymbol{z}_{ij} \right) \tag{5.4}$$

The other objective function is the total CO_2 emission, which increases linearly with the amount of water produced or electricity generated. The amount of CO_2 emitted by desalination varies with the type of technology (e.g., MSF, RO, MED, etc.) and likewise the amount of CO_2 emitted by electricity generation varies with the type of primary fuel (e.g., oil, natural gas, etc.). Hence, the CO_2 emission can be written in the form:

$$\text{CO}_2 = \sum_{(i,j)\in\mathcal{A}} \left({\boldsymbol{c}_{ij}^{x^+}}^{\mathrm{T}} \boldsymbol{x}_{ij}^{+} + {\boldsymbol{c}_{ij}^{x^-}}^{\mathrm{T}} \boldsymbol{x}_{ij}^{-} \right) \tag{5.5}$$

All the coefficients in Eqs. (5.3)-(5.5) can be determined using the assumptions listed in Table B.1 in Appendix B. In order to evaluate CAPEX and OPEX in the same units of annual cost [USD/year], we annualize CAPEX by dividing it by the average lifetime of the infrastructure, which we assume is 25 years unless otherwise specified.

We establish the combined objective function:

$$\mathcal{J} = w \left(\frac{\text{cost}}{s_{\text{cost}}} \right) + (1 - w) \left(\frac{\text{CO}_2}{s_{\text{CO}_2}} \right) \tag{5.6}$$

where w is the weight for the cost ($0 \leq w \leq 1$) and cost = CAPEX + OPEX. When $w = 1$, we minimize the cost only; when $w = 0$, we minimize the CO_2 emission only. In order to avoid a scaling effect, both the cost and CO_2 emission are divided by the rescaling factors s_{cost} and s_{CO_2}, respectively. These rescaling factors are determined such that $\mathcal{J}$ for $w = 0$ and $w = 1$ are equal.

5.2.3 Supply and Demand

Next we define supply/demand $\boldsymbol{b}_i$ at each node. In a typical network flow problem of the same sort, the capacity of a plant is used as the supply of that node. Instead, in the GMCNF model, the capacity of a plant is rather used as the capacity of a loop edge associated with that node. One important thing in this model is that a facility is modeled as a loop edge instead of a node and therefore a node is merely a point at which the mass balance constraint is evaluated. For example, a desalination process is modeled as a loop edge transforming feed water into potable water. Since the edge capacity is defined by the capacity of this plant, we can only produce potable water up to that capacity at most even if we have an infinite supply of feed water. For the modeling purposes, we make a fictitious assumption that a desalination plant has an infinite supply of feed water and a power plant has an infinite supply of power resource. On the other hand, cities have supplies of waste water. The supply of waste water is assumed to be 80% of the water consumption [68]. If a city consumes water of 10,000 cubic meters per day, the city simultaneously generates waste water of 8,000 cubic meters per day. A city with waste water treatment capability has a loop edge associated with it, transforming waste water into non-potable water with the loop edge capacity being the capacity of waste water treatment of that city.

As opposed to the above trick to deal with the supply and capacity, the demand is simply the water demand at each city node. Table B.2 in Appendix B lists water consumption in various regions during 2010 [68]. We estimate the demand for water of each city from the city's population times the average daily water consumption per capita for the region to which the city belongs. In order to evaluate the significance of the waste water treatment, we also consider non-potable water. Non-potable water is water that is not of drinking water quality but may still be used for other purposes. In general the toilet is said to use a quarter of household water. Based on this fact, we assume that 30% of daily water demand can also be satisfied with non-potable water. For example, if a city demands water of 10,000 cubic meters per day, 7,000 cubic meters must be potable water but 3,000 cubic meters can be both potable and non-potable water. This can be implemented in the model by (1) setting potable water demand to be 7,000 [m^3/day] and non-potable water demand to be 3,000 [m^3/day], and (2) attaching a loop edge transforming potable water into non-potable water at no cost to the city node. This loop edge allows us to be free to use potable water

for non-drinking purposes as well and the optimization results should give a solution to how non-potable water demand should be satisfied (potable water vs. waste water treatment). There is no need to define the demand for electricity because electricity is consumed through the $\boldsymbol{A}_{ij}^{+}$ matrix.

The following two sections describe how to determine the requirement matrix $\boldsymbol{A}_{ij}^{\pm}$ and transformation matrix $\boldsymbol{B}_{ij}^{\pm}$. Note that the concurrency matrix $\boldsymbol{C}_{ij}^{\pm}$ is not applicable to this case study.

5.2.4 Requirement Matrix $\boldsymbol{A}_{ij}^{\pm}$

In this case, the requirement matrix $\boldsymbol{A}_{ij}^{\pm}$ can be used in two ways: power consumption for water processing and pumping energy. The former involves a loop edge modeling facility while the latter involves a regular edge modeling pipeline.

Power Consumption for Water Processing

Water processing includes desalination, ground water processing, and waste water treatment, which are all modeled as a loop edge associated with a node. If a desalination plant with a certain technology consumes P of electricity per unit feed water, then the plant is required to provide:

$$\boldsymbol{A}_{ii}^{+}\boldsymbol{x}_{ii}^{+} = \begin{bmatrix} 1 & 0 & 0 & 0 & 0 & 0 \\ 0 & 1 & 0 & 0 & 0 & 0 \\ 0 & 0 & 1 & 0 & 0 & 0 \\ 0 & 0 & 0 & 1 & 0 & 0 \\ 0 & 0 & 0 & 0 & 1 & 0 \\ P & 0 & 0 & 0 & 0 & 1 \end{bmatrix}_{ii}^{+} \begin{bmatrix} \text{feed water} \\ \text{potable water} \\ \text{non-potable water} \\ \text{waste water} \\ \text{power resource} \\ \text{electricity} \end{bmatrix}_{ii}^{+} \tag{5.7}$$

In the actual implementation, cubic meter per day [m^3/day] is used as units of water-related variables and kilowatt hour per day [kWh/day] is used as units of electricity-related variables. For instance, a desalination plant with sea water reverse osmosis (SWRO) consumes 4.7 kWh per cubic meter of water produced. It is modeled by setting $P = 4.7$ in Eq. (5.7). Here we assume that the conversion rate between feed water and potable water is 1 for modeling purposes. In actuality, the recovery rate of feed water to potable water

produced is less than 100% but the detailed modeling of feed water is beyond the scope of this case study. Since this 4.7 kWh/m^3 of electricity is consumed for potable water produced, one might model this in another way, that is, the $(6, 2)$ entry of $\boldsymbol{A}_{ii}^-$ is set to -4.7. This is also correct. However, since $\boldsymbol{A}_{ii}^-\boldsymbol{x}_{ij}^-$ is subtracted (not added) in the mass balance constraint, we must use a negative value, which is counter-intuitive. For this reason, all the power consumption for water processing is modeled in the $\boldsymbol{A}_{ii}^+$ matrix, assuming that the conversion rate is 1 for simplicity. Power consumption for each water processing used in this analysis is given in Table B.3 in Appendix B.

Pumping Energy

Pumping energy represents energy required to pump water into the pipeline. Hydraulics of pipelines has been studied as a discipline [69]. In this study, we define pumping energy simply as:

$$E_\mathrm{p} = m_\mathrm{p} g_0 H_\mathrm{p} \tag{5.8}$$

where m_p is mass of water pumped, g_0 is the standard gravity, and H_p is the pumping head. Hydraulic head (or piezometric head) is usually measured as a liquid surface elevation, expressed in units of length. In other words, head is equal to the fluid's energy per unit weight. If H_p is simply an elevation, E_p is energy required to lift m_p of water by H_p (cf. potential energy). However, we must also overcome the pipeline friction. Therefore H_p includes the friction loss as well as the elevation difference (static lift):

$$H_\mathrm{p} = \max\left(\Delta h + H_\mathrm{f}, 0\right) \tag{5.9}$$

where H_f is the friction head loss. The max function here is to avoid a negative value of H_p when pumping from high to low; otherwise we gain electricity at the tail node. There are other minor losses that occur at a pipe entrance, elbow, orifice, valve, and so on, but for a long-distance pipeline, these losses are negligibly small compared with the friction loss. We assume that Δh is the elevation difference between two nodes. The friction head loss is estimated using the Darcy-Weisbach equation, one of the accepted methods to calculate friction losses resulting from fluid motion in pipes:

$$H_\mathrm{f} = f\left(\frac{L}{D}\right)\left(\frac{v^2}{2g_0}\right) \tag{5.10}$$

where f is the Darcy-Weisbach friction coefficient (dimensionless), L is the pipe length, D is the pipe diameter, and v is the flow velocity. While the Darcy-Weisbach friction coefficient f varies with the roughness of the pipe's surface and the Reynold's number of the flow, we uniformly assume $f = 0.01$ for all pipelines. We also choose $v = 2.0$ [m/s] for all pipelines as a typical flow velocity of the water pipe. With some unit conversions, tail node i is required to provide:

$$\boldsymbol{A}_{ij}^{+}\boldsymbol{x}_{ij}^{+} = \begin{bmatrix} 1 & 0 & 0 & 0 & 0 & 0 \\ 0 & 1 & 0 & 0 & 0 & 0 \\ 0 & 0 & 1 & 0 & 0 & 0 \\ 0 & 0 & 0 & 1 & 0 & 0 \\ 0 & 0 & 0 & 0 & 1 & 0 \\ \frac{g_0 H_{\mathrm{p}}}{3600} & \frac{g_0 H_{\mathrm{p}}}{3600} & \frac{g_0 H_{\mathrm{p}}}{3600} & \frac{g_0 H_{\mathrm{p}}}{3600} & 0 & 1 \end{bmatrix}_{ij}^{+} \begin{bmatrix} \text{feed water} \\ \text{potable water} \\ \text{non-potable water} \\ \text{waste water} \\ \text{power resource} \\ \text{electricity} \end{bmatrix}_{ij}^{+} \tag{5.11}$$

5.2.5 Transformation Matrix $\boldsymbol{B}_{ij}^{\pm}$

Likewise, the transformation matrix $\boldsymbol{B}_{ij}$ is used in two ways: water processing/electricity generation and water/electricity loss during transmission. The former involves a loop edge while the latter involves a regular edge.

Water Processing/Electricity Generation

Let us take a desalination/power plant as an example. A desalination/power plant transforms feed water into potable water as well as power resource into electricity. This process is expressed using the $\boldsymbol{B}_{ii}$ matrix as:

$$\boldsymbol{B}_{ii}\boldsymbol{x}_{ii}^{+} = \begin{bmatrix} 0 & 0 & 0 & 0 & 0 & 0 \\ 1 & 0 & 0 & 0 & 0 & 0 \\ 0 & 0 & 0 & 0 & 0 & 0 \\ 0 & 0 & 0 & 0 & 0 & 0 \\ 0 & 0 & 0 & 0 & 0 & 0 \\ 0 & 0 & 0 & 0 & 1 & 0 \end{bmatrix}_{ii} \begin{bmatrix} \text{feed water} \\ \text{potable water} \\ \text{non-potable water} \\ \text{waste water} \\ \text{power resource} \\ \text{electricity} \end{bmatrix}_{ii}^{+} = \boldsymbol{x}_{ii}^{-} \tag{5.12}$$

The $(2, 1)$ and $(6, 5)$ entries are 1, meaning that feed water/power resource is transformed into potable water/electricity with a conversion rate of 1, respectively. As discussed in the

previous section, this conversion rate does not the actual rate. Other entries are 0, which means that commodities other than feed water and power resource are just lost even though they are sent into this loop edge. Ground water processing also transforms feed water into potable water with a conversion rate of 1. Hence, the $(2, 1)$ entry of $\boldsymbol{B}_{ii}$ is set to 1. Waste water treatment transforms waste water into non-potable water. Since we assume a recovery rate of 90%, the $(3, 4)$ entry of $\boldsymbol{B}_{ii}$ is set to 0.9. A power plant is a subset of the above example and therefore the $(6, 5)$ entry of $\boldsymbol{B}_{ii}$ is set to 1.

Water/Electricity Loss during Transmission

Over a long-distance pipeline, a certain percentage of water is lost due to leaks, evaporation, etc. Similarly, over a long-distance powerline, there is a resistive loss of electricity. These losses are modeled in the diagonal entries of the $\boldsymbol{B}_{ij}$ matrix. Let r_{w} and r_{e} be the loss rate per unit distance of water over the pipeline and electricity over the powerline, respectively. The $\boldsymbol{B}_{ij}$ matrix of a pipeline/powerline is written as:

$$\boldsymbol{B}_{ij} = \begin{bmatrix} 0 & 0 & 0 & 0 & 0 & 0 \\ 0 & 1 - r_{\mathrm{w}}L & 0 & 0 & 0 & 0 \\ 0 & 0 & 1 - r_{\mathrm{w}}L & 0 & 0 & 0 \\ 0 & 0 & 0 & 1 - r_{\mathrm{w}}L & 0 & 0 \\ 0 & 0 & 0 & 0 & 0 & 0 \\ 0 & 0 & 0 & 0 & 0 & 1 - r_{\mathrm{e}}L \end{bmatrix}_{ij} \tag{5.13}$$

where L is the length of the pipeline/powerline. Feed water and power resource are not allowed to move in this model. In this case study, we assume $r_{\mathrm{w}} = 5.0 \times 10^{-4}$ and $r_{\mathrm{e}} = 3.0 \times 10^{-5}$, meaning that we lose 5% of water per every 100 km of pipeline and 0.3% of electricity per every 100 km of powerline. For example, if a pipeline/powerline is 400 km long, we lose 20% of water and 1.2% of electricity and then the transformation matrix

becomes:

$$\boldsymbol{B}_{ij} = \begin{bmatrix} 0 & 0 & 0 & 0 & 0 & 0 \\ 0 & 0.8 & 0 & 0 & 0 & 0 \\ 0 & 0 & 0.8 & 0 & 0 & 0 \\ 0 & 0 & 0 & 0.8 & 0 & 0 \\ 0 & 0 & 0 & 0 & 0 & 0 \\ 0 & 0 & 0 & 0 & 0 & 0.988 \end{bmatrix}_{ij} \tag{5.14}$$

All we need for implementing the GMCNF MILP model has been described up to this point. Tables B.4, B.5, and B.6 in Appendix B present lists of cities, desalination plants, and power plants created in this analysis, respectively. The following section discusses the optimization results.

5.3 Optimization Results and Discussions

This section presents two sets of optimization results, followed by the discussions. In defining supply and demand, we must first determine a *basis year* and a *target year* as inputs to the model. A *basis year* represents the "current" year that the infrastructure capacity is based on. In this study, the basis year is fixed at 2010. Therefore we are supposed to possess the infrastructure capacity as of 2010 given in Tables B.4-B.6. A *target year* represents the "future" year that the water demand corresponds to. If a target year is set to 2030, the problem is to optimize the investment and operation to meet the expected demand in 2030 on top of the 2010 supply capability. Since the capacity expansion variable $\boldsymbol{y}_{ij}^{\pm}$ has been implemented in the model, the demand is allowed to exceed the supply; if the demand exceeds the supply, the capacity can be expanded at the cost of CAPEX. We estimate the water demand simply from the expected population. We have the 2010 city population from the national census data. For example, if the total population in the Kingdom doubles, we assume that each city's population and water demand would simply double as well. We know this could only be a rough estimation. The macro-level system dynamics (SD) model actually models the future population and water demand in much more detail but for the scope of this case study, we use that simple estimation.

As described in Chapter 3, the GMCNF MILP problem is solved using the CPLEX `cplexmilp` function within MATLAB. Since the problem size is quite large, for the most part the problem is not completely solved within a reasonable time. Hence, we instead stick to a maximum optimality gap less than 5%, which guarantees that in all instances the solutions are within 5% of optimality. The following two sections present the results for target years of 2030 and 2050, respectively.

5.3.1 Target Year of 2030

The total population in the Kingdom in 2030 is expected to be about 42 million, which is about 1.5 times that of 2010. As in Table B.4, we include 97 cities in the optimization problem, covering about 80% of the total population. We assume this coverage remains the same in 2030 and therefore the total demand for water in this problem is 8.03 million cubic meters per day [Mm^3/day]. Of this, 5.62 Mm^3/day can only be satisfied with potable water while the rest 2.41 Mm^3/day can be satisfied with either potable or non-potable water

Table 5.3: List of optimization results for 2030

Weight		Total Cost [BUSD/year]	CAPEX (annualized) [BUSD/year]	OPEX [BUSD/year]	CO_2 Emission [Mmt/year]	Total Water Production [Mm^3/year]	Total Electricity Generation [GWh/year]	Optimality Gap
Cost	CO_2							
0.999	0.001	6.68	0.65	6.03	17.82	2468	20070	0.70%
0.9	0.1	6.71	0.66	6.06	15.45	2464	19987	2.98%
0.8	0.2	6.76	0.67	6.09	15.15	2457	19893	3.46%
0.7	0.3	6.89	0.73	6.16	14.20	2474	19279	2.70%
0.6	0.4	6.99	0.72	6.27	13.88	2434	18776	1.98%
0.5	0.5	7.01	0.72	6.29	13.83	2435	18738	1.85%
0.4	0.6	7.15	0.78	6.37	13.69	2428	18675	1.70%
0.3	0.7	7.27	0.82	6.45	13.58	2410	18631	1.11%
0.2	0.8	9.64	0.82	8.82	12.23	2202	18445	0.90%
0.1	0.9	10.22	0.85	9.37	12.01	2145	18527	0.33%
0.001	0.999	11.00	1.16	9.84	11.99	2130	18829	0.01%

(recycled waste water). Meanwhile, the desalination capacity totals 3.27 Mm^3/day and the ground water capacity totals 2.29 Mm^3/day. The 2010 capacity falls a bit short of the potable water demand in 2030 even without geographical consideration. Thus it is inevitable to expand the capacity of the existing infrastructure, construct a new infrastructure, or both. One of the objectives of the micro model is to find the optimal strategy to meet the future demand in consideration of the unique geographical features within the Kingdom. As discussed earlier in Section 5.2.2, the objective function used in the analysis is

$$\mathcal{J} = w\left(\frac{\text{cost}}{s_{\text{cost}}}\right) + (1-w)\left(\frac{\text{CO}_2}{s_{\text{CO}_2}}\right) \tag{5.15}$$

where w is the weight for the cost ($0 \leq w \leq 1$), cost = CAPEX + OPEX, and s_{cost} and s_{CO_2} are the rescaling factors. First we solve two optimization problems that minimize either of the total cost or the total CO_2 emission only to determine these rescaling factors such that $\mathcal{J}$ for $w = 0$ and $w = 1$ are equal. Then we vary the weight w from 1 to 0 with 0.1 intervals and see how the solutions behave.

Table 5.3 lists the results with the leftmost column representing w and Figure 5-7 plots the total costs and CO_2 emissions. For the case of $w = 0$, the total CO_2 emission is almost equal to that of $w = 0.001$ while the total cost is almost twice that of $w = 0.001$ because the case of $w = 0$ is totally insensitive to the cost. For this reason, the two extremes are replaced with $w = 0.999$ and $w = 0.001$. The maximum optimality gap is 3.46%.

For the case of $w = 0.999$, the total cost is 6.68 billion USD per year [BUSD/year], of which 0.65 billion is CAPEX and 6.03 billion is OPEX, and the CO_2 emission is 17.82

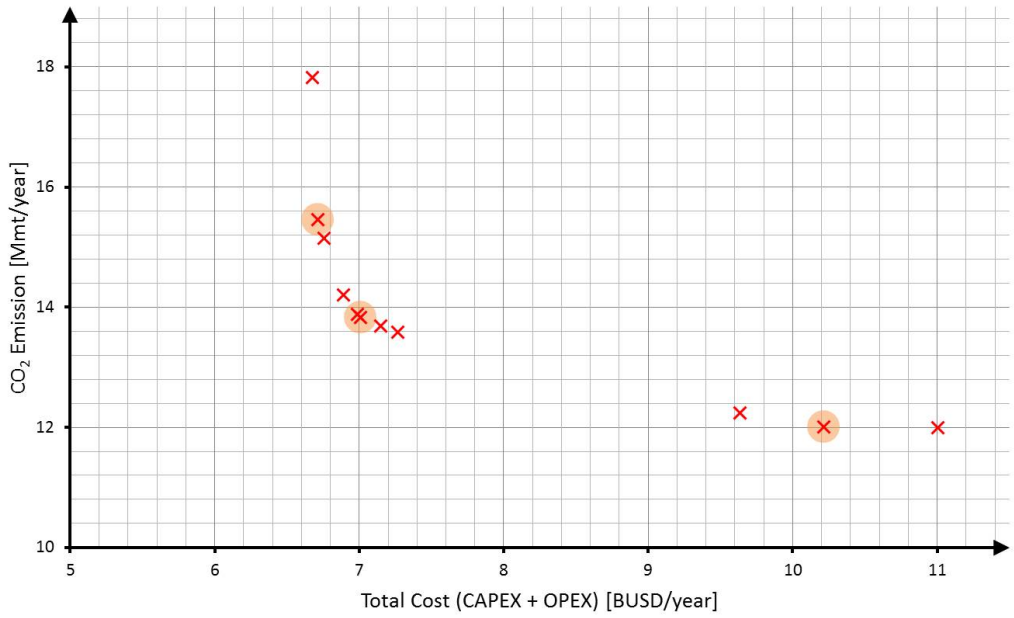

Figure 5-7: Total cost vs. CO_2 emission for 2030 demand

million metric tons per year [Mmt/year]. Note that CAPEX is divided by the lifetime, which is assumed to be 25 years unless otherwise specified. For the case of $w = 0.001$, on the other hand, the total cost is 11.00 BUSD/year, of which 1.16 billion is CAPEX and 9.84 billion is OPEX, and the CO_2 emission is 11.99 Mmt/year.

For $w = 0.9$ through $w = 0.1$, we observe that as w decreases, the total cost increases from 6.71 to 10.22 and the CO_2 emission decreases from 15.45 to 12.01. The total water production ranges between 2474 and 2130 Mm^3/year and the total electricity generation ranges between 18445 and 20070 GWh/year though they do not behave monotonically.

In Figure 5-7, since none of these 11 points are dominated, they all form a "Pareto-optimal" set. A Pareto-optimal set is a set of the solutions of a multi-objective optimization problem, in which an improvement in one of the objective functions can only be achieved by degrading at least one of the other objective functions. As representative examples, the resulting network graphs of the three points with light red circles are presented.

For the first example, Figure 5-8 shows the resulting network for $w = 0.5$, that is, equal weights on the cost and CO_2 emission. Green and red nodes are city nodes with and without waste water treatment, respectively, blue nodes are desalination plant nodes, and yellow nodes are power plant nodes. The size of a city node still represents the city population but note that it is not necessarily equivalent to the city's water demand because

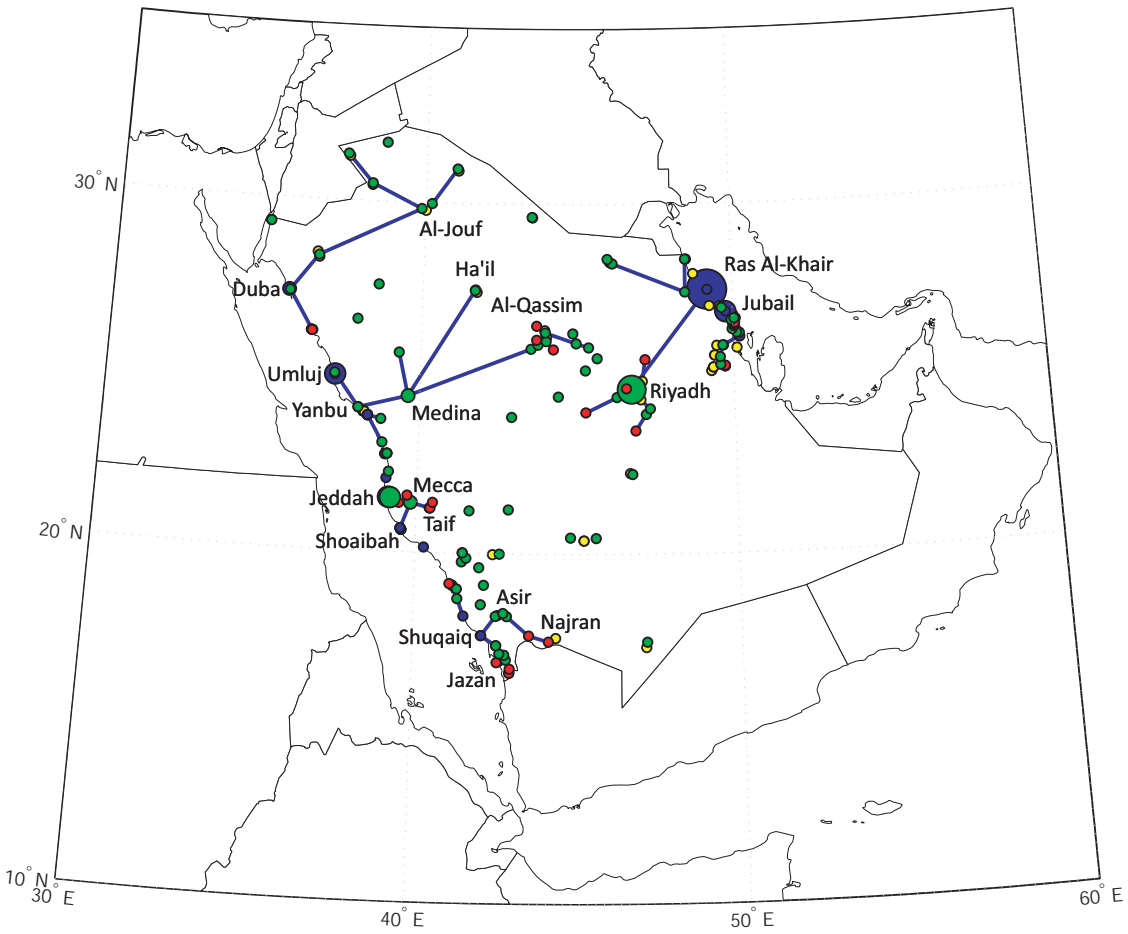

Figure 5-8: Resulting network graph for 2030 demand: cost 50% – CO_2 50%

the average daily water consumption per capita is different by region. On the other hand, the size of a desalination plant node or a power plant node represents the amount of water produced or electricity generated in the resulting network flow. Blue lines are the pipelines that are in use and they are not necessarily the existing ones. The existing ones that are not in use in the resulting network are not shown. For example, we can observe that the big blue node in the upper right representing the Ras Al-Khair SWRO plant produces a large amount of potable water. This is not surprising because Riyadh, the largest city in the Kingdom, is supplied by Ras Al-Khair through the 479-km long pipeline, through which the water transported is assumed to be lost up to 24% due to leaks and evaporation.

In the upper left, we observe that Duba, the green city on the shore of the Red Sea, supplies water to several cities in the regions of Al-Jouf and Northern Borders. To the south of the Duba network is the relatively large blue node, Umluj, connecting to the Yanbu-

Table 5.4: Top 10 CAPEX investment purposes for 2030

Rank	CAPEX (annualized) [MUSD/year]	Investment Purpose	Location	Technology	Capacity (new/expanded)	Distance [km]
1	200.99	Desal Plant Construction	Ras Al-Khair	SWRO	2512300 [m^3/day]	
2	87.73	Desal Plant Capacity Expansion	Jeddah	SWRO	1096600 [m^3/day]	
3	74.51	Desal Plant Capacity Expansion	Jubail	SWRO	931300 [m^3/day]	
4	73.13	Desal Plant Capacity Expansion	Umluj	BWRO	914090 [m^3/day]	
5	21.86	Desal Plant Capacity Expansion	Duba	BWRO	273230 [m^3/day]	
6	19.16	Pipeline Construction	Ras Al-Khair - Riyadh			479
7	18.40	Pipeline Construction	Medina - Ha'il			460
8	17.84	Pipeline Construction	Medina - Ar-Rass			446
9	16.84	Pipeline Construction	Tabuk - Dumat Al-Jandal			421
10	15.86	Power Plant Construction	Ras Al-Khair	Gas	793 [MW]	

Medina network. Medina serves as a hub for supplying water up to Ha'il and several cities in the central (Al-Qassim) region. Since cities in the central region are currently connected from the east coast via Riyadh, it is interesting that the resulting network has chosen the supply from west. Further down south is the Shoaibah-Jeddah-Mecca-Taif network and in the southernmost we observe the Shuqaiq plant serving to several cities in the Jazan region, cities in the Asir region, and up to Najran. On the east coast (Persian Gulf), the biggest blue Ras Al-Khair supplies water to the north east cities (Nairyah, Khafji, and Hafr Al-Batin) as well as Riyadh and several nearby cities. To the south of the Ras Al-Khair network is the relatively large blue node, Jubail, serves to several cities along the east coast and down to the inland cities such as Abqaiq, Al-Uyun, Hofuf, and Al-Taraf. Other isolated nodes are the cities that expand both the ground water capacity and the waste water treatment capacity (because they are all green) to supply themselves.

For reference, Table 5.4 lists the top 10 CAPEX investment purposes for this instance. Not surprisingly, the largest CAPEX investment is the construction of Ras Al-Khair SWRO desalination plant, which is represented by the biggest blue node in the north east. The new capacity is about 2.51 Mm^3/day, which is almost 2.5 times that of the actual plant under construction. The next 4 (top 2 through 5) investments fall into the capacity expansion of the existing desalination plants. Especially, the Umluj and Duba plants utilize brackish water/river water, which can produce water of the same quality/quantity while consuming less electricity and emitting less CO_2. This is probably because the current model assumes infinite supplies of feed water. Top 6 through 9 are the construction of new long-distance pipelines. The pipeline from Ras Al-Khair to Riyadh is actually under construction while

the rest three are found in this optimization result. The last one is the construction of power plant in Ras Al-Khair, whose capacity is about 793 MW. The Ras Al-Khair plant currently under construction is a desalination/power plant and this power capacity is well within the plan. This result would support the geographical advantage of Ras Al-Khair.

Other two instances are shown in Figures 5-9 ($w = 0.9$) and 5-10 ($w = 0.1$). Figure 5-9 puts a weight of 90% on minimizing the total cost while Figure 5-10 puts a weight of 90% on minimizing the CO_2 emission. In Figure 5-9, the network is topologically similar to that of $w = 0.5$ to some extent except that the cities in the central region are supplied by Ras Al-Khair via Riyadh. Hence, Ras Al-Khair in this instance is yet larger than that of the previous example. This is understandable partly because this instance prefers to minimize the total cost and uses the existing network to avoid the construction of a new long-distance pipeline connecting the west coast and the central region.

In Figure 5-10, on the other hand, the network looks less connected, more isolated. Even Riyadh and the central region are not connected to either of the coasts. Instead, there are many green nodes, which means many cities utilize waste water treatment. This result implies that the more isolated a network is, the less CO_2 is emitted as a whole. One possible explanation is that the transport of water makes more CO_2 because extra CO_2 must be produced for the water lost during transport and for the electricity to transport water through the network.

As can be seen from the three examples, the network topology seems to vary with what is to be minimized. The next section discusses another target year.

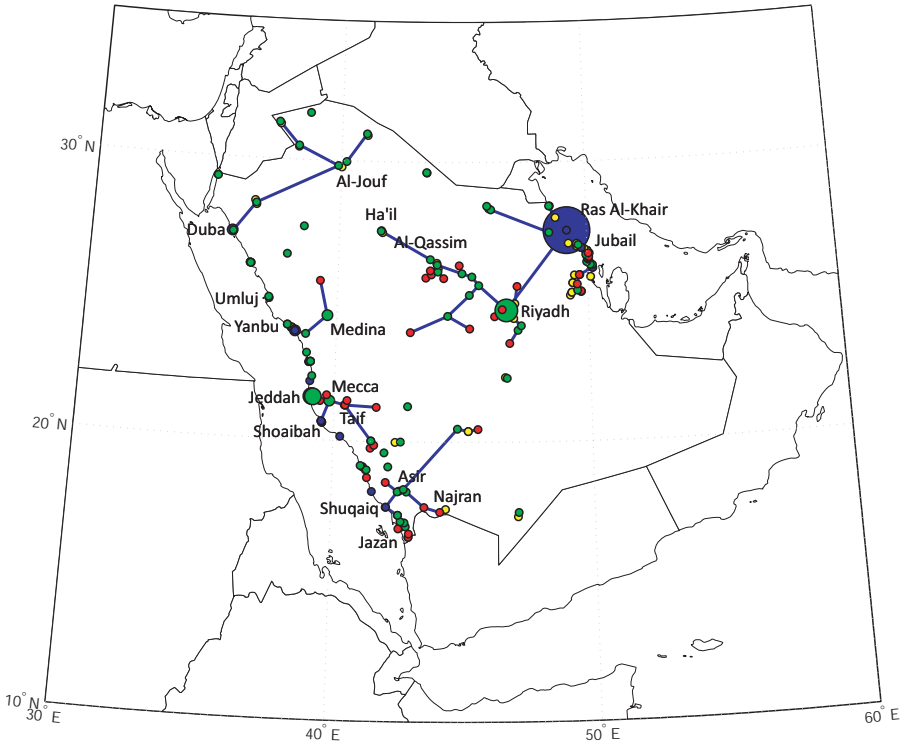

Figure 5-9: Resulting network graph for 2030 demand: cost 90% – CO_2 10%

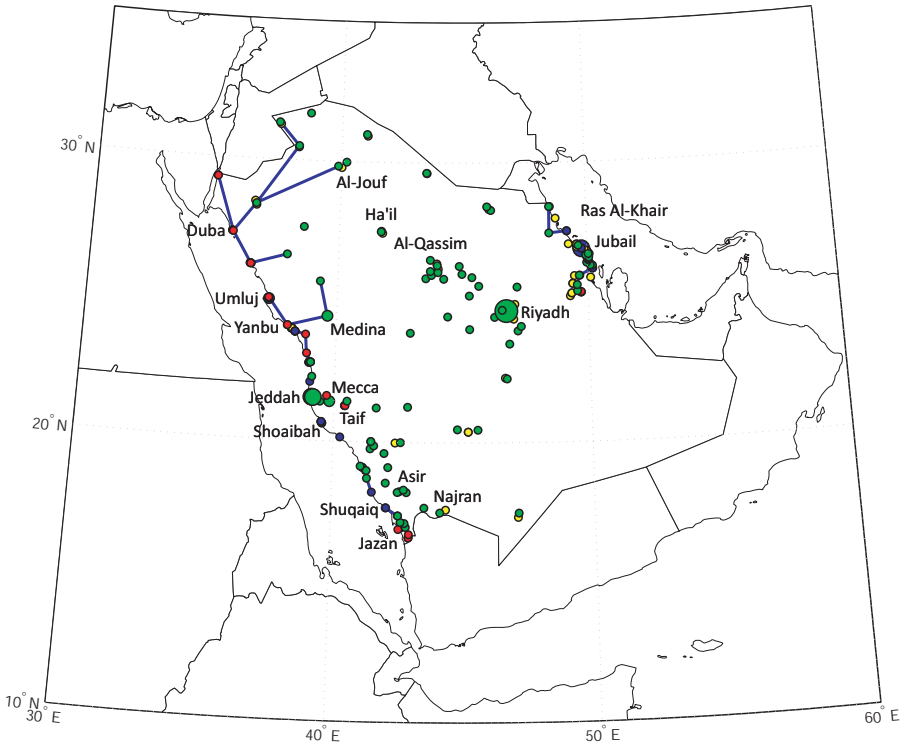

Figure 5-10: Resulting network graph for 2030 demand: cost 10% – CO_2 90%

Table 5.5: List of optimization results for 2050

Weight		Total Cost [BUSD/year]	CAPEX (annualized) [BUSD/year]	OPEX [BUSD/year]	CO_2 Emission [Mmt/year]	Total Water Production [Mm^3/year]	Total Electricity Gneration [GWh/year]	Optimality Gap
Cost	CO_2							
0.999	0.001	8.47	0.86	7.60	22.61	3173	25658	0.40%
0.9	0.1	8.53	0.89	7.64	19.99	3190	25796	2.00%
0.8	0.2	8.64	0.94	7.71	18.76	3197	25376	2.40%
0.7	0.3	8.72	0.95	7.77	18.18	3179	24718	1.69%
0.6	0.4	8.83	0.94	7.88	17.92	3146	24329	1.50%
0.5	0.5	8.89	0.98	7.91	17.80	3135	24175	1.60%
0.4	0.6	8.99	0.98	8.00	17.63	3134	24000	1.19%
0.3	0.7	9.19	1.04	8.15	17.45	3099	23918	1.00%
0.2	0.8	12.38	1.13	11.25	15.68	2836	23649	0.70%
0.1	0.9	13.04	1.12	11.92	15.45	2758	23807	0.25%
0.001	0.999	14.07	1.55	12.52	15.42	2739	24201	0.01%

5.3.2 Target Year of 2050

This section sets the target year to 2050 while keeping the basis year the same 2010. The total population in the Kingdom in 2050 is estimated to be 54 million, which is about twice that of 2010. Again we assume the same population coverage of 97 cities though it is less likely if looking ahead as far as 2050. The total demand for water is 10.32 Mm^3/day, of which 7.22 million can only be satisfied with potable water and 3.10 million can be satisfied with either potable or non-potable water (recycled waste water). Since the basis year stays 2010, the desalination capacity and the ground water capacity are still 3.27 Mm^3/day and 2.29 Mm^3/day, respectively, which obviously falls short of the 2050 demand for water. Similarly to the previous section, we first solve two single-objective optimization problems to determine each of the rescaling factors and then vary the weight w from 1 to 0 with 0.1 intervals.

Table 5.5 lists the optimization results with the maximum optimality gap being 2.4%. Figure 5-11 plots the total costs and CO_2 emissions along with those of 2030 for reference. We can observe that the Pareto front looks parallel shifted to the upper right while keeping the similar shape, which is intuitive because the demand has only been changed. The minimum total cost amounts 8.47 BUSD/year, which increases 26.8% from that of 2030, while the minimum CO_2 emission amounts 15.42 Mmt/year, which increases 28.6% from that of 2030. Again three representative examples of the resulting network graphs are presented below.

Figure 5-12 shows the resulting network for $w = 0.5$, which puts equal weights on the cost and CO_2 emission. The network topology is very similar to that of 2030, including Duba

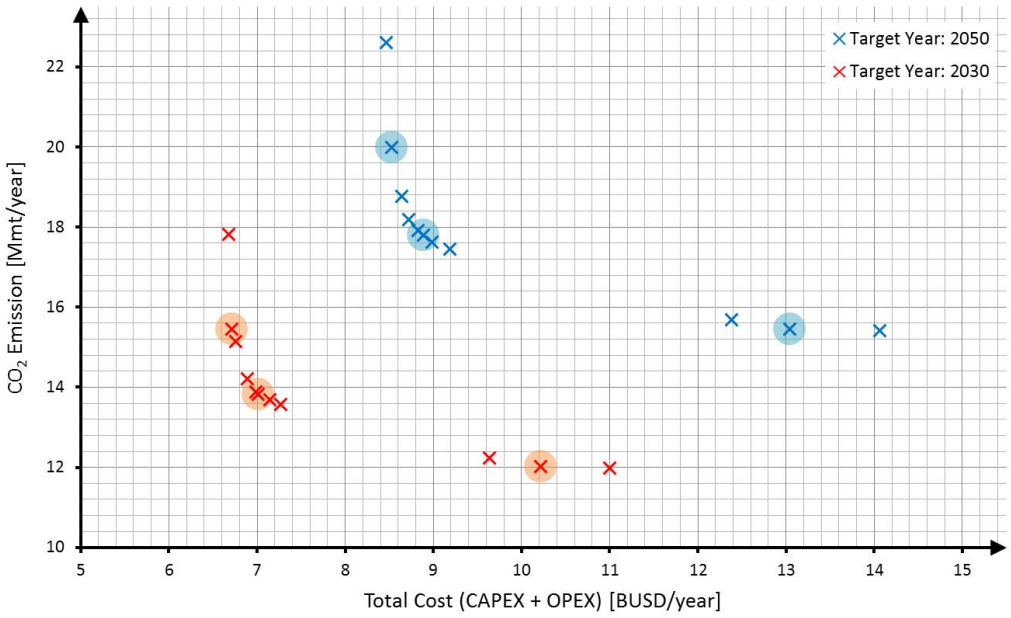

Figure 5-11: Total cost vs. CO_2 emission for 2050 demand

serving to cities in Al-Jouf and Northern Borders, Medina serving as a hub for Ha'il and cities in the central region, the Shoaibah-Jeddah-Mecca-Taif network, Shuqaiq serving to cities in Jazan, Asir, and Najran, Ras Al-Khair serving to Riyadh and nearby cities, and the Jubail network covering most cities in Eastern Province. Two recognizable differences from that of 2030 are that Shuqaiq supplies water to Wadi Ad-Dawasir and As-Sullayyil (inland cities in the Riyadh region) through the long-distance pipeline from Khamis Mushayt in Asir and that small to midsize cities between Al-Qassim and Riyadh such as Al-Zilfi and Al-Majma'ah are served by Ras Al-Khair on the east coast instead of the west coast. One major thing in common is the long-distance connection from Medina to Ha'il and Ar-Rass in Al-Qassim.

Additional two instances are shown in Figure 5-13 ($w = 0.9$) and 5-14 ($w = 0.1$). Again both networks are topologically very close to the corresponding ones of 2030, respectively. The case of $w = 0.9$ is more connected, primarily utilizing the existing pipeline networks, while the case of $w = 0.1$ is more isolated, in which many cities supply themselves by expanding both the ground water and the waste water treatment capacities.

It should be noted that the reason why the trends are very similar between 2030 and 2050 is because essentially the demand for water is just scaled up by population. The underlying assumptions do not reflect the time background such as change in lifestyle and daily water

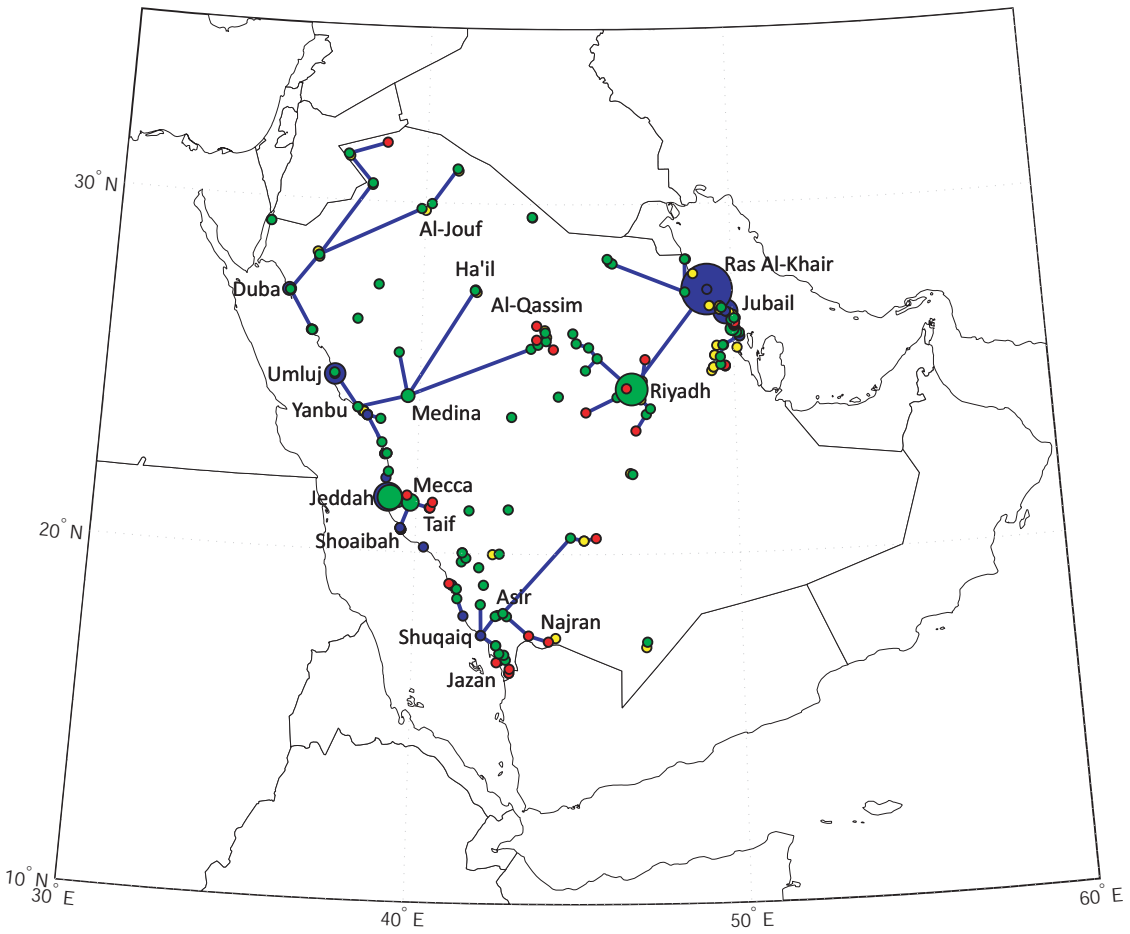

Figure 5-12: Resulting network graph for 2050 demand: cost 50% – CO_2 50%

consumption per capita, power consumption by desalination technologies, CAPEX and OPEX, CO_2 emission by technologies, etc. However, they are all subject to change along with technology advancements. Population growth rates are also different by city; every city will not necessarily keep growing at the same pace or even grow. Discussing the results in more detail obviously requires more accurate data, fine-tuned assumptions, and credible and reasonable estimates of supply/demand.

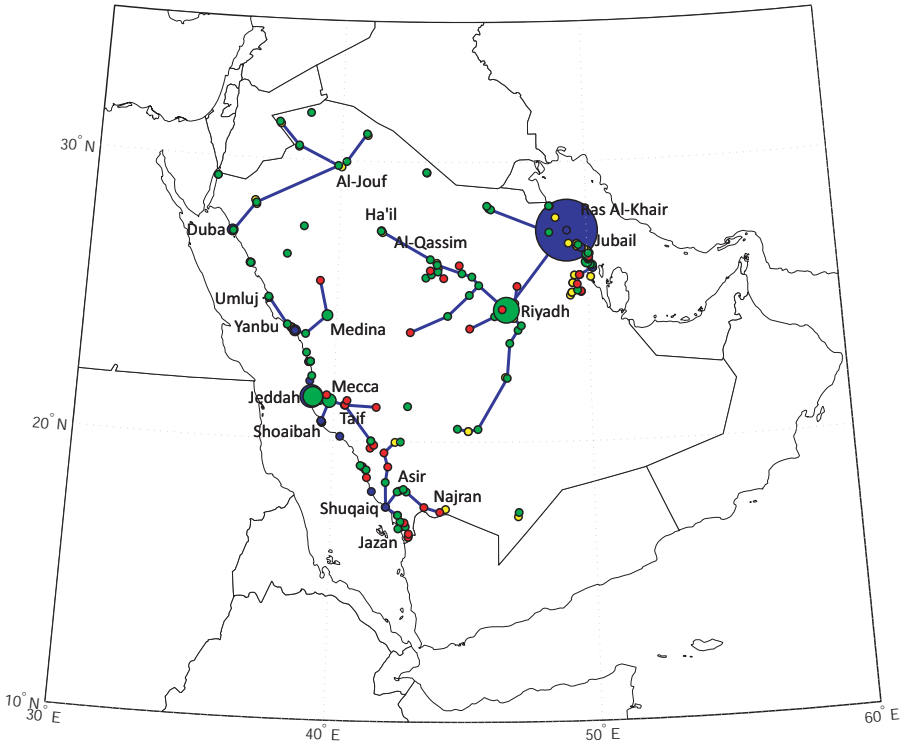

Figure 5-13: Resulting network graph for 2050 demand: cost 90% – CO_2 10%

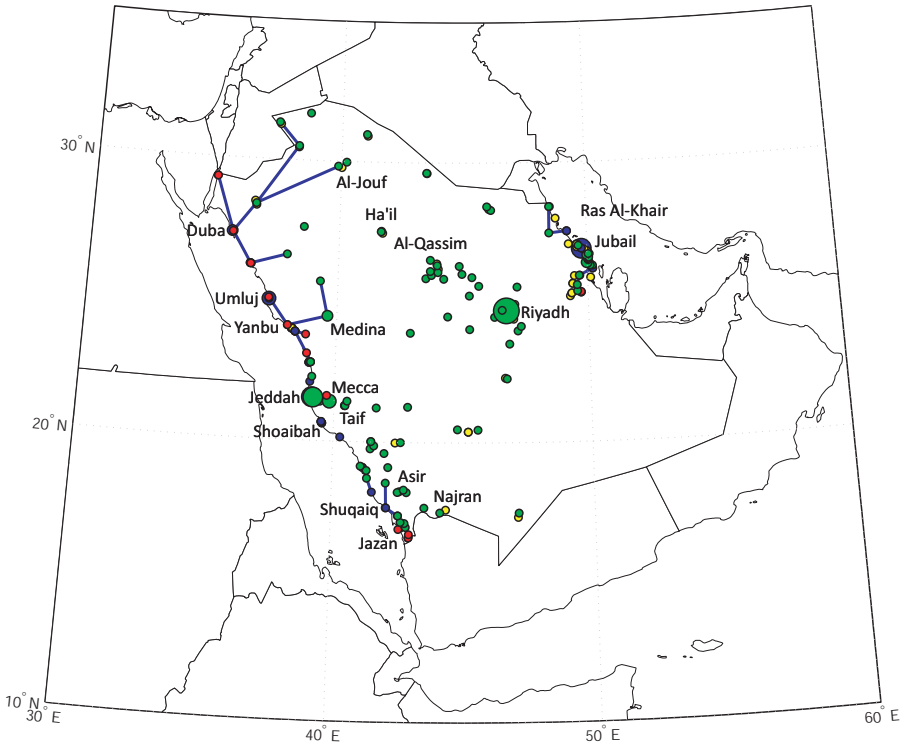

Figure 5-14: Resulting network graph for 2050 demand: cost 10% – CO_2 90%

5.3.3 Discussions

While most of the discussions of the results have been presented in the previous sections, two high-level insights are summarized here.

Water Supplying Network Topology

As we have seen six examples of the resulting network graph, the network topology highly depends on what is to be optimized. For the case of $w = 0.9$ putting more emphasis on minimizing the total cost, it seems that the resulting network makes the most use of the existing network to minimize the cost for new investments. For the case of $w = 0.1$ putting more emphasis on minimizing the CO_2 emission, the resulting network looks less connected, more isolated. In this case many isolated cities expand both ground water and waste water treatment capacity to support themselves without relying on the supply network. This implies that the transport of water makes more CO_2 because extra CO_2 must be produced for the water lost during transport and for the electricity to transport water through the network. For the case of $w = 0.5$ putting equal weights on the cost and CO_2 emission, we observe an interesting combination of investments in the construction of new plants and pipelines and the capacity expansion of the existing plants. However, the network topology is subject to change depending on the supply/demand, the input data accuracy, the underlying assumptions, and the objective functions. Therefore, care needs to be taken when discussing the results in more detail.

Trans-Peninsula Pipeline Network

Particularly in the case of $w = 0.5$, the possibility of the long-distance pipeline from Medina to Ar-Rass and cities in the central (Al-Qassim) region is one of the interesting findings in this study. Cities in the central region are currently connected from the east coast via Riyadh. Therefore it is natural to supply water to these cities from the east coast using the existing pipeline network. However, the resulting network chooses the west coast supplier via Medina at the cost of CAPEX for pipeline construction. One possible reason is simply that Ar-Rass and several cities in the central region are closer to Red Sea rather than Persian Gulf in terms of pipeline distance. For example, the pipeline distance from the east coast to Ar-Rass is 455 km from Jubail to Riyadh plus 379 km from Riyadh to Buraydah

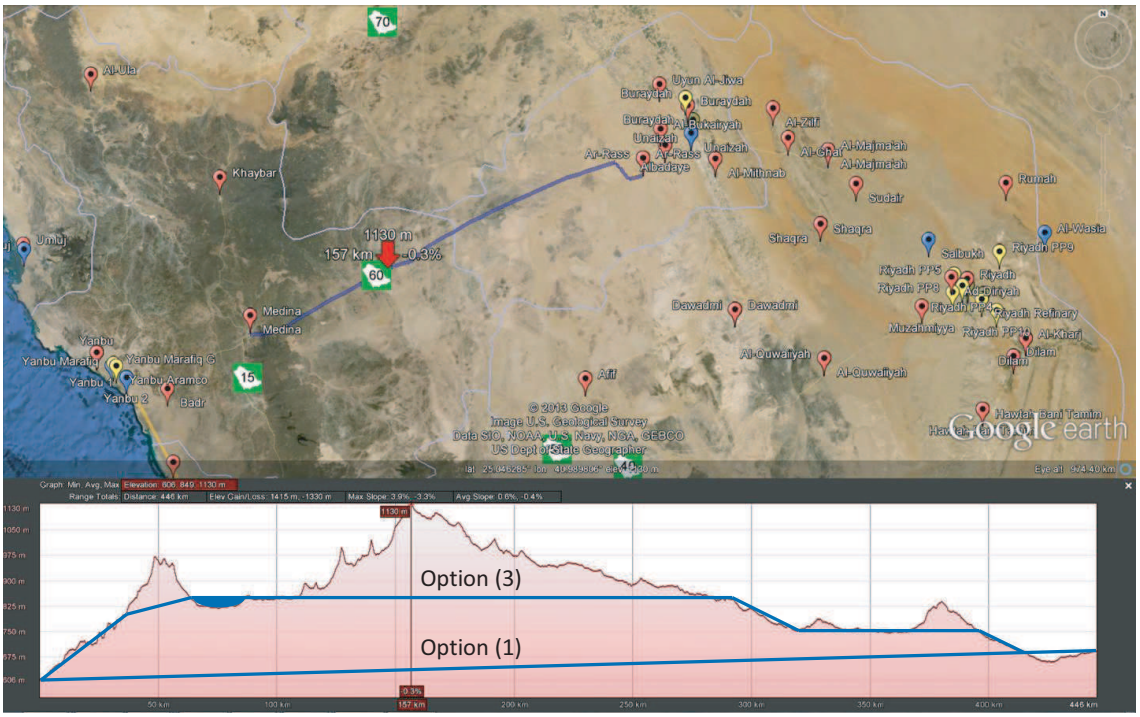

Figure 5-15: Medina to Ar-Rass elevation profile

plus 91 km from Buraydah to Ar-Rass, amounting to 925 km, while the pipeline distance from the west coast to Ar-Rass is 197 km from Yanbu to Medina plus 446 km from Medina to Ar-Rass, amounting to 643 km. Since water is lost 5% every 100 km, the pipeline from the west coast loses less amount of water. But one significant assumption in the model is that the construction of a new pipeline only considers the elevation difference between two end nodes and does not take into account the elevation profile between them.

Figure 5-15 shows the elevation profile between Medina and Ar-Rass. While the elevations of Medina and Ar-Rass are 613 m and 693 m, respectively, there is a mountain region in between with the highest point up to 1130 m. Therefore, we must consider either (1) drilling a tunnel, (2) pumping water to a higher point than two end nodes, or (3) a combination of both. As an example, option (1) and option (3) with storage are illustrated in Figure 5-15. If we drill a tunnel, the same assumption about pipeline CAPEX does not hold; drilling a tunnel is expected to be much higher than just laying down a pipe. Likewise, if we pump water to a higher point, the pumping energy requirement must be modified. Thus, while the feasibility of this pipeline still needs to be investigated in more detail, it is worth exploring the possibility. Once this pipeline is constructed, it forms a "trans-peninsula" pipeline network along with the currently existing network from the east

coast to the central region. One possible advantage of this trans-peninsula network is that it provides robustness and redundancy to the unexpected supply disruption from either of the two. While a fully connected trans-peninsula pipeline would never appear as a solution in the current model because the current model always chooses the better one of the two sides, if robustness optimization is implemented, it would probably fully connect the network by taking into consideration a pipeline failure.

Chapter 6

Conclusions

This chapter summarizes the key results of the preceding chapters, the thesis contributions and limitations, and concludes the thesis with the recommendations for future work.

6.1 Thesis Summary

With the advent of a new era of human space exploration, the research presented in this thesis originates from the question of what the next-generation space logistics paradigm should be. Chapter 1 presents the research background, motivation, and objective. From the literature review, it is found that the past studies on space logistics have been mainly focused on a "vehicle" perspective with the arbitrarily determined logistics network. The objective of this thesis is to develop a comprehensive graph-theoretic modeling framework to quantitatively evaluate and optimize space exploration logistics from a "network" perspective.

In an attempt to create such a modeling framework, we develop a novel network flow model referred to as the generalized multi-commodity network flow (GMCNF) model. Chapter 2 reviews fundamentals of network flow theory and its limitations, and subsequently presents the GMCNF model with examples of a requirement matrix $\boldsymbol{A}_{ij}^{\pm}$, a transformation matrix $\boldsymbol{B}_{ij}$, and a concurrency matrix $\boldsymbol{C}_{ij}^{\pm}$, followed by the introduction of two important graph-theoretic concepts: multi-graph and graph-loop.

In Chapter 3, a linear programming (LP) formulation and a mixed integer linear programming (MILP) formulation of the GMCNF model are described in preparation for the two case studies. For the MILP formulation, in addition to the flow variables $\boldsymbol{x}_{ij}^{\pm}$, we in-

troduce two more variables, capacity expansion $\boldsymbol{y}_{ij}^{\pm}$ and decision binary $\boldsymbol{z}_{ij}$, and additional constraints including the big-$\mathcal{M}$ method. Implementation and optimization environment is also mentioned.

Chapter 4 presents the first case study in the space application. This case study applies the GMCNF LP model to human exploration of Mars and compares the results with NASA's Mars DRA 5.0. First we solve the baseline problem with the demand that is equivalent to that of the Mars DRA 5.0 scenario. It is found that the solution saves 67.5% from the Mars DRA 5.0 reference scenario in terms of the initial mass in low-Earth orbit (IMLEO) primarily because chemical (LOX/LH_2) propulsion is used along with oxygen-rich ISRU. We also present one possible scenario with two "gateway" resource depots at GTO and DTO with orbital transfer vehicles (OTVs). Then we solve variant problems that have different settings to see the effect of each factor. Findings include: taking advantage of oxygen-rich ISRU, LOX/LH_2 is preferred to nuclear thermal rocket (NTR), the aerobraking option as well as ISRU availability on the Moon make great contributions in reducing the initial mass at KSC, the zero boil-off (ZBO) does not make a big difference in the initial mass within the scope of this case study, and as the ISRU resource production decreases, ISRU in each location becomes worthless at a certain threshold and the network topology changes.

Chapter 5 presents the other case study in the terrestrial application. This case study applies the GMCNF MILP model to the complex infrastructure system in Saudi Arabia, focusing on the couplings between water and energy. Considering the capacity of the online infrastructures as of 2010 as a basis, we solve the problems with the 2030 demand and the 2050 demand. The objective function is a weighted sum of the total cost (= CAPEX + OPEX) and the total CO_2 emission. The key findings include: the network tends to be less connected, more isolated when putting more emphasis on minimizing the CO_2 emission, and some of the resulting networks suggest the possibility of the long-distance pipeline network connecting the west coast and the east coast via the central region.

6.2 Contributions and Limitations

This thesis develops the generalized multi-commodity network flow (GMCNF) model. The LP formulation of this model is applied to space exploration logistics while the MILP formulation is applied to terrestrial infrastructure system. These two applications address

substantially different types of problems: the terrestrial application solves a typical network flow problem whereas the space application solves more like a vehicle routing problem (VRP). In a typical network flow problem as in the terrestrial application, the resulting network flow is interpreted straightforwardly while if it is applied to a VRP-type problem, the resulting network flow could imply several interpretations. This model could be applied to any network flow problem (or any problem that is translatable into a network flow problem) in which multiple commodities interact with each other in the form of requirement at nodes, transformation on edges, and concurrency within edges. Also, allowing multiple edges between the same end nodes enables built-in trades between multiple options while allowing graph-loops associated with nodes enables modeling of a facility that requires other commodities and transforms a commodity into another.

As discussed in Section 4.3.3, the limitations of the GMCNF model primarily arise in three areas: risk analysis, model linearity, and time evolution of network flow/topology. The current model assumes that all transports occur with certainty and all demands are purely deterministic. The risks of node and edge failures are not treated in the model. Robustness optimization needs to be implemented to take into account those risks. As shown in Chapter 5, for example, a fully-connected trans-peninsula pipeline would never appear as a solution in the current model because the current model always chooses the better one of the two sides. However, robustness optimization would probably fully connect the network in case of pipeline failure.

The second limitation of the model is model linearity. In the current model, both the objective function and the constraints are all written in linear forms. While nonlinearity in the predetermined parameters can be built in such as ΔV and TOF, nonlinear objective function or constraints on the flow cannot be handled in this model. For example, we assume a linear scalability between the size of an ISRU plant and the amount of resources produced in the space application and a linear relationship between the amount of water sent into the pipeline and the pumping energy required in the terrestrial application. If we perform subsystem-level detailed design and planning, we would need a high fidelity model. At the same time, however, there is a great advantage in linear formulation, that is, LP problems can be solved quickly so that we can solve many instances, which helps make trade studies more efficient.

The third limitation of the model is time evolution of network flow/topology. This

model simulates a static network flow for a given snapshot of supply/demand and therefore it does not consider the time evolution of the network flow or the network topology. Since it determines the optimal flow such that it only satisfies the mass balance at each node, it cannot capture the "flow" of events. This is also true in Chapter 5. The current model is limited to the optimization between two points: from capacity (basis) to demand (target). The gradual evolution of infrastructure system during that time is not taken into account. Therefore, considering these two limitations, this model is probably more useful for high level system trades such as mission architectures and infrastructure concepts.

6.3 Recommendations for Future Work

While one obvious future work is to implement the GMCNF model in SpaceNet as a front-end tool for network auto-generation, the recommendations for mode general future work are based on the current limitations. One possible way to add robustness optimization to the model is to introduce probabilistic failure of node/edge in any way. In that case, however, the model would not keep its current linear form any longer and therefore this will relate to the second limitation as well.

Removing the limitation of model linearity seems straightforward because a number of solution methods and solvers are available for nonlinear programming (NLP) problems and mixed integer nonlinear programming (MINLP) problems. However, it should be noted that the effectiveness of LP would be sacrificed in return for the generality in the problem structures.

Removing the other limitation seems more challenging. The GMCNF model presented in this thesis can only handle the optimization between two points. As seen in the example of ISRU plant deployment, the current model counts chickens before they hatch. If the temporal dimension is somehow embedded, this contradiction inherent in the current model will be solved. One possible solution is the time-expanded network, in which a set of nodes of the underlying static network is copied for each discrete time step (building a time layer). However, it will raise another issue that due to the size of the time-expanded network that is generated, the problem can become quite large with millions of variables and constraints, which requires much more computational effort. It might be worth exploring a smarter solution to this "back to the future" paradox.

Appendix A

Case I: Background Information

This appendix lists the detailed background information for Case I. These data are used to define the supply/demand at each node and the $\boldsymbol{ABC}$ matrices for each edge.

Tables A.1 and A.2 provide a summary of the surface systems and a summary of Mars transit habitat (MTH) in the Mars DRA 5.0 scenario, respectively [59]. Figure A-1 lists the ΔV_{ij} value for each edge [13, 61, 62]. Note that these ΔV values assume high thrust propulsion and the Oberth maneuver if possible. Cells shaded in light red represent aerobraking options, in which ΔV for arrival capture can be saved but the aeroshell is needed that adds to mass. For example, when we transfer from LEO to LMO, it requires 6.12 km/s of ΔV without aerocapture and 3.82 km/s of ΔV with aerocapture. Figure A-2 lists the times of flight (TOFs). The TOF for Mars transfer as well as the ΔV are time-variant but we assume a "fast" trajectory of 180 days as with Mars DRA 5.0.

Table A.1: Mass summary for the surface systems of Mars DRA 5.0

Surface Systems	**Quantity**	**Mass [kg]**
Science	–	1,000
Robotic Rover	2	500
Drill	1	1,000
Unpressurized Rover	2	500
Pressurized Rover	2	8,000
Pressurized Rover Growth	–	1,600
Pressurized Rover Power	2	1,000
Traverse Cache	–	1,000
Habitat	1	16,500
Habitat Growth	–	5,000
Stationary Power System	4	15,600
Total Surface Systems	–	51,700

Table A.2: Mass summary for Mars transit habitat (MTH) of Mars DRA 5.0

Transit Habitat Mass Estimate	**Mass [kg]**
Power System	5,840
Avionics	290
Environmental Control & Life Support	3,950
Thermal Management System	1,260
Crew Accommodations	4,210
EVA Systems	870
Structure	2,020
Margin (30%)	4,920
Additional Spares	4,180
Crew Exploration Vehicle (CEV)	10,000
Total Transit Habitat Mass	37,540

ΔV [km/s]	KSC	PAC	LEO	GTO	GEO	LSP	LLO	EML1	EML2	EML4/5	DTO	DEIM	PTO	PHOB	LMO	GC
KSC			9.50													
PAC																
LEO		9.50 0.00		2.50	4.33		4.04	3.77	3.43	3.97	4.92 3.82		5.22 3.82		6.12 3.82	10.22 3.82
GTO		12.00 0.23	2.50 0.23		1.83		1.54	1.27	0.93	1.47	2.42 1.32		2.72 1.32		3.62 1.32	7.72 1.32
GEO		13.83 2.06	4.33 2.06	1.83			2.05	1.38	1.47	1.71	3.00 1.90		3.30 1.90		4.20 1.90	8.30 1.90
LSP							1.87									
LLO		13.54 1.31	4.04 1.31	1.54	2.05	1.87		0.64	0.64	0.98	3.10 2.00		3.40 2.00		4.30 2.00	8.40 2.00
EML1		13.27 0.77	3.77 0.77	1.27	1.38		0.64		0.14	0.33	1.84 0.74		2.14 0.74		3.04 0.74	7.14 0.74
EML2		12.93 0.33	3.43 0.33	0.93	1.47		0.64	0.14		0.34	1.84 0.74		2.14 0.74		3.04 0.74	7.14 0.74
EML4/5		13.47 0.84	3.97 0.84	1.47	1.71		0.98	0.33	0.34		2.13 1.03		2.43 1.03		3.33 1.03	7.43 1.03
DTO		14.42 1.10	4.92 1.10	2.42 1.10	3.00		3.10	1.84	1.84	2.13		0.70	0.30 0.00		1.20 0.00	5.30 0.00
DEIM											0.70					
PTO		14.72 1.40	5.22 1.40	2.72 1.40	3.30		3.40	2.14	2.14	2.43	0.30			0.50	0.90 0.00	5.00 0.00
PHOB													0.50			
LMO		15.62 2.30	6.12 2.30	3.62 2.30	4.20		4.30	3.04	3.04	3.33	1.20		0.90			4.10 0.00
GC															4.10	

Aeroshell needed for aerobraking

Figure A-1: ΔV values [km/s] used in the analysis

TOF [days]	KSC	PAC	LEO	GTO	GEO	LSP	LLO	EML1	EML2	EML4/5	DTO	DEIM	PTO	PHOB	LMO	GC
KSC			1													
PAC																
LEO		1 1		1	1		4	3	4	4	180 180		180 180		180 180	180 180
GTO		1 1	1 1		1		4	3	4	4	180 180		180 180		180 180	180 180
GEO		1 1	1 1	1			4	3	4	4	180 180		180 180		180 180	180 180
LSP							1									
LLO		4 4	4 4	4	4	1		1	1	4	180 180		180 180		180 180	180 180
EML1		3 3	3 3	3	3		1		1	4	180 180		180 180		180 180	180 180
EML2		4 4	4 4	4	4		1	1		4	180 180		180 180		180 180	180 180
EML4/5		4 4	4 4	4	4		4	4	4		180 180		180 180		180 180	180 180
DTO		180 180	180 180	180 180	180		180	180	180	180		1	1 1		1 1	1 1
DEIM											1					
PTO		180 180	180 180	180 180	180		180	180	180	180	1			1	1 1	1 1
PHOB													1			
LMO		180 180	180 180	180 180	180		180	180	180	180	1		1			1 1
GC															1	

Aeroshell needed for aerobraking

Figure A-2: Time of flight (TOF) [days] used in the analysis

Appendix B

Case II: Background Information

This appendix lists the detailed background information for Case II. These data are used to define the supply/demand at each node and the $\boldsymbol{ABC}$ matrices and the capacity for each edge.

Table B.1 lists the assumptions about CAPEX/OPEX and CO_2 emission used in determining the coefficients in the objective functions. Table B.2 lists water consumption in various regions during 2010 [68]. The rightmost column calculates the average daily water consumption per capita by dividing the total amount of water consumption by the population. Table B.3 gives power consumption for each water processing used in the analysis. Tables B.4, B.5, and B.6 present lists of cities, desalination plants, and power plants created in this analysis, respectively.

Table B.1: Assumptions about CAPEX/OPEX and CO_2 emission

	Unit Cost/Amount	**Relevant Variable***
CAPEX:		
Capacity expansion		
Desalination	2,000 [USD/(m^3/day)]	y_{ii} (potable water)
Ground water processing	5,000 [USD/(m^3/day)]	y_{ii} (potable water)
Waste water treatment	2,500 [USD/(m^3/day)]	y_{ii} (waste water)
Electricity generation	500,000 [USD/MW]	y_{ii} (electricity)
Pipeline construction	1,000,000 [USD/km]	z_{ij} (potable water)
Powerline construction	2,000,000 [USD/km]	z_{ij} (electricity)
OPEX:		
Desalination	1.5 [USD/m^3]	x_{ii} (potable water)
Ground water processing	5.0 [USD/m^3]	x_{ii} (potable water)
Waste water treatment	0.5 [USD/m^3]	x_{ii} (waste water)
Electricity generation	0.1 [USD/kWh]	x_{ii} (electricity)
Pipeline maintenance	36,500 [USD/km/year]	z_{ij} (potable water)
Powerline maintenance	36,500 [USD/km/year]	z_{ij} (electricity)
CO_2 Emission:		
Desalination		
Reverse osmosis (RO)		
Sea water (SWRO)	1.78 [kg/m^3]	x_{ii} (potable water)
Brackish water (BWRO)	1.00 [kg/m^3]	x_{ii} (potable water)
Multi-stage flash distillation (MSF)	23.41 [kg/m^3]	x_{ii} (potable water)
Multi-effect distillation (MED)	18.05 [kg/m^3]	x_{ii} (potable water)
Ground water processing	0.5 [kg/m^3]	x_{ii} (potable water)
Waste water treatment	1.50 [kg/m^3]	x_{ii} (waste water)
Electricity generation		
Natural gas	0.443 [kg/kWh]	x_{ii} (electricity)
Crude/diesel/heavy fuel oil (HFO)	0.778 [kg/kWh]	x_{ii} (electricity)

*Subscripts ii and ij represent loop ii and edge ij, respectively.

Table B.2: Water consumption in various regions during 2010

Region	**Amount [m^3]**	**Population***	**Average daily water per capita [L/day]**
Riyadh	722,614,778	6,777,146	292
Makkah	540,983,519	6,915,006	214
Madinah	150,787,017	1,777,933	232
Al-Qassim	116,785,197	1,215,858	263
Eastern Province	515,502,427	4,105,780	344
Asir	58,269,765	1,913,392	83
Tabuk	57,453,884	791,535	199
Ha'il	29,547,619	597,144	136
Northern Borders	16,787,044	320,524	143
Jazan	17,369,545	1,365,110	35
Najran	9,888,592	505,652	54
Al-Bahah	9,064,775	411,888	60
Al-Jouf	38,373,392	440,009	239
Total	**2,283,427,553**	**27,136,977**	**231**

*National Census Data 2010, General Statistics and Information Department.

Table B.3: Power consumption for water processing

	Power Consumption [kWh/m^3]
Desalination	
Reverse osmosis (RO)	
Sea water (SWRO)	4.7 [kWh] per unit feed water [m^3]
Brackish water (BWRO)	2.1 [kWh] per unit feed water [m^3]
Multi-stage flash distillation (MSF)	13.0 [kWh] per unit feed water [m^3]
Multi-effect distillation (MED)	7.5 [kWh] per unit feed water [m^3]
Ground Water Processing	10.0 [kWh] per unit feed water [m^3]
Waste water treatment	3.0 [kWh] per unit waste water [m^3]

Table B.4: List of cities

City	Administration		ID	Latitude [deg N]	Longitude [deg E]	Elevation [m]	Population (2010)	Water Demand [m^3/day]		Ground Water Capacity [m^3/day]	Waste Water Generation [m^3/day]	Treatment Capacity [m^3/day]
	Region	Abbr.						Potable	Non-Potable			
Haql	Tabuk	TBK	1	29.286097	34.938583	47	25649	5530	2370	4262	6320	0
Tabuk	Tabuk	TBK	2	28.390409	36.5732	769	512629	110520	47366	85181	126309	60000
Tayma	Tabuk	TBK	3	27.627741	38.56012	827	30411	6556	2810	5053	7493	0
Duba	Tabuk	TBK	4	27.34926	35.69619	6	25568	5512	2362	4249	6300	0
Al-Wajh	Tabuk	TBK	5	26.22879	36.469059	2	30512	6578	2819	5070	7518	0
Umluj	Tabuk	TBK	6	25.050006	37.265108	23	37757	8140	3489	6274	9303	0
Al-Ula	Madinah	MDM	7	26.612829	37.922918	778	32413	8147	3492	1248	9311	0
Khaybar	Madinah	MDM	8	25.698611	39.2925	774	45489	11434	4900	1752	13067	0
Medina	Madinah	MDM	9	24.4609	39.62019	613	1100093	276505	118502	42367	316006	198017
Yanbu	Madinah	MDM	10	24.0867	38.058552	11	233236	58623	25124	8982	66998	41983
Badr	Madinah	MDM	11	23.78	38.790556	130	28999	7289	3124	1117	8330	0
Masturah	Makkah	MKM	12	23.110901	38.850689	12	266	62	26	0	70	0
Rabigh	Makkah	MKM	13	22.8	39.033333	6	55304	12822	5495	36	14654	0
Thuwal	Makkah	MKM	14	22.283333	39.1	4	274	64	27	0	73	0
Al-Jumum	Makkah	MKM	15	21.61989	39.699587	229	25601	5935	2544	16	6783	0
Jeddah	Makkah	MKM	16	21.543489	39.172989	15	3430697	795393	340883	2203	909021	471107
Al-Hawiyah	Makkah	MKM	17	21.441111	40.4975	1508	148151	34348	14721	95	39255	0
Mecca	Makkah	MKM	18	21.416667	39.816667	330	1534731	355821	152495	985	406653	210751
Bahrah	Makkah	MKM	19	21.401667	39.450833	97	75213	17438	7473	48	19929	0
Al-Khurmah	Makkah	MKM	20	21.273232	40.427258	1669	27032	6267	2686	17	7163	0
Taif	Makkah	MKM	21	21.27066	40.417068	1676	579970	134464	57627	372	153673	79642
Ranyah	Makkah	MKM	22	21.262738	42.85404	920	21656	5021	2152	14	5738	0
Turabah	Makkah	MKM	23	21.222639	41.647301	1157	25937	6013	2577	17	6872	0
Al-Qunfudhah	Makkah	MKM	24	19.128142	41.078739	3	24512	5683	2436	16	6495	0
Al-Qouz	Makkah	MKM	25	18.980531	41.30595	47	23391	5423	2324	15	6198	0
Hali	Makkah	MKM	26	18.7	41.333333	22	1000	232	99	1	265	0
Al-Bahah	Al-Bahah	BAH	27	20.012991	41.460449	2175	95089	6181	2649	5705	7064	0
Baljurashi	Al-Bahah	BAH	28	19.858062	41.57123	2031	43493	2827	1212	2610	3231	0
Al-Makhwah	Al-Bahah	BAH	29	19.75604	41.436246	378	21999	1430	613	1320	1634	0
Bisha	Asir	ASI	30	20	42.6	1165	86201	7751	3322	1138	8859	21320
Sabt Alalayah	Asir	ASI	31	19.597836	41.978993	1975	19956	1794	769	263	2051	0
An-Nimas	Asir	ASI	32	19.098994	42.127934	2420	27021	2430	1041	357	2777	0
Muhayil	Asir	ASI	33	18.547395	42.05344	520	56953	5121	2195	752	5853	14086
Khamis Mushayt	Asir	ASI	34	18.3	42.733333	2004	430828	38741	16603	5686	44275	106558
Abha	Asir	ASI	35	18.220221	42.50816	2215	236157	21236	9101	3117	24269	58409
Ahad Rafidah	Asir	ASI	36	18.212171	42.844291	2079	57112	5136	2201	754	5869	14126
Dhahran Al-Janub	Asir	ASI	37	17.665225	43.517421	2156	23758	2136	916	314	2442	0
Baish	Jazan	JAZ	38	17.374003	42.53625	78	30835	1169	501	779	1336	0
Sabya	Jazan	JAZ	39	17.148992	42.625923	36	63143	2394	1026	1596	2736	5138
Damad	Jazan	JAZ	40	17.10638	42.777481	80	24056	912	391	608	1042	0
Abu Arish	Jazan	JAZ	41	16.968889	42.8325	67	61047	2315	992	1543	2646	4967
Jazan	Jazan	JAZ	42	16.89192	42.549751	6	127743	4844	2076	3228	5536	10395
Ahad Al-Masarihah	Jazan	JAZ	43	16.709722	42.955	80	25007	948	406	632	1084	0
Samtah	Jazan	JAZ	44	16.597222	42.943889	62	32458	1231	527	820	1407	0
Najran	Najran	NJR	45	17.49173	44.13229	1313	298288	17451	7479	16108	19944	0
Sharurah	Najran	NJR	46	17.483333	47.116667	727	75237	4402	1886	4063	5030	0

Hafr Al-Batin	Eastern Province	SHQ	47	28.434151	45.9753	315	271642	101237	43387	59524	115700	95158
Khafji	Eastern Province	SHQ	48	28.416667	48.5	1	67012	24975	10703	14684	28542	23475
Al-Qaisumah	Eastern Province	SHQ	49	28.309722	46.1275	363	22538	8400	3600	4939	9600	0
Nairyah	Eastern Province	SHQ	50	27.47234	48.481171	51	26470	9865	4228	5800	11274	0
Jubail	Eastern Province	SHQ	51	27.012563	49.658128	0	337778	125885	53951	74017	143869	118326
Ras Tanura	Eastern Province	SHQ	52	26.701864	50.049572	3	54166	20187	8652	11869	23071	18975
Safwa	Eastern Province	SHQ	53	26.65	49.95	14	50447	18801	8058	11054	21487	17672
Tarout	Eastern Province	SHQ	54	26.566667	50.066667	5	77757	28979	12420	17039	33119	27239
Qatif	Eastern Province	SHQ	55	26.55905	49.995689	7	172922	64446	27620	37892	73652	60576
Ank	Eastern Province	SHQ	56	26.519577	50.026727	6	23125	8618	3694	5067	9850	0
Saihat	Eastern Province	SHQ	57	26.475	50.041667	6	75794	28247	12106	16609	32283	26551
Dammam	Eastern Province	SHQ	58	26.392666	49.977714	5	903312	336653	144280	197941	384746	316436
Dhahran	Eastern Province	SHQ	59	26.288768	50.114103	46	120521	44917	19250	26410	51333	42219
Khobar	Eastern Province	SHQ	60	26.283333	50.2	16	457745	170596	73112	100305	194966	160351
Abqaiq	Eastern Province	SHQ	61	25.933335	49.666667	99	36207	13494	5783	7934	15422	0
Al-Uyun	Eastern Province	SHQ	62	25.6	49.566667	113	33042	12314	5278	7240	14074	0
Hofuf	Eastern Province	SHQ	63	25.383333	49.583333	153	660788	246267	105543	144797	281448	231478
Al-Taraf	Eastern Province	SHQ	64	25.35252	49.72433	137	23543	8774	3760	5159	10028	0
Al-Zilfi	Riyadh	RYD	65	26.313754	44.849229	700	60867	19255	8252	9544	22006	9044
Al-Ghat	Riyadh	RYD	66	26.026668	44.960833	706	8497	2688	1152	1332	3072	0
Al-Majma'ah	Riyadh	RYD	67	25.91053	45.35886	712	47743	15104	6473	7486	17261	0
Sudair	Riyadh	RYD	68	25.601243	45.630314	730	14316	4529	1941	2245	5176	0
Rumah	Riyadh	RYD	69	25.563706	47.160584	565	20276	6414	2749	3179	7331	0
Shaqra	Riyadh	RYD	70	25.249359	45.261669	712	26651	8431	3613	4179	9635	0
Ad-Diriyah	Riyadh	RYD	71	24.733222	46.564421	654	43269	13688	5866	6785	15644	0
Riyadh	Riyadh	RYD	72	24.711667	46.724167	635	5188286	1641318	703422	813544	1875792	770887
Dawadmi	Riyadh	RYD	73	24.504444	44.393889	977	61834	19561	8383	9696	22356	9187
Muzahmiyya	Riyadh	RYD	74	24.48147	46.25576	629	30164	9542	4090	4730	10906	0
Al-Kharj	Riyadh	RYD	75	24.14833	47.305	438	234607	74218	31808	36787	84821	34858
Al-Quwaiiyah	Riyadh	RYD	76	24.046339	45.265612	854	22519	7124	3053	3531	8142	0
Dilam	Riyadh	RYD	77	23.993521	47.174129	446	40114	12690	5439	6290	14503	0
Afif	Riyadh	RYD	78	23.91	42.920278	1048	45525	14402	6172	7139	16459	0
Hawtah Bani Tamim	Riyadh	RYD	79	23.525188	46.844661	616	26270	8311	3562	4119	9498	0
Layla	Riyadh	RYD	80	22.283333	46.733333	538	30906	9777	4190	4846	11174	0
Wadi Ad-Dawasir	Riyadh	RYD	81	20.471998	44.785584	684	93036	29432	12614	14588	33637	13823
As-Sullayyil	Riyadh	RYD	82	20.459722	45.574444	606	26639	8427	3612	4177	9631	0
Uyun Al-Jiwa	Al-Qassim	QSM	83	26.526068	43.68789	660	33042	9415	4035	8082	10760	0
Buraydah	Al-Qassim	QSM	84	26.333333	43.966667	624	467410	133180	57077	114324	152206	86229
Al-Bukairyah	Al-Qassim	QSM	85	26.126419	43.69088	658	29547	8419	3608	7227	9622	0
Unaizah	Al-Qassim	QSM	86	26.084761	43.994301	665	152895	43565	18671	37397	49788	28206
Albadaye	Al-Qassim	QSM	87	25.98118	43.733409	668	46620	13284	5693	11403	15181	0
Ar-Rass	Al-Qassim	QSM	88	25.86834	43.51289	693	92501	26357	11296	22625	30122	17065
Al-Mithnab	Al-Qassim	QSM	89	25.852668	44.230216	632	29210	8323	3567	7144	9512	0
Ha'il	Ha'il	HAL	90	27.516667	41.683333	1007	310897	45808	19632	42282	52352	12000
Turaif	Northern Borders	HDS	91	31.674191	38.656399	828	48108	7453	3194	6879	8518	0
Ar'ar	Northern Borders	HDS	92	30.980829	41.025009	538	167057	25881	11092	23889	29579	18244
Rafha	Northern Borders	HDS	93	29.633301	43.510929	447	52712	8166	3500	7538	9333	5756
Al-Qurayyat	Al-Jouf	JWF	94	31.312979	37.374888	501	116162	30078	12891	27763	34375	11772
Tabarjal	Al-Jouf	JWF	95	30.5	38.216667	546	48525	12565	5385	11597	14360	0
Sakakah	Al-Jouf	JWF	96	29.970869	40.205009	558	150257	38906	16674	35911	44464	15228
Dumat Al-Jandal	Al-Jouf	JWF	97	29.818202	39.868198	600	32613	8445	3619	7795	9651	0

Table B.5: List of desalination plants

Desalination Plant	Administration		Technology	Primary Fuel	ID	Latitude [deg N]	Longitude [deg E]	Elevation [m]	Online Year	Water Production Capacity [m^3/day]	Power Consumption [kWh/m^3]	CO_2 Emission [kg/m^3]	Power Capacity [MW] (if any)
	Region	Abbr.											
Existing Desalination Plants as of 2010 (Online or Presumed Online)													
Haql D SWCC	Tabuk	TBK	SWRO		101	29.290733	34.929889	11	1988	6000	4.7	1.78	0
Duba D SWCC	Tabuk	TBK	BWRO		102	27.362429	35.66257	11	1992	42250	2.1	1.00	0
Al-Wajh D SWCC	Tabuk	TBK	MED		103	26.239238	36.450558	6	2008	18100	7.5	18.05	0
Umluj MED D SWCC	Tabuk	TBK	MED		104	25.002671	37.274977	4	2009	9000	7.5	18.05	0
Umluj RO D SWCC	Tabuk	TBK	BWRO		105	25.002671	37.274977	4	1999	35000	2.1	1.00	0
Yanbu 2 DP SWCC	Madinah	MDM	MSF	HFO	106	23.872239	38.364825	6	1998	144000	13.0	23.41	162.8
Yanbu RO D SWCC	Madinah	MDM	SWRO		107	23.872239	38.364825	6	1998	127800	4.7	1.78	0
Yanbu 1 DP SWCC	Madinah	MDM	MSF	HFO	108	23.867581	38.369019	1	1981	110000	13.0	23.41	357
Rabigh D SWCC	Makkah	MKM	MED		109	22.77895	38.961911	0	2008	18000	7.5	18.05	0
Rabigh D Huta	Makkah	MKM	SWRO		110	22.77895	38.961911	0	2008	30000	4.7	1.78	0
Aziziyah D SWCC	Makkah	MKM	MED		111	22.095696	39.032558	6	1987	4500	7.5	18.05	0
Jeddah 4 DP SWCC	Makkah	MKM	MSF	HFO	112	21.553061	39.116313	11	1980	227100	13.0	23.41	590
Jeddah 3 DP SWCC	Makkah	MKM	MSF	HFO	113	21.550639	39.114814	10	1980	90840	13.0	23.41	341
Jeddah RO2 D SWCC	Makkah	MKM	SWRO		114	21.553061	39.116313	11	1994	56800	4.7	1.78	0
Jeddah RO1 D SWCC	Makkah	MKM	SWRO		115	21.553061	39.116313	11	1988	56800	4.7	1.78	0
Jeddah RO D	Makkah	MKM	SWRO		116	21.553061	39.116313	11	2008	27600	4.7	1.78	0
Jeddah WW D GOV	Makkah	MKM	SWRO		117	21.543489	39.172989	15	1990	30000	4.7	1.78	0
Shoaiba 3 DP SWEC	Makkah	MKM	MSF	HFO	118	20.681198	39.520305	7	2009	880000	13.0	23.41	1190.7
Shoaiba Ex D SEPC	Makkah	MKM	SWRO		119	20.676091	39.52321	8	2009	150000	4.7	1.78	0
Shoaiba 2 DP SWCC	Makkah	MKM	MSF	HFO	120	20.671396	39.526242	9	2002	454000	13.0	23.41	520
Shoaiba 1 DP SWCC	Makkah	MKM	MSF	HFO	121	20.627626	39.555765	7	1988	223000	13.0	23.41	262.8
Shoaiba Barge D RAKA	Makkah	MKM	SWRO		122	20.627626	39.555765	7	2008	52000	4.7	1.78	0
Al-Lith D SWCC	Makkah	MKM	MED		123	20.150511	40.26685	3	2009	9000	7.5	18.05	0
Qunfudhah D SWCC	Makkah	MKM	MED		124	19.075763	41.164482	5	2009	9000	7.5	18.05	0
Al-Birk D SWCC	Makkah	MKM	SWRO		125	18.209489	41.525435	5	2001	2200	4.7	1.78	0
Shuqaiq 2 DP SqWEC	Jazan	JAZ	SWRO	Crude	126	17.658759	42.076809	7	2010	213000	4.7	1.78	1020
Shuqaiq 1 DP SWCC	Jazan	JAZ	MSF	HFO	127	17.660904	42.063008	14	1989	97014	13.0	23.41	128
Khafji D SWCC	Eastern Province	SHQ	MSF		128	28.414542	48.530718	6	1985	36000	13.0	23.41	0
Jubail MSF DP SWCC	Eastern Province	SHQ	MSF	HFO	129	26.897219	49.778863	10	1983	1461210	13.0	23.41	1585
Jubail RO D SWCC	Eastern Province	SHQ	SWRO		130	26.897219	49.778863	10	2007	261809	4.7	1.78	0
Khobar 2 DP SWCC	Eastern Province	SHQ	MSF	Gas	131	26.178118	50.210179	12	1984	267000	13.0	23.41	710
Khobar 3 DP SWCC	Eastern Province	SHQ	MSF	HFO	132	26.175467	50.207548	9	1997	280000	13.0	23.41	478.8
Future Desalination Plants (under Construction or Planned)													
Al-Wajh 4 D SWCC	Tabuk	TBK	MED		501	26.239238	36.450558	6	2020	11000	7.5	18.05	0
Yanbu 3 DP SWCC	Madinah	MDM	MSF	HFO	502	23.872239	38.364825	6	2016	550000	13.0	23.41	1700
Yanbu MED D SWCC	Madinah	MDM	MED		503	23.872239	38.364825	6	2012	68190	7.5	18.05	0
Yanbu 1 D Marafiq	Madinah	MDM	MED		504	23.972716	38.215687	8	2013	54552	7.5	18.05	0
Yanbu 2 DP Marafiq	Madinah	MDM	MED	HFO	505	23.972716	38.215687	8	2013	60348	7.5	18.05	690
Rabigh 4 D SWCC	Makkah	MKM	SWRO		506	22.77895	38.961911	0	2020	600000	4.7	1.78	0
Jeddah RO3 D SWCC	Makkah	MKM	SWRO		507	21.553061	39.116313	11	2012	240000	4.7	1.78	0
Ras Al-Khair DP SWCC	Eastern Province	SHQ	MSF	Gas	508	27.539057	49.196598	2	2014	768750	13.0	23.41	2400
Ras Al-Khair RO D SWCC	Eastern Province	SHQ	SWRO		509	27.539057	49.196598	2	2014	256250	4.7	1.78	0
Jubail RO2 D Marafiq	Eastern Province	SHQ	SWRO		510	26.897219	49.778863	10	2013	58500	4.7	1.78	0

Table B.6: List of power plants

Power Plant	Administration		Primary Fuel	ID	Latitude [deg N]	Longitude [deg E]	Elevation [m]	Power Capacity [MW]	CO_2 Emission [kg/kWh]
	Region	Abbr.							
Tabuk 1 P SEC	Tabuk	TBK	Diesel	201	28.330835	36.584622	767	134.20	0.778
Tabuk 2 P SEC	Tabuk	TBK	Diesel	202	28.469697	36.51738	751	335.60	0.778
Duba P SEC	Tabuk	TBK	Diesel	203	27.367544	35.659148	12	162.00	0.778
Al-Wajh P SEC	Tabuk	TBK	Diesel	204	26.223823	36.488845	8	86.00	0.778
Medina P SEC	Madinah	MDM	Diesel	205	24.4609	39.62019	613	452.80	0.778
Yanbu P Aramco	Madinah	MDM	Gas	206	23.970644	38.262468	7	82.50	0.443
Yanbu P Marafiq G	Madinah	MDM	Gas	207	23.991673	38.23296	8	524.60	0.443
Yanbu P Marafiq H	Madinah	MDM	HFO	208	23.991673	38.23296	8	508.00	0.778
Yanbu P SEC	Madinah	MDM	Diesel	209	24.0867	38.058552	11	54.50	0.778
Rabigh P SEC C	Makkah	MKM	Crude	210	22.8	39.033333	7	3113.46	0.778
Rabigh P SEC H	Makkah	MKM	HFO	211	22.8	39.033333	7	1575.60	0.778
Jeddah P SEC D	Makkah	MKM	Diesel	212	21.543489	39.172989	15	806.90	0.778
Jeddah P SEC C	Makkah	MKM	Crude	213	21.543489	39.172989	15	1630.00	0.778
Mecca P SEC	Makkah	MKM	Diesel	214	21.41667	39.81667	330	1147.10	0.778
Taif P SEC	Makkah	MKM	Diesel	215	21.282224	40.406195	1673	200.40	0.778
Shoaiba P SEC	Makkah	MKM	HFO	216	20.627516	39.555705	7	4323.00	0.778
Tihama P SEC	Makkah	MKM	Diesel	217	19.095824	41.157887	10	697.09	0.778
Al-Bahah P SEC	Al-Bahah	BAH	Diesel	218	20.012991	41.460449	2175	85.60	0.778
Bisha P SEC	Asir	ASI	Diesel	219	19.987241	42.393704	1220	365.40	0.778
Asir CPS P SEC	Asir	ASI	Diesel	220	18.246183	42.578331	2172	639.72	0.778
Baish P SEC	Jazan	JAZ	Diesel	221	17.374003	42.53625	78	26.40	0.778
Jazan P SEC	Jazan	JAZ	Diesel	222	16.937474	42.633229	24	1353.65	0.778
Samtah P SEC	Jazan	JAZ	Diesel	223	16.597222	42.943889	62	25.00	0.778
Najran P SEC	Najran	NJR	Diesel	224	17.596377	44.33737	1254	436.00	0.778
Sharurah P SEC	Najran	NJR	Diesel	225	17.331103	47.093045	759	105.92	0.778
Qaisumah P SEC	Eastern Province	SHQ	Diesel	226	28.348841	46.048965	369	153.80	0.778
Safaniyah P SEC	Eastern Province	SHQ	Gas	227	28.000165	48.75334	10	94.80	0.443
Khursaniyah P Aramco	Eastern Province	SHQ	Gas	228	27.065248	49.261289	24	298.00	0.443
Jubail P JEC	Eastern Province	SHQ	Gas	229	27.055052	49.596196	14	250.00	0.443
Jubail P JWPC	Eastern Province	SHQ	Gas	230	27.055052	49.596196	14	733.33	0.443
Berri P Aramco	Eastern Province	SHQ	Gas	231	26.956166	49.589445	18	298.00	0.443
Berri P SEC	Eastern Province	SHQ	Gas	232	26.956166	49.589445	18	278.10	0.443
Ghazlan P SEC	Eastern Province	SHQ	Gas	233	26.854569	49.895607	13	4256.00	0.443
Juaymah P SEC G	Eastern Province	SHQ	Gas	234	26.793366	50.006868	7	158.70	0.443
Juaymah P SEC D	Eastern Province	SHQ	Diesel	235	26.793366	50.006868	7	10.80	0.778
Juaymah P TPGC	Eastern Province	SHQ	Gas	236	26.793366	50.006868	7	310.00	0.443
Qatif P Aramco	Eastern Province	SHQ	Gas	237	26.788265	49.944084	5	144.00	0.443
Ras Tanura P TPGC	Eastern Province	SHQ	Gas	238	26.698637	50.097106	6	153.00	0.443
Dammam P SEC	Eastern Province	SHQ	Gas	239	26.381623	50.093836	47	582.50	0.443
Abqaiq P Aramco	Eastern Province	SHQ	Gas	240	25.928889	49.687778	97	129.00	0.443
Ain Dar P SCC	Eastern Province	SHQ	Gas	241	25.925676	49.469298	146	76.80	0.443
Qurayyah P SEC	Eastern Province	SHQ	Gas	242	25.859581	50.115573	6	4532.00	0.443
Shedgum P SEC	Eastern Province	SHQ	Gas	243	25.652018	49.391654	298	1429.50	0.443
Shedgum P TPGC	Eastern Province	SHQ	Gas	244	25.652018	49.391654	298	310.00	0.443
Hofuf P SCC G	Eastern Province	SHQ	Gas	245	25.332825	49.722984	138	81.00	0.443
Hofuf P SCC C	Eastern Province	SHQ	Crude	246	25.332825	49.722984	138	108.00	0.778
Uthmaniyah P SEC	Eastern Province	SHQ	Gas	247	25.312005	49.343107	293	412.20	0.443
Uthmaniyah P TPGC	Eastern Province	SHQ	Gas	248	25.312005	49.343107	293	310.00	0.443
Faras P SEC	Eastern Province	SHQ	Gas	249	25.210032	49.285314	261	1568.70	0.443
Riyadh PP9 P SEC	Riyadh	RYD	Gas	250	24.945655	47.065096	668	3760.60	0.443
Riyadh PP5 P SEC	Riyadh	RYD	Crude	251	24.759032	46.592737	680	608.00	0.778
Riyadh PP3 P SEC	Riyadh	RYD	Diesel	252	24.652952	46.726875	590	65.00	0.778
Riyadh PP4 P SEC	Riyadh	RYD	Diesel	253	24.65254	46.672353	610	336.49	0.778
Riyadh PP8 P SEC	Riyadh	RYD	Gas	254	24.597212	46.571972	740	2060.50	0.443
Riyadh PP7 P SEC	Riyadh	RYD	Gas	255	24.569941	46.885403	566	1315.78	0.443
Riyadh P Aramco	Riyadh	RYD	Gas	256	24.522474	46.866235	567	66.00	0.443
Riyadh PP10 P SEC	Riyadh	RYD	Crude	257	24.415381	47.013971	511	1118.00	0.778
Layla P SEC	Riyadh	RYD	Crude	258	22.309044	46.662492	558	102.00	0.778
Juba P SEC C	Riyadh	RYD	Crude	259	20.39297	45.206759	630	230.35	0.778
Juba P SEC D	Riyadh	RYD	Diesel	260	20.39297	45.206759	630	100.08	0.778
Buraydah P SEC	Al-Qassim	QSM	Diesel	261	26.402126	43.944573	624	104.50	0.778
Qassim Central P SEC	Al-Qassim	QSM	Crude	262	26.203288	44.014917	622	1138.06	0.778
Ha'il 1 P SEC	Ha'il	HAL	Diesel	263	27.535063	41.701593	994	48.40	0.778
Ha'il 2 P SEC	Ha'il	HAL	Crude	264	27.468809	41.741723	1004	340.40	0.778
Ar'ar P SEC	Northern Borders	HDS	Diesel	265	30.927203	41.055819	545	273.80	0.778
Rafha P SEC	Northern Borders	HDS	Diesel	266	29.619087	43.52629	458	126.40	0.778
Qurayyat P SEC	Al-Jouf	JWF	Diesel	267	31.251532	37.427176	517	116.80	0.778
Tabarjal P SEC	Al-Jouf	JWF	Diesel	268	30.455557	38.212876	552	99.90	0.778
Al-Jouf P SEC	Al-Jouf	JWF	Crude	269	29.777394	40.01158	673	238.00	0.778

Bibliography

[1] Robert Zubrin. *The Case for Mars: The Plan to Settle the Red Planet and Why Must.* Simon & Schuster, NY, 1997.

[2] Robert Zubrin. Human Mars Exploration: The Time Is Now. *Journal of Cosmology*, 12:3549–3557, 2010.

[3] George W. Bush. A Renewed Spirit of Discovery: The President's Vision for U.S. Space Exploration. The White House, Washington, D.C., January 2004.

[4] Review of U.S. Human Spaceflight Plans Committee. Seeking A Human Spaceflight Program Worthy of A Great Nation. Washington, D.C., October 2009.

[5] Fiscal Year 2011 Budget Estimates. NASA, February 2010.

[6] Barack Obama. Remarks by the President on Space Exploration in the 21st Century. John F. Kennedy Space Center, Merritt Island, FL, April 2010.

[7] Charlie Bolden. Statement by Charlie Bolden. NASA Budget Press Conference, February 2010.

[8] Takuto Ishimatsu, Paul T. Grogan, and Olivier L. de Weck. Interplanetary Trajectory Analysis and Logistical Consideration of Human Mars Exploration. *Journal of Cosmology*, 12:3588–3600, 2010.

[9] Paul T. Grogan. A Flexible, Modular Approach to Integrated Space Exploration Campaign Logistics Modeling, Simulation, and Analysis. Master's Thesis, Massachusetts Institute of Technology, Cambridge, MA, September 2010.

[10] American Institute of Aeronautics and Astronautics. Space Logistics Technical Committee. URL: https://info.aiaa.org/tac/smg/sltc [cited March 6, 2013].

[11] David Simchi-Levi, Xin Chen, and Julien Bramel. *The Logic of Logistics: Theory, Algorithms, and Applications for Logistics and Supply Chain Management.* Springer, 2005.

[12] Takuto Ishimatsu, Jeffrey A. Hoffman, and Olivier L. de Weck. Interplanetary Trajectory Analysis for 2020-2040 Mars Missions including Venus Flyby Opportunities. AIAA 2009-6470, AIAA SPACE 2009 Conference & Exposition, Pasadena, CA, September 2009.

[13] Takuto Ishimatsu, Jeffrey A. Hoffman, and Olivier L. de Weck. Method for Rapid Interplanetary Trajectory Analysis using ΔV Maps with Flyby Options. *Journal of the British Interplanetary Society*, 64:204–213, 2011.

[14] Takuto Ishimatsu, Olivier L. de Weck, and Jeffrey A. Hoffman. Mid-Course Plane-Change Trajectories Expanding Launch Windows for Mars Missions including Venus Flyby Opportunities. AAS 11-520, AAS/AIAA Astrodynamics Specialist Conference, Girdwood, AK, August 2011.

[15] Olivier L. de Weck and David Simchi-Levi. Haughton-Mars Project Expedition 2005. Final Report, NASA/TP 2006-214196, January 2006.

[16] Sarah A. Shull, Erica L. Gralla, Olivier L. de Weck, and Robert Shishko. The Future of Asset Management for Human Space Exploration: Supply Classification and an Integrated Database. AIAA 2006-7232, AIAA SPACE 2006 Conference & Exposition, San Jose, CA, September 2006.

[17] Christine Taylor, Miao Song, Diego Klabjan, Olivier L. de Weck, and David Simchi-Levi. Modeling Interplanetary Logistics: A Mathematical Model for Mission Planning. AIAA 2006-5735, AIAA SpaceOps 2006 Conference, Rome, Italy, June 2006.

[18] Christine Taylor, Miao Song, Diego Klabjan, Olivier L. de Weck, and David Simchi-Levi. A Mathematical Model for Interplanetary Logistics. SOLE 2006, Dallas, TX, August 2006.

[19] Christine Taylor. *Integrated Transportation System Design Optimization*. PhD Thesis, Massachusetts Institute of Technology, Cambridge, MA, February 2007.

[20] Matthew R. Silver and Olivier L. de Weck. Time-Expanded Decision Network: A New Framework for Designing Evolvable Complex Systems. AIAA 2006-6964, AIAA/ISSMO Multidisciplinary Analysis and Optimization Conference, Portsmouth, VA, September 2006.

[21] Erica L. Gralla, Sarah A. Shull, Olivier L. de Weck, Gene Y. Lee, and Robert Shishko. A Modeling Framework for Interplanetary Supply Chains. AIAA 2006-7229, AIAA SPACE 2006 Conference & Exposition, San Jose, CA, September 2006.

[22] Sarah A. Shull, Erica L. Gralla, Nii Armar, and Olivier L. de Weck. An Integrated Modeling Tool for Sustainable Space Exploration. IAC 06-D3.3.1, International Astronautical Congress 2006, Valencia, Spain, October 2006.

[23] Olivier L. de Weck, Matthew R. Silver, and Robert Shishko. Measures of Effectiveness for SpaceNet. Unpublished, v3.3, March 2006.

[24] Afreen Siddiqi, Olivier L. de Weck, and Sarah A. Shull. Matrix Methods Analysis of International Space Station Logistics. AIAA 2008-7605, AIAA SPACE 2008 Conference & Exposition, San Diego, CA, September 2008.

[25] Afreen Siddiqi, Olivier L. de Weck, Gene Y. Lee, and Sarah A. Shull. Matrix Modeling Methods for Spaceflight Campaign Logistics Analysis. *Journal of Spacecraft and Rockets*, 46(5):1037–1048, 2009.

[26] Paul T. Grogan, Afreen Siddiqi, and Olivier L. de Weck. A Flexible Architecture and Object-oriented Model for Space Logistics Simulation. AIAA 2009-6548, AIAA SPACE 2009 Conference & Exposition, Pasadena, CA, September 2009.

[27] Paul T. Grogan, Afreen Siddiqi, and Olivier L. de Weck. Matrix Methods for Optimal Manifesting of Multi-Node Space Exploration Systems. AIAA 2010-8805, AIAA SPACE 2010 Conference & Exposition, Anaheim, CA, August-September 2010.

[28] Paul T. Grogan, Afreen Siddiqi, and Olivier L. de Weck. Matrix Methods for Optimal Manifesting of Multi-Node Space Exploration Systems. *Journal of Spacecraft and Rockets*, 48(4):679–690, 2010.

[29] Massachusetts Institute of Technology Strategic Engineering Research Group. SpaceNet. URL: http://spacenet.mit.edu [cited March 6, 2013].

[30] Olivier L. de Weck, David Simchi-Levi, Robert Shishko, Jaemyung Ahn, Erica L. Gralla, Diego Klabjan, Jason Mellein, Sarah A. Shull, Afreen Siddiqi, Brian K. Bairstow, and Gene Y. Lee. SpaceNet v1.3 User's Guide. NASA/TP 2007-214725, January 2007.

[31] Sarah A. Shull. Integrated Modeling and Simulation of Lunar Exploration Campaign Logistics. Master's Thesis, Massachusetts Institute of Technology, Cambridge, MA, June 2007.

[32] Sarah A. Shull and Olivier L. de Weck. Modeling and Simulation of Lunar Campaign Logistics. AIAA 2007-6244, AIAA SPACE 2007 Conference & Exposition, Long Beach, CA, September 2007.

[33] Gene Y. Lee, Elizabeth Jordan, Robert Shishko, Olivier L. de Weck, Nii Armar, and Afreen Siddiqi. SpaceNet: Modeling and Simulating Space Logistics. AIAA 2008-7747, AIAA SPACE 2008 Conference & Exposition, San Diego, CA, September 2008.

[34] Nii Armar and Olivier L. de Weck. Cargo Revenue Management for Space Logistics. AIAA 2009-6723, AIAA SPACE 2009 Conference & Exposition, Pasadena, CA, September 2009.

[35] Olivier L. de Weck, Elizabeth O. Jordan, Gene Y. Lee, Paul T. Grogan, Takuto Ishimatsu, and Afreen Siddiqi. SpaceNet 2.5 User's Guide. September 2009.

[36] Olivier L. de Weck, Elizabeth O. Jordan, Gene Y. Lee, Paul T. Grogan, Takuto Ishimatsu, and Afreen Siddiqi. SpaceNet 2.5 Quick Start Tutorial. September 2009.

[37] Howard Yue. Propulsive and Logistical Feasibility of Alternative Future Human-Robotic Mars Exploration Architectures. Master's Thesis, Massachusetts Institute of Technology, Cambridge, MA, June 2011.

[38] Paul T. Grogan, Howard K. Yue, and Olivier L. de Weck. Space Logistics Modeling and Simulation Analysis using SpaceNet: Four Application Cases. AIAA 2011-7346, AIAA SPACE 2011 Conference & Exposition, Long Beach, CA, September 2011.

[39] National Aeronautics and Space Administration. In-Situ Resource Utilization. URL: http://www.nasa.gov/centers/ames/research/technology-onepagers/in-situ_resource_Utiliza14.html [cited March 9, 2013]. 2013.

[40] Gerald B. Sanders, William E. Larson, Kurt R. Sacksteder, and Carole A. Mclemore. NASA In-Situ Resource Utilization (ISRU) Project - Development & Implementation. AIAA 2008-7853, AIAA SPACE 2008 Conference & Exposition, San Diego, CA, September 2008.

[41] Ariane Chepko. Technology Selection and Architecture Optimization of In-Situ Resource Utilization Systems. Master's Thesis, Massachusetts Institute of Technology, Cambridge, MA, June 2009.

[42] Gerald B. Sanders, William C. Carey, Jean-Claude Piedboeuf, and Andrea Lorenzoni. Lunar In-Situ Resource Utilization in the ISECG Human Lunar Exploration Reference Architecture. IAC-10.A5.1.7, IAF 61st International Astronautical Congress, Prague, Czech, October 2010.

[43] Gerald B. Sanders, Landon Moore, David S. McKay, Tom M. Simon, Dale E. Lueck, Clyde F. Parrish, Kenneth R. Johnson, Greg Mungas, Mike Pelletier, Kurt Sacksteder, Michael Duke, Jeffrey Taylor, Larry Taylor, and Dale Boucher. Regolith & Environment Science, and Oxygen & Lunar Volatile Extraction (RESOLVE) for Robotic Lunar Polar Lander Mission. International Lunar Conference, Toronto, Canada, September 2005.

[44] Gerald B. Sanders, Kris A. Romig, William E. Larson, Robert Johnson, Don Rapp, Ken R. Johnson, Kurt Sacksteder, Diane Linne, Peter Curreri, Michael Duke, Brad Blair, Leslie Gertsch, Dale Boucher, Eric Rice, Larry Clark, Ed McCullough, and Robert Zubrin. Results from the NASA Capability Roadmap Team for In-Situ Resource Utilization (ISRU). International Lunar Conference, Toronto, Canada, September 2005.

[45] Layton J. Wittenberg. In-Situ Extraction of Lunar Soil Volatiles. Technical Report WC SAR-TR-AR3-9311-3, Wisconsin Center for Space Automation and Robotics, University of Wisconsin, November 1993.

[46] Lunarpedia. Volatiles. URL: http://www.lunarpedia.org/index.php?title=Volatiles [cited March 18, 2013]. 2013.

[47] Tom Simon and Kurt Sacksteder. NASA In-Situ Resourec Utilization (ISRU) Development & Incorporation Plans. Presentation at Technology Exchange Conference, Galveston, TX, November 2007.

[48] William Larson and Gerald Sanders. NASA In-Situ Resourec Utilization (ISRU) Development & Field Testing. Presentation at Hawaii's Aerospace Industry: The Next Frontier, Hawaii State Capital Auditorium, Honolulu, HI, August 2008.

[49] Bruce M. Cordell. The Moons of Mars: A Source of Water for Lunar Bases and LEO. *Lunar Bases and Space Activities of the 21st Century*, 1:809–816, 1985.

[50] Anthony C. Muscatello, Robert P. Mueller, Gerald B. Sanders, and William E. Larson. Phobos and Deimos Sample Collection and Prospecting Missions for Science and ISRU. *LPI Contributions*, 1679(4296), 2012.

[51] Ravindra K. Ahuja, Thomas L. Magnanti, and James B. Orlin. *Network Flows – Theory, Algrithims, and Applications.* Prentice Hall, 1993.

[52] Frank Harary. *Graph Theory.* Westview Press, 1994.

[53] Sriram Pemmaraju and Steven Skiena. *Computational Discrete Mathematics: Combinatorics and Graph Theory with Mathematica* ®. Cambridge Univerysity Press, 2003.

[54] Daniel Zwillinger. *CRC Standard Mathematical Tables and Formulae, 31st Edition.* Chapman and Hall/CRC, 2002.

[55] Jonathan L. Gross and Jay Yellen. *Graph Theory and Its Applications, Second Edition.* Chapman and Hall/CRC, 2005.

[56] Nora Hartsfield and Gerhard Ringel. *Pearls in Graph Theory: A Comprehensive Introduction.* Academic Press, 1994.

[57] Thomas H. Cormen, Charles E. Leiserson, Ronald L. Rivest, and Clifford Stein. *Introduction to Algorithms, Second Edition.* The MIT Press, 2001.

[58] Bret G. Drake. Human Exploration of Mars: Challenges and Design Reference Architecture 5.0. *Journal of Cosmology*, 12:3578–3587, 2010.

[59] Bret G. Drake. Human Exploration of Mars Design Reference Architecture 5.0. NASA/SP 2009-566, NASA Johnson Space Center, Houston, TX, July 2009.

[60] Frank Zegler and Bernard Kutter. Evolving to a Depot-Based Space Transportation Architecture. AIAA 2010-8638, AIAA SPACE 2010 Conference & Exposition, Anaheim, CA, August-September 2010.

[61] Richard C. Oeftering. A Cis-Lunar Propellant Infrastructure for Flexible Path Exploration and Space Commerce. AIAA 2011-7113, AIAA SPACE 2011 Conference & Exposition, Long Beach, CA, September 2011.

[62] Wikipedia. Delta-v budget. URL: http://en.wikipedia.org/wiki/Delta-v_budget [cited April 3, 2013].

[63] Ministry of Economy and Planning. Ninth Development Plant (2010-2014). Kingdom of Saudi Arabia, 2009.

[64] Anas Alfaris, Afreen Siddiqi, Charbel Rizk, Olivier L. de Weck, and Davor Svetinovic. Hierarchical Decomposition and Multi-Domain Formulation for the Design of Complex Sustainable Systems. *Journal of Mechanical Design*, 132:091003–1, 2010.

[65] Mark W. Maier. Architecting Principles for Systems-of-Systems. *Systems Engineering*, 1(4):267–284, 1998.

[66] City Population. Saudi Arabia: Regions & Major Cities - Statistics & Maps on City Population. URL: http://www.citypopulation.de/SaudiArabia.html [cited March 26, 2013].

[67] DesalData.com. Plant browser. URL: http://desaldata.com/projects [cited March 26, 2013].

[68] Ministry of Water and Electricity. Annual Report 1431-1432 A.H. (2010 A.D.). Kingdom of Saudi Arabia, 2010.

[69] Paul J. Tullis. *Hydraulics of Pipelines: Pumps, Valves, Cavitation, Transients.* Wiley-Interscience, 1989.